Determining effect of cementitious repair materials on embedded steel reinforcement exposed to chloride environment using electrochemical NDT methods

by

Perla Rodulfo Gomez
B.Sc., Universidad Santa Maria, 1998

A Thesis submitted in Partial Fulfillment of the
Requirement for the Degree of

MASTER OF APPLIED SCIENCE

in the Department of Civil Engineering

University of Victoria

We acknowledge and respect the lək̓ʷəŋən peoples on whose traditional territory the university stands and the Songhees, Esquimalt and W̱SÁNEĆ peoples whose historical relationships with the land continue to this day.

Supervisory Committee

Determining effect of cementitious repair materials on embedded steel reinforcement exposed to chloride environment using electrochemical NDT methods

by

Perla Rodulfo Gomez

B.Sc., Universidad Santa Maria, 1998

Supervisory Committee

Dr. Rishi Gupta, Department of Civil Engineering
Supervisor

Dr. Lina Zhou, Department of Civil Engineering
Departmental Member

Dr. Josh Giles, Department of Mechanical Engineering
Departmental Member

Abstract

For many years, Reinforced Concrete has been used to construct buildings all around the globe. Corrosion-affected RC structures may lose durability, possibly reducing life expectancy or failing catastrophically if timely action is not taken. Critical content of chloride accumulated at the rebar-concrete interface may break the protective passive film of the rebar surface by the diffusion of chloride through the concrete cover. Specialized cementitious repair materials can be used to restore and extend the service life of RC structures that have been exposed and damaged due to corrosion caused by a marine environment. This research evaluated three different types of cementitious repair materials and a control mix.

Electrochemical NDT techniques: Half-Cell Potential (HCP), Macrocell current and Linear Polarization Resistance (LPR) were used in this study to measure and monitor corrosion potential, current passed and the corrosion current on the three types of cementitious repair materials and control under examination throughout the duration of the research. The effectiveness of repair materials assessed in this study when monitoring the corrosion potential, current passed and corrosion current, when exposed to a chloride environment was compared to that of regular concrete using Ordinary Portland Cement. From the Electrochemical NDT results, it was found that Mix F outperformed Mix M, Mix P and control when exposed to a chloride environment.

Further examination of the three different repair cementitious materials was done through Scanning Electron Microscope (SEM) and Energy Dispersive X-ray (EDX) analysis. Through the EDX microscopy analysis, it was found that Mix F cementitious repair material was the one showing the least amount of chloride per % atomic weight of sample compared to Mixes P, M and Control. As a result, Mix F was the most effective in delaying or retarding the transport of chloride ions reaching the rebar through the concrete matrix and initiating the corrosion process.

Furthermore, observation of all the repair materials through SEM showed that the Mix F repairs have the densest microstructure. The results obtained in this study helped in the determination of the best cementitious repair material for the inhibition of corrosion of RC structures in contact with marine environments.

Table of Contents

List of Tables

List of Figures

List of Abreviations

ACI	American Concrete Industry
ASTM	American Society for Testing Materials
CCD	Corrosion Current Density
CCR	Corrosion Current Rate
CM	Cementitious Materials
CE	Counter Electrode
Control (P)	Control Ponding
Control (NP)	Control No Ponding
C-S-H	Calcium Silicate Hydrates
CTE	Coefficient of Thermal Expansion
EDX	Energy Dispersive X-ray
FA	Fly Ash
HCP	Half Cell Potential
Icorr	Corrosion rate
LPR	Linear Polarization Resistance
MC	Macrocell Current
MIX M (PRO)	Mix M Ponding Repair Only
MIX P (PRO)	Mix P Ponding Repair Only
MIX F (PRO)	Mix F Ponding Repair Only
MIX M (PR&S)	Mix M Ponding Repair & Substrate
MIX P (PR&S)	Mix P Ponding Repair & Substrate
MIX F (PR&S)	Mix F Ponding Repair & Substrate
MIX M (NP)	Mix M No Ponding

MIX F (NP)	Mix F No Ponding
NDT	Non-Destructive Test
OPC	Ordinary Portland Cement
RC	Reinforced Concrete
RE	Reference Electrode
RH	Relative Humidity
Rp	Resistance Polarization
SEM	Scanning Electron Microscope
SF	Silica Fume
WE	Working Electrode
%at	Atomic percentage weight

Unit Abbreviation

Coulombs	C
Kilograms per cubic meter	kg/m3
Mega Pascals	MPa
Micro-ampere per centimeter square	$\mu A/cm^2$
Micrometer	µm
Micrometer per year	µm/year
Millivolts	mV
Nanometer	nm

Acknowledgements

I would like to gratefully acknowledge my Supervisor Dr. Rishi Gupta, for his guidance, encouragement and support throughout my research project; Drs. Lina Zhou and Josh Giles for accepting being part of the committee of my defense and for their teaching during my graduate studies; Prof. Ricardo Bonilla, my graduate classmates, lab and research partner Boyu Wang, Drs. Milton Wang and Elaine Humphrey at the AMF, and technical staff at the Material's lab under the Supervision of Dr. Armando Tura.

Dedication

I would like to dedicate this thesis to my parents, my brothers and sisters and my family for encouraging me to keep pursuing my goals. I would also like to thank my professors at University of Victoria, Universidad Santa Maria and Universidad Central de Venezuela Civil Engineering Graduate studies faculty for their invaluable help and guidance.

Chapter 1 Introduction

1.1 Overview

Concrete that has been structurally designed and has embedded steel reinforcement is known as reinforced concrete. The steel and concrete work together to utilize their best qualities, including the tensile strength of steel and the compressive strength of concrete so that stresses over considerable spans can be sustained.

One of the reasons why concrete and carbon steel work well together is due to their similarity of coefficients of thermal expansion, 1.1×10^{-5} $^{\circ}C^{-1}$ and 1.2×10^{-5} $^{\circ}C^{-1}$ respectively. These similar values suggest that the two materials have great thermal compatibility, which is crucial when two materials are connected and acting as a system.

Concrete is a versatile material suitable for many construction applications that require heavy load bearing capacity [1]. Although a material with intrinsic durability, concrete's resistance to a specific set of exposure circumstances depends on the proportions of its mixture, the reinforcement materials, finishing and sometimes the covering or protection used. There are many factors which can contribute to the deterioration of concrete, including freezing and thawing, exposure to salt as in marine environments, and wetting and drying. These factors and others can seriously affect the lifespan of any reinforced concrete structure [2].

A passive layer protects the most common steel used in RC. Adequate formation of this layer depends on a high alkaline environment. The possibility of corrosion is increased if this layer is absent or deteriorated. In reinforced concrete, corrosion may occur in both the concrete matrix and the reinforcing bars, and it can occur in any environment.

Deterioration of concrete tends to accelerate over time once initiated. Cracking allows ingress of chemical agents that further the corrosion process [3]. Salts from road de-icing and marine environments are major factors contributing to RC structure damage from corrosion. The exposure of RC to wet / dry cycles, like the one an RC structure will experience in a marine environment, can lead to capillary suction of water. Such capillary suction brings salts to the interface between the reinforcing steel and the concrete. Movement of Chloride ions in aggressive environments is a major cause of RC corrosion [4].

Factors affecting durability of a repair material for the purpose of corrosion repair:

1. Permeability
2. Electrical resistivity
3. Resistance to chemical attacks
4. Bonding / adhesion to concrete substrate
5. Low shrinkage
6. Freeze / thaw resistance

Many types of special cementitious repair materials are available and offered in the market for RC corrosion repair. Effective repair material choice depends on consideration of the exposure environment and the existing substrate. The goal is for repairs to have as much longevity as possible, ideally beyond the intended lifetime of the structure. When selecting RC repair materials, planners must take into account substrate and repair material compatibility, particularly electrochemical, and the modulus of elasticity. In this research it is hypothesized that the microstructure of repair mixes would have a determining effect in the delay/inhibition of corrosion of steel when under cyclic wet/dry ponding.

Durable repairs must have good bonding between substrate and the new material. Low permeability in the repair material will enhance protection from future chloride penetration. Existing substrates are normally older concrete. Therefore, drying shrinkage is not normally occurring in the substrate. Consequently, low shrinkage repair materials are a good choice in order to promote good bonding and crack prevention [5]. Electrochemical methods will be used to assess the effectiveness of the repair materials considered in this study. They are the most theoretically sound methods of monitoring corrosion since corrosion is an electrochemical process. In this study, rebar corrosion's electrochemical processes are analyzed through HCP, Macrocell Current, and LPR.

1.2 Proposed work

The purpose of this work is to assess three different types of repair and control materials for corrosion repair of RC when exposed to a ponding methodology of wet and dry cycles simulating a marine environment. Ponding is here defined as an accumulation of water on an RC surface leading to a concentration of ions in the confined area, which react to cause corrosion of RC [6]. A wet/dry ponding procedure was done following ASTM G-109. The intention of the wet/dry ponding cycle was to simulate a real case scenario of an RC structure exposed to a tidal zone area of a marine environment on site. Additionally, assessment of corrosion repair and control materials in 50% RH and 20°C Temperature conditions at a Lab environment were also evaluated when not exposed to wet / dry cycles of NaCl. The exposure conditions considered in the present work are wet / dry cycles of sodium chloride ponding of RC specimens using concrete containing an Ordinary Portland Cement (OPC) mix as a substrate material. Cementitious-based and polypropylene-modified materials bonded to the existing concrete (substrate) were used as repair materials. Carbon reinforcement steel bars embedded and passing through both materials (concrete substrate material + repair material) are also part of the experimental set up. The same specimen configurations including substrate and repair materials were also assessed for corrosion repair. The specimens were prepared according to ASTM concrete standards for steel rebar preparation. The repair mixes were prepared according to manufacturer's specifications. ASTM Standards G-109, ASTM C876, ASTM G-59 were also used for non destructive testing.

The set-up models represent the following. See Figure 1.1:

- RC structural member situated in the tidal zone of a marine environment

- RC structural members exposed to known RH and Temp in a lab environment (not exposed to wet / dry cycles of NaCl)

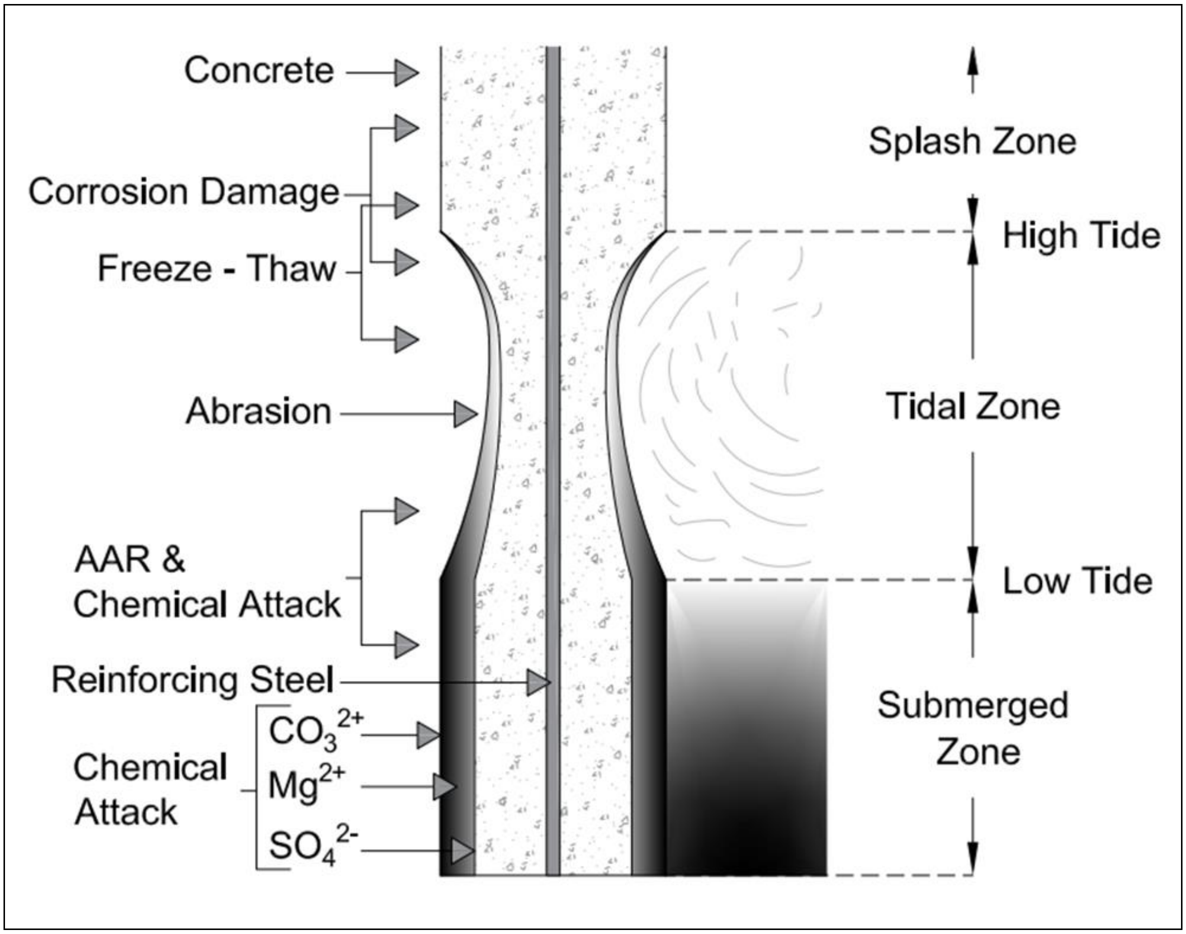

Figure 1.1 Reinforced concrete pile exposed to different zones in a marine environment [7]

Figure 1.1 above shows a RC pile exposed to three zones in a marine environment. For the purpose of this research, this study will simulate the impact on a RC structure exposed to the tidal zone area.

The exposure area at the splash zone is the marine environment zone where the RC area is wet, the surface of the RC is well-aerated, and there is no presence of fouling. An exposure area at the tidal zone is regarded as a marine environment zone where marine fouling is present, and oxygen is available. An exposure area at shallow water is regarded as a marine environment where seawater is usually saturated with oxygen. An exposure area deeply submerged in the ocean is a marine environment where oxygen content is lower than at the surface [8].

Mixes	**NDT Tests**			**Exposure**			**Microscopy**	
	*HCP	*LPR	*MC	*PRO	*PR&S	*NP	*SEM	*EDX
M	√	√	√	√	√	√	√	√
P	√	√	√	√	√	√	√	√
F	√	√	√	√	√	√	√	√
Control	√	√	√	√	√	√	√	√

Table 1.1 Summary of experimental research. Type of mixes, NDT tests, Exposure and Microscopy tests.

*HCP = Half Cell Potential
*LPR = Linear Polarization Resistance
*MC = Macrocell Current
*PRO =Ponding Repair Only
*PR&S= Ponding Repair & Substrate
*NP = No Ponding
*SEM = Scanning Electron Microscopy
*EDX = Energy Dispersive X-Ray

The potential for corrosion, corrosion rate, and macrocell current were calculated with the help of the electrochemical techniques mentioned above, and the results will be presented for each one of the three repair materials and Control. At the end of the testing period, SEM image and EDX analyses were performed on each of the repair material specimens and will help in determining the advantageous properties of the repair materials used in this study. The relationship of the experimental NDT results using these electrochemical methods to measure corrosion potential, corrosion rate, and macrocell current was determined.

The results of Macrocell corrosion, Linear Polarization and HCP performed in this study showed a correlation regarding the level of corrosion where each of the different types of cementitious repair materials stand when under chloride exposure. The chemical constituents of each of the three repair materials plus control under the set-up conditions mentioned above and at the end of testing are presented.

Chapter 2. Background and Literature Review

2.1 Concrete as a steel protector

In RC, a passive oxide layer that surrounds the steel when in contact with an alkaline medium like the one that concrete offers, shields the reinforcing steel from corroding [9]. This alkaline medium is achieved during the hydration of Portland Cement. In this environment, thermodynamically stable compounds of iron and iron-base alloys form oxides and hydroxides. When RC is exposed to a salt concentration, the chloride ion content raises to a certain level known as the corrosion threshold. If the concrete surrounding the steel does not provide adequate protection and the passive layer has broken down, the corrosion of the steel continues at a higher rate.

In an environment with a pH close to 12, a passive film forms on the surface of the rebar serving as protection from corrosion as shown in Figure 2.1 [10]**.** Portland cement, one of the main components of concrete hydrates, together with the calcium silicates, will react to form calcium silicate hydrates and calcium hydroxide [$Ca(OH)_2$].

Concretes containing an adequate amount of the minerals mentioned above are more resistant to chloride penetration from the environment. In terms of the aggregates contained in concrete, if they are highly porous or chloride contaminated, then the chances of reinforcement corrosion will increase [11].

The penetration of chlorides into concrete highly depends on the concrete curing periods. The shorter the concrete curing periods, the higher the possibility of chloride ion penetration. In the case of blended cements, their pozzolanic reaction will make them more resistant to chloride penetration compared to the capacity of Portland cement's hydration reaction and its resistance to chloride penetration. For blended cements, the water cement ratio (w/c), and the fineness of the cement and the pozzolanic components will determine the porosity and pore-size distribution. Blended cements containing fly ash, slag, and silica fume will reduce and refine the porosity of the concrete matrix [12]. Steel reinforcement embedded in concrete with a pH of approximately 12 to 13 environment normally has corrosion protection. A thin oxide layer at a high pH (12-13) will form on the steel and prevent metal atoms from dissolving [13].

Concrete's constituent parts are what define its overall porosity, pore-size distribution, and pore-solution pH [14]. Low permeability in concrete can greatly reduce the onset and propagation of corrosion. By using pozzolans and reducing the proportion of water to cementitious elements in the concrete, low-permeability concrete may be obtained. The corrosion rate of steel can be decreased by the use of pozzolans and slag. ACI 318-14, Building Code Requirements for Structural Concrete, provides useful information regarding measures to protect steel reinforcement embedded in concrete from corrosive materials. The use of corrosion inhibiting admixtures, and sealers and membranes on the concrete surface are some additional measures to protect steel reinforcement from corrosion [15].

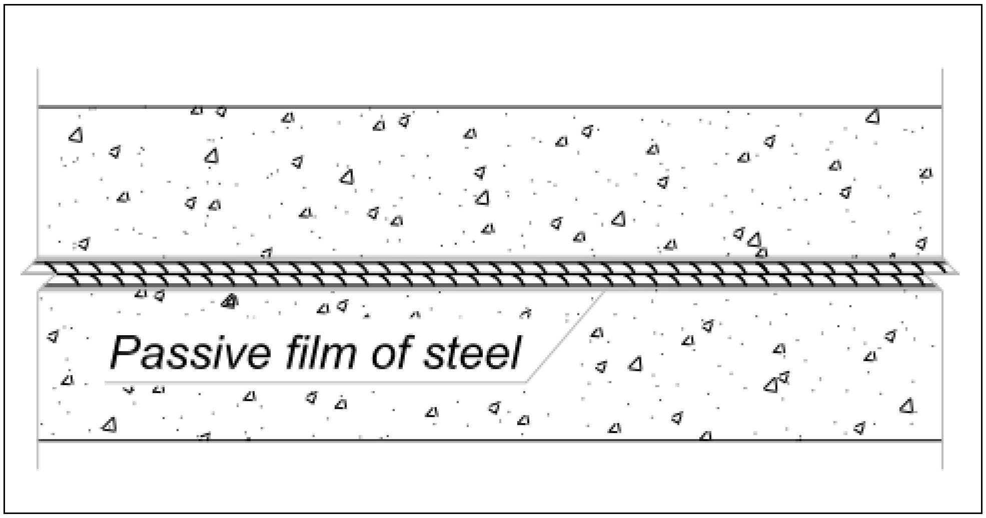

Figure 2.1 Protective layer of steel [10]

2.2 Corrosion of steel embedded in concrete

Corrosion will affect the structural performance of RC. This process happens by loss of steel in the rebar and by the effect of spalling concrete or breakdown of the steel-concrete bond [16]. The steel reinforcement that will be considered in this study is carbon steel. Carbon steel reinforcement consists of iron and carbon in a small proportion. Iron is mostly found in nature in a stable state as iron ore. It oxides as magnetite (Fe_3O_4) and hematite (Fe_2O_3) [17]. Corrosion of iron or steel is an electrochemical process occurring through electrochemical reactions and involving the passage of electrical charge. It consists in two half cell reactions: oxidation, or anodic reaction and cathodic or reduction reaction. In this process, electrons are given off in the oxidation reaction, **Eq. (1)** and used in the reduction reaction, **Eq. (2)** [1].

$Fe \rightarrow Fe^{2+} + 2e^-$ (1) Anodic or Oxidation reaction (dissolution of irons)

$2e^- + H_2O + 1/2\ O_2 \rightarrow 2OH^-$ (2) Cathodic or Reduction reaction (oxygen reduction)

The anodic and cathodic reactions are the beginning of the rust creation process. Both the anodic and cathodic reactions are necessary for the corrosion process to occur, as is water and oxygen. Anodes are the portions of steel reinforcement that are actively corroding. Iron atoms lose electrons in this region of activity and travel as iron ions into the nearby concrete. **Eq. (1).** The electrons that are still in the bar then go to cathode locations where they mix with the oxygen and water in the concrete. Reduction reaction is the name of the process occurring at the cathode. **Eq. (2).** Figure 2.2 below represents the electrochemical process of corrosion of embedded steel described above.

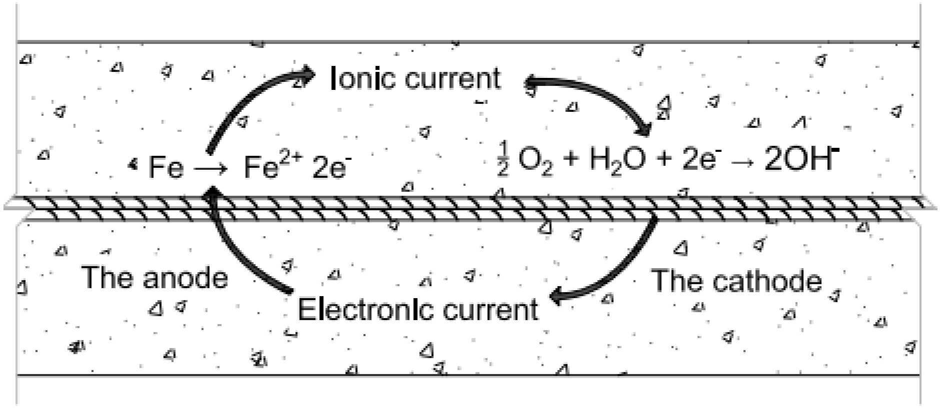

Figure 2.2 Corrosion process of embedded steel through anodic, cathodic, oxidation and hydration reaction [1].

As the electrochemical process progresses, the Fe ions move through the concrete pore water to the cathodic sites where together they form iron hydroxides, which tend to react further with oxygen that is surrounding the embedded reinforcing steel. Equations 3, 4 and 5 show ferrous hydroxide becoming ferric hydroxide and then ferric oxide.

$Fe^{2+} + 2OH^- \rightarrow Fe(OH)_2$ Ferrous Hydroxide (3)

$4Fe(OH)^2 + O_2 + 2H_2O \rightarrow 4Fe(OH)_3$ Ferric Hydroxide (4)

$2Fe(OH)_3 \rightarrow Fe_2O_3 \cdot H_2O + 2H_2O$ Hydrated ferric oxide (rust) (5)

The corrosion process and mechanism of steel in concrete has been discussed in much literature [1], [13–15], and it continues to be an important area of ongoing research. The main components of a corrosion cell are:

- Anode
- Cathode
- Electrolyte

Every length of rebar can have anode and cathode sites. The anode is the location on a steel reinforcing bar where corrosion is taking place and metal is being lost. Iron atoms lose electrons at the anode and change into iron ions (Fe^{2+}). Anodic reaction is the name given to this oxidation process. The location on a steel bar where metal is not consumed is called the cathode [18]. When the reaction products react further with dissolved oxygen, the volume of the reaction forming rust increases. The formation of rust creates internal stress within the concrete matrix that will cause cracking and spalling of the concrete cover [14] .

Rusted rebar expands in volume. Decrease in strength and ductility as well as concrete cover cracking of RC can be caused by reinforcement corrosion due to volumetric expansion of corrosion products [18]. Deterioration of the steel – concrete interface bonding will cause loss of the cover confinement [19]. The diminished mechanical properties of corroded rebars will in turn decrease the load capacity of a structural member, converting a ductile failure mode into a brittle failure [20]. All of these factors can contribute to the risk of RC structural failure.

Extensive research on the repair of corrosion in RC structures has shown that corrosion of embedded metals in concrete can be delayed. Durability of structures can be increased by placing special types of cementitious repair that are chemically more resistant to chloride attacks, especially in the case of structures that are exposed to a marine environment [22–25]. Another focus of research has been conducting experiments demonstrating that reducing the permeability of concrete also can increase the corrosion resistance when using specialized Permeability Reducing Admixtures [24].

2.3 Concrete repair materials

As concrete structures increase in age, concrete repair and increased maintenance is frequently required. In order to slow the corrosion's deterioration process in reinforced concrete structures, new materials and repair techniques are being developed and made available on the market. Their effectiveness in preventing the ingress of aggressive external agents such as chloride ions is examined in this study. Concrete repair evaluation and selection should be made considering the physical properties of repair materials, including the importance of specific material properties for various repair applications and environments. The application of repair materials should be done with proper equipment, and with the removal of all chloride-contaminated concrete surrounding the steel. Surface rust must be removed. The new repair material is then applied at the metal concrete interface [25].

Repair materials needed for concrete deteriorated due to steel rebar corrosion can be categorized as follows:

a) Cement-based materials
b) Polymer modified cement-based materials
c) Polymer or Resin materials [26]

The repair material used in the experimental work of this study is overlay cement-based and polymer-based repair materials for corrosion repair. These three different kinds of repair materials were chosen for this experimental study as they are all advertised as corrosion repair materials. Identification and discussion of relevant material properties will be described. One important aspect to be considered when selecting an appropriate repair material for RC corrosion repair is the compatibility between the properties of concrete replacement and overlay materials and the properties of the substrate [2].

The coefficient of thermal expansion should be similar to that of the substrate in concrete repair applications. All the relevant properties affecting the compatibility of the substrate and repair material must be identified and addressed prior to the repair [27].

Some relevant properties of repair materials that must be considered:

1. **Volume stability:** The negative effects of inadequate volume stability include shear stresses at the interface, cracking or debonding of the repair material.
2. **Mechanical properties:** Effective bonding is essential. Substrate and repair materials must act as a system to avoid failure.

To some extent, other properties can compensate for less-than-ideal chemical or physical properties. Researchers have performed assessment in bonding of repair materials using NDT methods [28]. Among the more relevant mechanical properties of repair materials:

    1.1 Elasticity
    1.2 Static modulus of elasticity
    1.3 Coefficient of thermal expansion
    1.4 Creep
    1.5 Bond strength
    1.6 Compressive strength
    1.7 Tensile strength
    1.8 Flexural strength

One of the most important elements for a successful patch repair is the repair material's compatibility with the substrate. Electrochemical potential differences between substrate and repair can lead to the formation of macrocell corrosion. For compatibility, similarities between physical and electrochemical properties, as well as volume changes must be considered [29–31].

Substrate-repair compatibility’s main factors:

- Repair and substrate drying shrinkage compatibility

- Minimalized thermal expansion or contraction differences

- The modulus of elasticity for repair and substrate should be close in value to reduce potential strains caused by poorly distributed load sharing.

- Differences in creep

Substrate and repair differing strengths and moduli of elasticity could potentially decrease the service life of corrosion repaired RC structures. High tensile strength and the formation of cracking that may reach the repair and substrate interface can be induced by the drying shrinkage of repair materials, consequently reducing the long-term efficiency of the RC structure. Additionally, the load-sharing ability of the patch may eventually become less effective due to creep of the repair material under prolonged stress [32].

It is widely acknowledged that the electrochemical property differences between the repair and substrate are the driving force of corrosion in repair systems. Electrochemical incompatibility causes electrochemical imbalance potential between different locations of the reinforcing steel because of the dissimilar environments caused by a repair. This promotes the initiation of corrosion and furthers or accelerates the process. It has been reported that incompatibility of a repair material against that of its substrate could have a great influence in the success of the repair, and hence its durability as a corrosion repair material-substrate system component [2], [32–34].

Industry partners involved in the area of restoration and rehabilitation of RC structures will be able to successfully design concrete repair projects by having a better understanding of the compatibility / incompatibility issues in concrete repair composite systems. Thermal expansion compatibility between repair and substrate materials is imperative to ensure mechanical properties like tensile stress and shrinking are maintained when the structural element is under stress forces. Moreover, coefficient of thermal expansion (CTE) values between different layers in Portland cement concrete (PCC) such as in pavement, bridge decks, concrete exposed to marine environments, or in other concrete corrosion repairs should be compatible. Otherwise, splitting cracks or spalling will be observed as a consequence of thermal instability between two layers [35].

In this study, three different materials and a control will be evaluated using three NDTs and microscopy analysis. Velu Saraswathy et al [21], through experimental results reported that modified mortar systems treated with fly ash and micro silica have lesser permeable voids because of the smaller size of the micro silica particles compared to normal cement particles. Less permeable gaps and less water absorption occurred in the cement matrix's denser packing. D.D. L. Chung et al. [36], also investigated the corrosion resistance of cement-based materials containing silica fume content and found that SF improves a broad range of essential features, including steel corrosion resistance, freeze-thaw durability, abrasion resistance, bond strength, and chemical attack resistance, as compared to polymer-modified mortars. The NDTs performed and further microscopy analysis in this experiment will be seen to increase understanding of what is required to delay the onset or inhibit the corrosion process in RC repairs.

Safwan et al. [37], also investigated the resistance of SF concrete to corrosion-related damage and found it performed better than regular control concrete. Desi Wang et al. [38] studied the long-term durability of concrete against combined freezing-thawing and sulfate attack. Both FA and SF were proven to increase concrete resistance, agreeing with the findings of D.D. L. Chung. Desi Wang’s experimental results showed that, in comparison, SF performed better than FA leading to significant improvements in concrete durability.

Mailvaganam, N. P. and Taylor, D. A. [39] studied the compatibility of repair systems for concrete structures. Their experimental investigation revealed that it is necessary to think of the repair and substrate as components of a composite system, which consists of different materials. In order to understand how different factors affect the performance of repair systems, even though materials vary, the objective must be to improve physical and chemical property compatibility. The Daniel Cusson et al. [40] research study reported the importance of comprehensive data on the performance of repair products. A significant portion of early repair failures in North American concrete buildings have been linked to incompatibility between repair materials and that of substrate concrete.

The K. U. Aavani et al. [41] research found the use of silica fume beneficial for corrosion repair. Their studies show how SF material properties affect chloride transfer into concrete and highlights the importance of a material's porous structure. Silica fume's fine glassy spheres have a specific surface area of 20,025 m^2 / kg (97,650 ft^2 / lb). The silica fume's particle size, which enables them to fit into the microscopic gaps typically filled by water, results in a denser mixture. It is important to note the difference between the specific surface area of silica fume and that of Portland cement. Portland cement's specific area is 300 to 400 m^2/kg (1465 to 1950 ft^2/lb).

In summary, the use of concrete cementitious materials with low permeability is a crucial element in the long-term durability of RC structures repair. Chloride ion penetration or diffusion is better resisted by low permeability concrete, which prevents oxygen, water, and chlorides from getting to the steel reinforcing bars. Electrochemical compatibility of repair and substrate are also essential to durable repairs.

2.4 Electrochemical NDT methods

Numerous test techniques have been developed to evaluate the corrosion resistance of repair materials. Both destructive and non-destructive test techniques may be used to monitor corrosion initiation and diffusion. In destructive testing, a sample of the rebar is retrieved by taking a core from a structure and determining the rebar's loss in weight and therefore, the rate of corrosion can be assessed. In non-destructive testing, many electrochemical methods are available in the market. Destructive methods carry limitations in terms of disturbing the integrity of the structure and the repairs that need to be done afterwards [42].

In this study, three NDT methods were used to monitor the corrosion rate, corrosion potential, and macrocell current of three repair materials. They include Half Cell Potential method (HCP) [43-44], Linear Polarization Resistance (LPR) [45 - 46] and Macrocell current [47 - 48]. To augment what was learned from the experimental NDTs, SEM and EDX microscopy analysis was used to further investigate the morphology and chemical constituents of the repair materials tested.

2.4.1 Half-cell potential (HCP)

Half-cell potential (HCP), also known as corrosion potential *E*corr and open circuit potential (OCP) is one of the simplest techniques for evaluating and detecting corrosion in both the lab and the field after visual evaluation of rust spots and corrosion-induced cracking. The HCP performed in this study is measured with a three-electrode configuration—counter electrode, working electrode (steel reinforcement) and reference electrode, as shown in Figure 2.3 (a).

According to ASTM C876 [43], the HCP of steel may be used to determine the corrosion risk or likelihood. The copper sulphate reference electrode (CSE) is mostly used in field applications. This electrode is used to describe HCP values in ASTM C876. Standard silver / silver chloride (SSCE) electrodes and saturated calomel electrodes (SCE) are usually employed in laboratory experiments.

For the measurement of the corrosion potential of the reinforcing steel embedded in concrete, the half-cell potential employs a reference electrode that is sufficiently stable and capable of producing repeatable potential. The potential for corrosion of steel embedded in concrete or cement mortar is shown by a range of voltage values measured against the reference electrode. The main problem with this test is that corrosion potential does not clearly indicate the rate and nature of corrosion, even though half-cell data can be useful in determining the likelihood of corrosion for general uniform corrosion [49 - 50] . When conducting measurements on site, Ellie Sassine et al [51], significantly improved the interpretation of Half-cell potential data in terms of absolute / gradient values.

As previously indicated, the Half-cell potential test can only provide a qualitative evaluation of whether the steel rebar is corroded or not, not the rate of corrosion. When conducting a more thorough corrosion examination in the field, this electrochemical approach is often employed as a first and preliminary inspection. The half-cell potential approach just needs an electrical connection to the steel reinforcement.

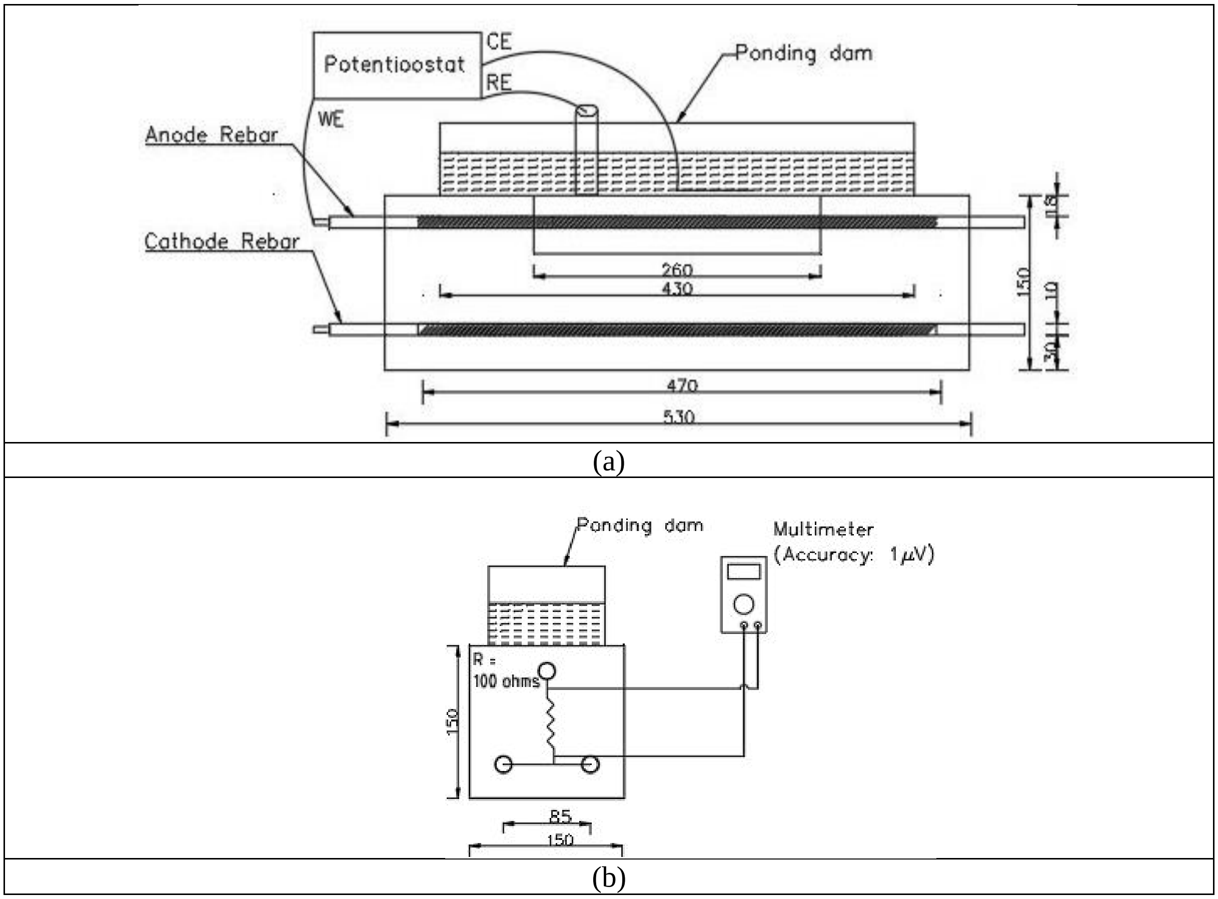

(a)

(b)

Figure 2.3 (a) Longitudinal Section view of beam specimen used for electrochemical measurement: LPR and HCP. (b) Cross section view of beam specimen showing Macrocell current measurement [47] .

Half-Cell Potential Reading (mV) [43] Copper-Copper Sulfate-Electrode (CSE)	Corrosion Activity	Corrosion Current Density (icorr) (µA/cm^2) [45]	Mean Corrosion Penetration Rate (CR) (µm/year)	Corrosion Classification	Total Charge Passed (C) [47]	Macrocell Corrosion Status
>-200	Greater than 90% probability of no corrosion	≤ 0.1	≤1.2	Very low or passive	≤150	Passive
-200 to -350	An increasing probability of corrosion	0.1 – 0.5	1.2 - 6	Low to moderate	>150	Active
<-350	Greater than 90% probability of corrosion	0.5 – 1	6 – 12	Moderate to high	-	-
		>1	>12	High	-	-

Table 2.1 Interpretation of corrosion activity of electrochemical methods

2.4.2 Macrocell current

Macrocell corrosion, also known as galvanic or localized corrosion, results in the formation of anodic and cathodic areas, appearing as corrosion macrocells. In this phenomenon, an exchange of electrons through a metallic connection between passive and active corrosion system occurs due to local differences in the steel electrochemical states. An illustration of macrocell corrosion formation can be observed in Figure 2.4. High concentration of chlorides, or partial carbonation of concrete may cause localized differences in the steel reinforcing network leading to a local depassivation of the steel.

In cold climates where de-icing is required, RC bridge decks and parking structures are particularly susceptible to macrocell corrosion when exposed to chloride ions (through salt application) and high moisture contents. In such cases, corrosion resistivity of the RC decreases, increasing the likelihood of macrocell corrosion [47].

Concrete electrical resistivity represents an important parameter in the formation of macrocell. Electrical conductivity influences the ionic microcell current intensity, leading to local dissolution of steel. The macrocell current method measures the current passing through a net of connected rebars. An illustration of macrocell current measurement can be observed in previously shown Figure 2.3 (b). According to observations made by V. Sarawasthy et al. [21], macrocell current results measured for different corrosion repair mortars can be greater than 100%, depending on the chemical constituents and compatibility of the repair materials. Additionally, Choorackal A. et al [55] found through their research that the severity of macrocell corrosion depends on the driving potential existing between the repair and substrate concrete.

Researcher Bernard Elshner et al. [56 - 57] also studied the factors influencing macrocell corrosion of steel in concrete. Through experimental studies, they observed that chloride induced corrosion is associated with micro and macrocell corrosion. Microcell corrosion occurs when anodes and cathodes are immediately adjacent and there is no macrocell current on the reinforcement.

Research work performed by Quian Shiyuan et al. [58] observed through theorical and experimental results on macrocell corrosion that, although the potential incompatibility between repair-substrate interface serves as a driving force for the corrosion, the degree of corrosion highly depends on the individual corrosion kinetics of the anode or cathode.

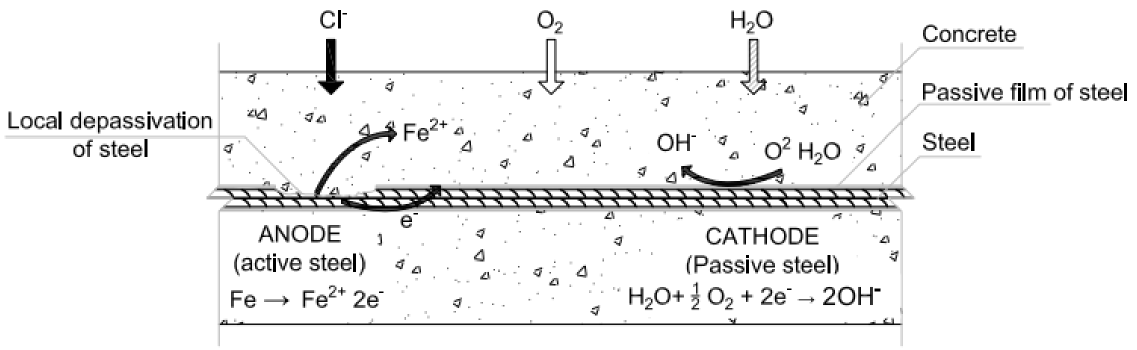

Figure 2.4 Localized (Macrocell) depassivation of steel due to chloride induced corrosion in RC [59]

2.4.3 Linear Polarization Resistance (LPR)

LPR is a non-destructive technique for corrosion measurement [60]. Linear Polarization is defined as the relationship between the potential applied to an RC structure and the current values obtained. The shift under the slope of a linear plot between the potential applied and the current indicates the Linear polarization resistance or Rp [61]. Resistance Polarization refers to the resistance of steel from oxidation, and is measured by applying an external voltage [62]. Polarization can be described as a kinetic deviation from equilibrium due to an electric current passing through a galvanic cell. Polarization may occur at the cathode (cathodic polarization) or at the anode (anodic polarization) [63]. LPR can also be converted to Icorr or corrosion current using the Stern-Geary equation [64 – 66], given in Eq. (7). The corrosion current density $i$corr is defined as the amount of electric current flowing through a unit cross sectional area and is expressed as the corrosion current per unit area of polarization as shown in Eq. (8). A constant value of B equal to 52 mV and 26 mV for steel in the passive and active modes, respectively is suggested according to Stern-Geary equations. The corrosion rate (CR) [67], is defined as the loss of the corroding metal in micrometers per year (µm/year) and it can be calculated following Faraday's law in terms of penetration rate or mass loss rate (MR) following Eq. (10).

$$Rp = \left(\frac{\partial \Delta \mathrm{E}}{\partial i}\right)\ i = 0, \frac{dE}{dt} \rightarrow 0 \qquad (6)$$

Where ΔE = E – Ecorr, E = applied potential, Ecorr = corrosion potential

$$I\mathrm{corr} = \frac{\mathrm{B}}{Rp} \qquad (7)$$

Where $I\mathrm{corr} =$ Corrosion Current (in A) and Rp is polarozation resistance (Ohm). ASTM G-59.

$$icorr = \frac{Icorr}{As} \qquad (8)$$

Where $i$corr = Corrosion current density (in A/cm^2) and A$_{s,}$ is the area of exposed steel in cm^2 .

$$B = \frac{\beta a\ \beta c}{2.303\ (\beta a\ \beta c)}) \qquad (9)$$

Where B = Stern-Geary constant (V), βa = anodic Tafel constant and βc = cathodic Tafel constant.

Corrosion rate (assuming uniform corrosion)

$$CR = \frac{Kaw}{nF\delta}\ icorr = \alpha icorr \ \ (\mu\mathrm{m/year}) \qquad (10)$$

Where K = 315.360, is a unit conversion factor, aw = is the atomic weight in grams, $n =$ is the number of moles of electrons transferred, $F =$ Faraday constant ($F =$ 96,485 C/ mol), $\delta =$ is the density of the metal in g/cm^3 , $icorr =$ corrosion current density in µa/cm^2)

A relationship between current and metal loss can be established for calculating the corrosion rate of a metal. A current of 1mA and a steel density of (7652kg/m^3) will result in a metal loss of 9.2g a year. This volume of metal can also be converted into a loss of section or diameter of steel once an area over where the loss of steel is calculated. For example, if a 16 mm diameter rebar is corroding with a 100 mA/m^2 for 20 years, then, the cross section would have reduced to 11.6 mm [68]. The area of steel considered is the surface area of the reinforcing bar in the measurement region being evaluated [69]. For a carbon steel bar a constant α will be approximately α_{Fe} 11.6 $\mu A/cm^2$ μm/year which is equivalent to a metal loss for a current density of 1$\mu A/cm^2$ considered for this experimental research [69].

The rate of corrosion of steel embedded in concrete will depend on the specific properties of the material and the environmental conditions to which the material is exposed. Table 2.1 shows information on different ranges of corrosion rate for RC structures.

Several electrochemical methods such as potentiodynamic polarization, (either lineal or cyclic), can be used to determine the resistance polarization. In the present investigation, a three-electrode configuration, including a working electrode (i.e. steel bar), a reference electrode, and a counter electrode was used to measure linear polarisation utilising potentiostat equipment. An illustration of LPR measurement is shown in previously indicated figure 2.3a. A carbon steel embedded bar is exposed and connected to a potentiostat (WE). A stainless-steel counter electrode (CE) and a reference electrode (RE) are also connected to a Potentiostat.

NDT Linear Polarization Resistance measures the rate of general corrosion rate for metals at or near the corrosion potential. In this method a small perturbation ΔE(t), is defined with respect to the corrosion potential or OCP to maintain linearity, the perturbation ($\Delta E = E - Ecorr$) is applied to a metal sample, once the value of ΔE is obtained, the resultant current is recorded, and the Rp is obtained. Figure 2.3 (a) shows a schematic view of LPR, HCP, and Macrocell NDTs.

The slope of the polarization curve is calculated in order to obtain the Rp of the system (i.e., potential-current curve), as given in Eq. (6). The calculated value of *R*p obtained from the above equation, is the sum of the true polarization resistance of steel and concrete resistance, which must be considered. Several authors, including Saraswathy Velu et al., [70 – 72] , state that LPR is a quick and non-intrusive corrosion monitoring technique that only needs to be connected to the reinforcing steel. The data offers more thorough information than a straightforward potential survey and offers a valuable insight into the steel reinforcement's instantaneous corrosion rate. LPR as an NDT offers a reliable, albeit time-consuming, assessment of corrosion measurement.

2.5 Microstructure and chemical analysis of cementitious repair materials

The implementation of Scanning Electron Microscope (SEM) with Energy Dispersive X-Ray (EDX) microanalysis of clinker and cementitious materials will provide information about the microstructure, morphology and the chemical constituents of concrete samples. Some of the advantages of this technology include the ability to show high-contrast images of the microstructure, and simultaneous chemical analysis [73]. SEM and EDX can provide data on the morphology and chloride content of samples from the field or from experimentation in the lab.

2.5.1 Scanning Electron Microscope images (SEM)

The SEM methodology employs a scan using a high-energy electron beam across a specimen surface while measuring signals from the interaction between the beam and the specimen. The information (or signal) from the sample is detected and images of the sample surface is shown on a screen monitor [74]. In addition to SEM, an X-ray detector can be attached to the SEM for conducting elemental analysis.

2.5.2. Energy Dispersive X-ray (EDX)

EDX Spectra is a graphical display that presents information about which chemical elements are present in the sample and in what concentration. X-ray signals from the electron beam-specimen interaction are obtained [75]. Peak positions in an EDX spectra are specific to a particular element, and their relative abundance is shown per the intensity (height) of the spectra peaks. The units shown on the horizontal axis represent the kiloelectronvolts (keV).

Information on the quantitative and qualitative chemical analysis can be obtained through the x-ray signal from the EDX analysis. An accelerating voltage of at least 12 to 20 keV range is necessary for cement products to get adequate beam energy without excessive absorption of lower energy x-rays. For SEM imaging higher beam energies are preferred as they result in greater resolution [73]. In this study, the EDX provided important information on the chemical constituents of the samples.

The figure below provides information about the expected performance of concrete when using materials according to a specific particle size and surface area. In the case of this experimental research, mix repairs containing Silica Fume are expected to result in high performance concrete due to SF’s particle size and large surface area compared to other repair mixes shown in Fig 2.5. This is particularly the case for mix F, containing Silica Fume. During the SEM / EDX examination of the repair hydrated mixes, it was also found that Mix F contained the lowest %at weight of chloride compared to the rest of the repair mixes.

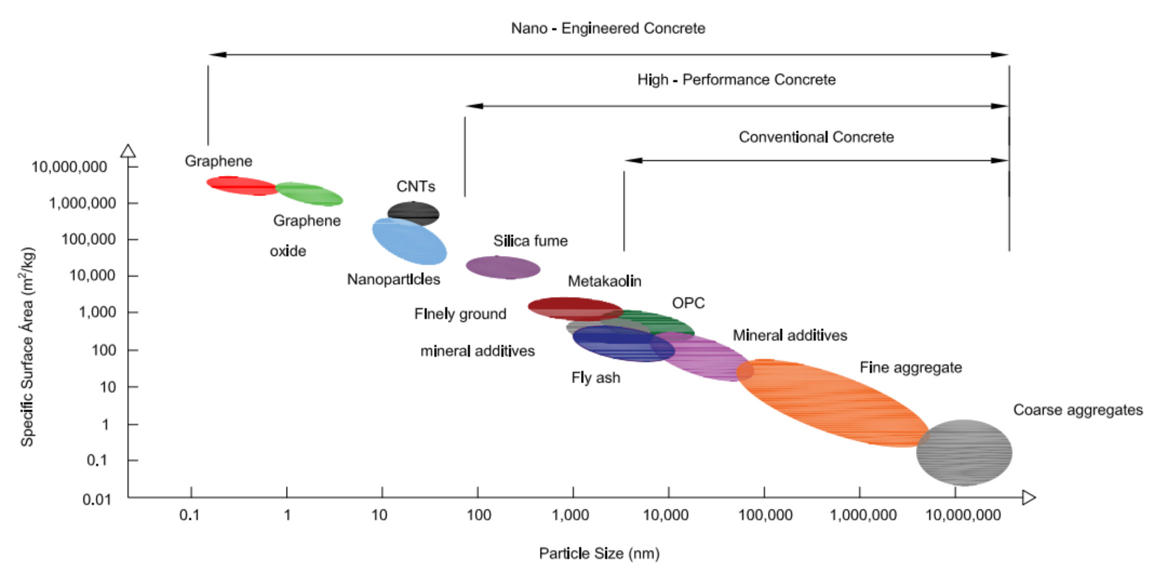

Figure 2.5 Particle-size and specific-surface-area scale related to concrete materials [76]

Chapter 3. Experimental Investigation

3.1 Material and Specimen preparation

Four types of materials were prepared: a normal concrete mix using Ordinary Portland Cement (OPC) and three types of cement-based repair materials. The preparation of the concrete mix material was done with the purpose for it to serve as the substrate or the parent material receiving the cement-based materials. The mix design for the concrete mix is shown in Table 3.1 Quikrete Portland cement GU, [77] also referred to as cement-type 1 with a w/c = 0.40 was utilized for the concrete mix in accordance with ASTM C150 [78]. Tap water was introduced as the mixing water. Fine aggregate was used, meeting the ASTM C33 [79] requirement. The fineness modulus of fine and coarse aggregates are 2.85 and 6.48 respectively [80]. Air entraining agent (AEA) meeting ASTM C260 [81] and a high-range reducing agent (HWRA) meeting ASTM C494 [82] was used to reduce water usage and increase the entrained air content.

The other three commercially available mixes, are termed as Mix M [83], P [84] and F [85]. Table 3.2 shows the corresponding water to material (w / m) ratio as recommended by each manufacturer.

The cementitious repair materials used in this research, mixes M, P and F, can be classified as cementitious mortar, polymer-modified cement mortar, and cementitious concrete repair, respectively. Table 3.3 shows the fresh properties of all the mixes. Air content and slump were assessed following ASTM standards ASTM 231 [86] and ASTM C143 [87]. Table 3.4 shows the properties of carbon steel, which is the steel reinforcement used in this study. All of the mixtures were cast according to ASTM C192 [88].

Sample ID/ Mix Proportions (kg / m^3)	Portland Cement (kg / m^3)	Coarse Aggregates (kg / m^3)	Sand (kg / m^3)	Water (kg / m^3)	HWA (kg / m^3)	AEA (kg / m^3)
Control	180	450	1053	762	2.25	2.25

Table 3.1 Mix design of Control

Sample ID/ Mix Proportions (kg / m^3)	Cement-Repair (kg / m^3)	Water (kg / m^3)
Mix M	1562	118.75
Mix P	1250	137.5
Mix F	1746	291

Table 3.2 Mix design of cementitious - repair material provided by manufacturers

Category	Mix	Slump (mm)	Air content (%)
Substrate	S	70	7
Repair	M	60	5.5
Repair	P	20	5
Repair	F	80	6

Table 3.3 Fresh Properties of concrete and repair mixes

Steel Reinforcement	Diameter (mm)	Modulus of Elasticity (MPa)	Tensile Strength (F_y) (MPa)	Grade of Steel (W)
Carbon Steel	11.3 mm	200,000 MPa	400 MPa	400

Table 3.4. Steel Reinforcement properties

3.2 Curing and additional preparation of RC / Cementitious material repair specimens for corrosion experiments.

Twenty-one RC beams measuring 530 x 150 x 150 mm (length x height x width) were constructed according to ASTM G109 [47], (see Figure 2.3). Seventeen of the twenty-one concrete beams were prepared to undergo the ponding wet / dry cycles. Four specimens were prepared to undergo corrosion at 50% RH and 20°C Temp lab set up (No wet/dry chloride cycles). A minimum of three samples per experimental set up is recommended as per ASTM G-109 to test the effect of different mixes to a chloride environment. The results of this testing aim to reflect what would happen in the real world (site) when using repair mixes, and a substrate material that is compatible to that of the repair and the same environmental conditions.

Specimen preparation of the RC beams is described below:

i) A total of three (3) 11.3 mm longitudinal carbon steel rebars of length 660.4 mm were placed inside a steel form beam mold for each RC specimen.

ii) The rebars were wire power brushed and rinsed with deionized water to remove any contaminants or pre-existing rust. This was performed with the purpose of facilitating the uniform formation of the rebar surface’s passive film.

iii) Each rebar had stainless steel screws installed and welded in place.

iv) An epoxy solution was used for sealing, and vinyl tubing was used for electrical insulation.

v) For the preparation of the concrete corrosion repair, an area of 250 mm x 100 x 50 mm (length, width, height) was reserved along the top surface of the RC beam. This was the active area of experimentation.

vi) Fresh concrete mixture was placed in each mold in three equal layers, each layer was vibrated for 10 seconds to achieve consistency in all the specimens.

vii) The steel molds were covered by plastic sheets for 24 hours.

viii) Ambient conditions were (18 +/- 2° C). Mixes M, P, F were applied to the indentations on the top surfaces of the beams. After 24 hours of curing in ambient conditions at (18 +/- 2° C), the inserted form blocks were removed from the substrate of 6 specimens and three types of repairs. Mix M, P, F were applied to the notches.

ix) The side surface of the repaired section was left unroughened as the current repair codes and standards [89] have no such stipulation.

x) After undergoing the repair, the specimens were moist cured for 28 days and covered with a burlap material in an ambient temperature (18 +/- 2° C).

xi) Four concrete beam specimens were also constructed and were left as no-ponding beams, one for each repair mix (M, P and F) and one for a regular concrete mix.

xii) The bottom and top surfaces were unsealed. The vertical sides were sealed with epoxy.

xiii) 3 mm Plexiglas was used for a salt solution ponding dam with dimensions of 431.7 x 114.4 x 76.2 mm. The dam was epoxied to the top surface of the 8 beam specimens.

xiv) Specimens were placed onto non-electrical-conducting supports of at least 13 mm (0.5 inch) thickness. This ensured adequate air flow during testing.

xv) A plastic loose fitting was placed on top of the ponding to minimize evaporation.

In the schematic view previously shown in Figure 2.3, moisture and chloride ions penetrate downward from the dam. The two bottom rebars (cathodes), which are dryer and have better access to oxygen than the top rebar, go through reduction while the top rebar (anode) experiences oxidation or corrosion.

Wetting-drying cycles were applied on the beam specimens after a thorough curing process. This alternate cyclic wetting and drying is often used, particularly to simulate marine environments, to evaluate the corrosion propagation phase in reinforced concrete structures, and it is also used to simulate the ingress of chloride ions and oxygen through the concrete cover. This wet/dry cycling condition will trigger the initiation of corrosion since for corrosion to take place it will need the presence of oxygen, water, and diffusion of chloride ions. Each wet / dry cycle involved two weeks of ponding salt solution (wetting cycle) and two weeks of drying (drying cycle). A three percent (3 %) by-weight salt solution was prepared and ponded on 17 beam specimens during the wetting cycle. An ACS grade sodium chloride solution chloride (NaCl) with 99% purity was used [90]. At the end of the second week (end of the wetting cycle), the salt solution was vacuumed off and the specimens were allowed to dry naturally (drying cycle) for two weeks.

Corrosion monitoring was periodically measured using a Multimeter and a Potentiostat [91]. A three-electrode arrangement was used to take measurements. The top rebar served as a working electrode (WE), a reference electrode (RE) known as copper-sulfate-electrode (SCE) was used. An AISI type 316 stainless steel shim was used as a counter electrode (CE), and immersed in the ponding dam [92]. A center line was drawn on top of the concrete specimens for proper placement of the RE and to ensure measurements were all constant between RE and WE.

3.3. Specimen Testing

3.3.1 Ponding test wet / dry cycles

A high impedance potentiostat [91] and a multimeter with 1μV resolution [93] were used to perform the tests. The tests were conducted following ASTM G109 [47] . In this work after 16 weeks of wet / dry cycles, NDT methods were used to determine the corrosion potential, corrosion rate and macrocell current of the repaired specimens.

3.4. Electrochemical Non-Destructive Test (NDT) methods

Three different types of electrochemical NDT techniques were used to monitor the corrosion activity on RC-repaired material specimens: Half cell potential, Corrosion rate, and Macrocell current.

3.4.1 Half Cell Potential

HCP data was collected at the end of the wetting cycle in all the specimens using commercially available non-destructive Gamry 600 + potentiostat equipment [91]. An embedded rebar inside the concrete specimens served as a working electrode and the CSE acted as a reference electrode. HCP readings were taken when the charge in potential over a 10-second interval was less than 0.2 mV. ASTM C0876-15 [43] was used to interpret corrosion activity results in terms of corrosion potential. As stated previously, HCP is a useful tool for monitoring the probability of corrosion. See Figure 2.3 (a).

3.4.2 Macro-cell corrosion rate

The macro-cell current was measured once every four weeks at the end of the wetting cycle on all the beams according to the ASTM G109 procedure [47]. A high impedance multimeter with an accuracy of 1 μV was used to measure the voltage across a resistor (R = 100 Ohm).

Exposure to chloride ions and moisture leads to the formation of macrocell corrosion in concrete beams. Under the specimens set up, the top reinforcement acts as an anode while the bottom rebars act as a cathode. A decrease in the concrete resistivity will cause separation between the cathodes and the anodes allowing the ingress of current flow and corrosion due to the potential difference between the anode and cathode [43], [54]. See Figure 2.3(b). According to Ohms law, the macrocell corrosion current is determined by dividing the measured voltage by the resistance value (100 ohms).

Testing of each sample was monitored, and NDT data was collected for 16 weeks.

3.4.3 Linear Polarization

The corrosion rate (CR) was measured in accordance with ASTM G59, at the end of the wetting cycle at different times of exposure using the Linear Polarization Method (LPR) [45]. For all specimens, a high impedance voltmeter built in a commercially available non-destructive Gamry 600+ potentiostat was used [91]. See Figure 2.3 (a). LPR is a reliable, non-destructive technique for measuring corrosion [60]. In this study, the resistance of the steel to be polarized is calculated by applying a fixed potential ΔE, for a fixed duration of 270 sec and the resulting ΔI is recorded.

The resultant Resistance polarization (Rp expressed in Ohms) is determined from the slope of a linear curve of an applied potential (E) vs. current density as per equation (6). The corrosion current density was calculated from the Stern-Geary equation formula using Rp values [94] and ASTM G59 [45]. Corrosion current (I*corr*) was calculated according to equation (7). The corrosion current density ($i$corr) was obtained as per equation (8).

As per RILEM recommendations [95], in this study B was assumed equal to 26 mV which indicates an (Ecorr < -0.3V) for steel in active condition, while for steel in passive conditions a value of B equal to 52 mV (Ecorr > -0.2 V) is normally used.

The corrosion penetration rate (CR), expressed in (µm / year), was calculated according to equation (10). The corrosion rate parameters were calculated according to Faraday's law as follows. K = 315,360; it refers to a unit's conversion factor, F is the Faraday constant (F = 96,485 Cmol $^{-1}$), n refers to the number of moles of electrons transferred, aw is the atomic weight in grams, δ is the density of the metal in g/cm^3, and i*corr* is the corrosion current density in μA / cm^2 [96].

3.5 Scanning Electron Microscope (SEM) and Energy Disperse X-Ray Spectra (EDX)

3.5.1 Equipment and specimen preparation

Four types of repair materials termed Mix M, P, F and Control were prepared for SEM and EDX analysis: a normal concrete mix containing regular (OPC), two types of cement-based repair materials and 1 type of polymer repair-based material.

A total of twenty (20) samples of powder hydrated cement-based and polymer-based repair materials were examined using SEM and EDX technology at the sub-micro scale level to determine the morphology, physical characteristics, and chemical composition as they are considered essential in the case of the study of cementitious based repair materials for corrosion repair. The repair mixes hydrated powder samples were extracted by using drill equipment from German Instruments Inc. They were then placed into Eppendorf tubes and taken to the Advanced Microscopy Facility.

The Advanced Microscopy Facility (AMF) of the University of Victoria was visited to conduct the micro-scale examination of the characteristics of the repair materials using a scanning electron microscopy linked with an energy-dispersive X-ray analyzer (SEM / EDX) equipment Hitachi S-4800 [97].

The procedure for the SEM observation of cementitious repair samples is as follows:

i) Specimen stubs: aluminium type, nonmagnetic stubs were used to mount the samples.
ii) Conductive tape: double sided carbon conductive tape was used for fixing sample to the specimen stub.
iii) Samples were fixed in place by attaching them to the conductive double-sided tape.
iv) Tweezers were used when sampling so as not to touch the sample surface.
v) Alignment of the SEM microscopy was performed as per S-4800 instruction manual [97].

The SEM microscope works under vacuum conditions, and it uses electrons instead of light to form images. There are three types of signals when using the SEM: SE: Second image, BSE: Back Scattered image and X-Rays. The SEM images captured in this research are Backscattered electron (BSE) [97].

Backscattered-Electron (BSE) Imaging works under the kinetic energy principle, where the interaction of the electrons produces signals and later an image. The SEM (BSE) has been used in many fields, including material science, nanoscience, biomedical, and microbiology, as well as for the chemical analysis and the research of cement / cementitious materials chemical components. Table 3.5 below shows a summary of all the SEM / EDX images obtained at the AMF lab.

Figure #	**Ponding Repair Only**	**Image**	**Image**
3.1 to 3.4.1	Mix M (PRO)	SEM	EDX
	Mix P (PRO)	SEM	EDX
	Mix F (PRO)	SEM	EDX
	Control (PRO)	SEM	EDX
	Ponding Repair+Subst		
3.5 to 3.8.1	Mix M (PR&S)	SEM	EDX
	Mix P (PR&S)	SEM	EDX
	Mix F (PR&S)	SEM	EDX
	Control (PR&S)	SEM	EDX
	No ponding Repair		
3.9 to 3.11.1	Mix M (NP)	SEM	EDX
	Mix P (NP)	SEM	EDX
	Mix F (NP)	SEM	EDX

Table 3.5 Description of SEM and EDX images according to the analysed elements

3.5.2 SEM /EDX IMAGES of Mixes M, P, F and Control (PRO)

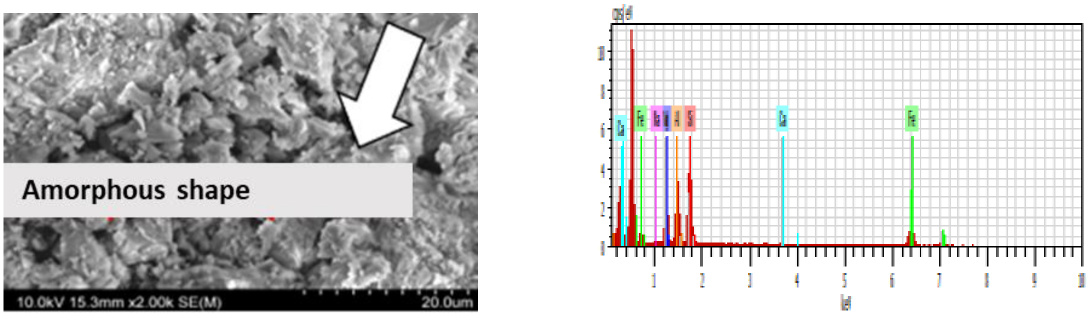

Figure 3.1 SEM Morphology of hydrated Mix M Figure 3.1.1 EDX Chemical constituents of Mix M

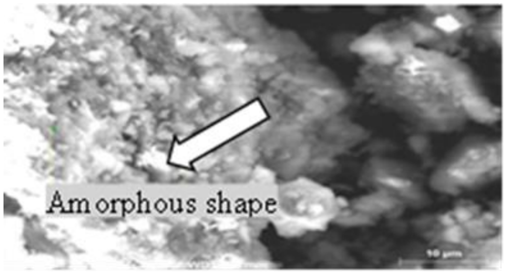

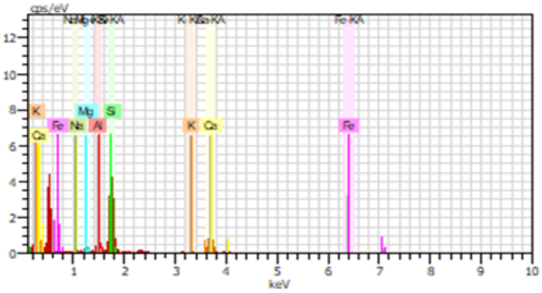

Figure 3.2 SEM Morphology of hydrated Mix P Figure 3.2.1 EDX Chemical constituents of Mix P

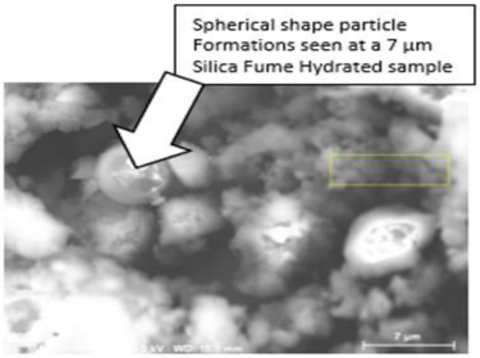

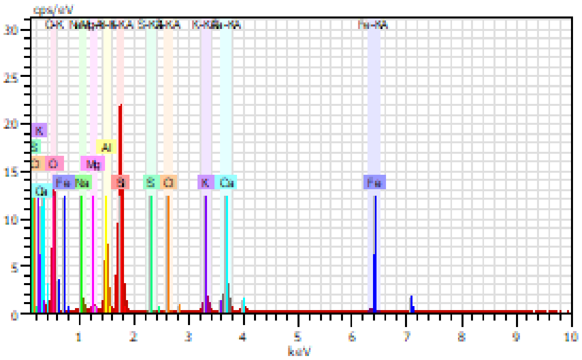

Figure 3.3. SEM Morphology of hydrated Mix F Figure 3.3.1. EDX Chemical constituents of Mix F

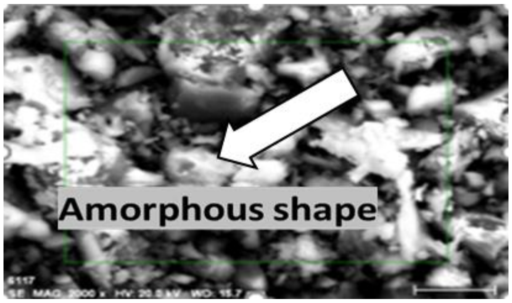

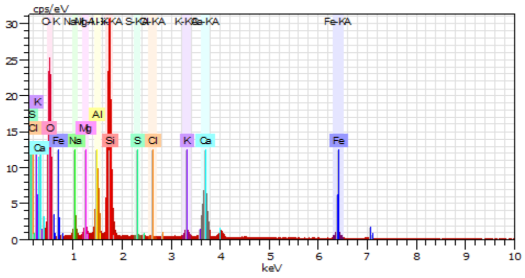

Figure 3.4. SEM Morphology of hydrated Control mix Figure 3.4.1. EDX Chemical constituents of Control

Figures 3.1 to 3.4 and 3.1.1 to 3.4.1 show the morphology and the chemical constituents respectively of 3 different cementitious materials and control mix hydrated for (PRO) samples.

3.5.3 SEM / EDX IMAGES of Mixes M, P, F and Control (PR&S)

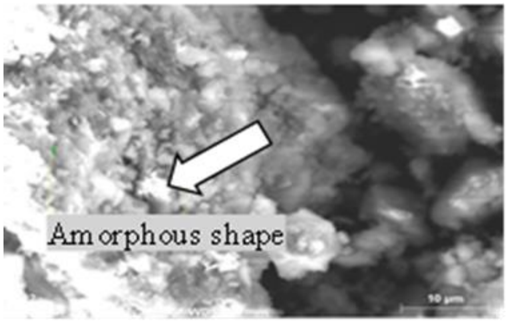

Figure 3.5 SEM Morphology of hydrated Mix M

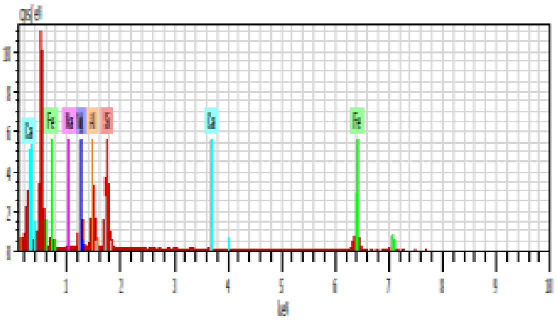

Figure 3.5.1 EDX Chemical constituents of Mix M

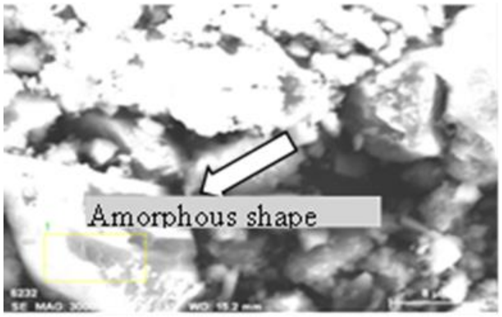

Figure 3.6 SEM Morphology of hydrated Mix P

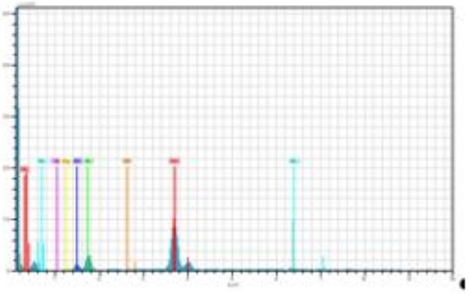

Figure 3.6.1 EDX Chemical constituents of Mix P

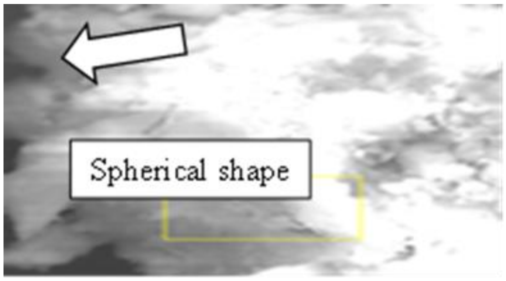

Figure 3.7 SEM Morphology of hydrated Mix F

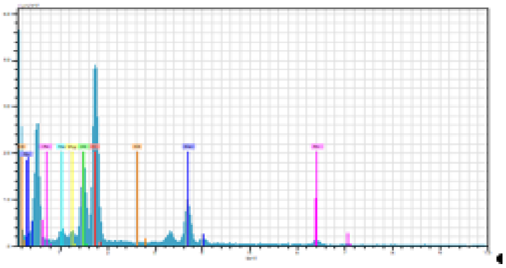

Figure 3.7.1 EDX Chemical constituents of Mix F

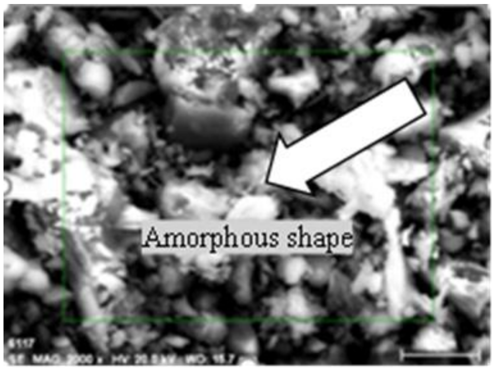

Figure 3.8 SEM Morphology of hydrated Control mix

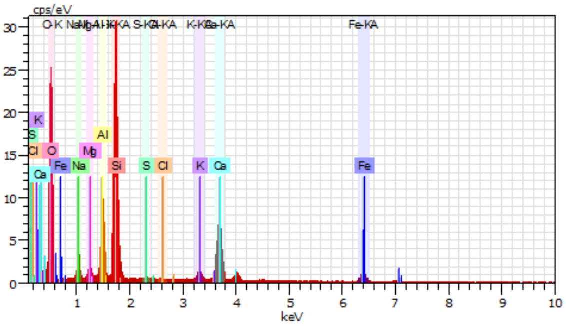

Figure 3.8.1 EDX Chemical constituents of Control mix

Figures 3.5 to 3.8 and 3.5.1 to 3.8.1 show the morphology and the chemical constituents respectively of 3 different cementitious materials and control mix hydrated for (PR&S) samples.

3.5.4 SEM / EDX IMAGES of Mixes M, P, F and Control (NP)

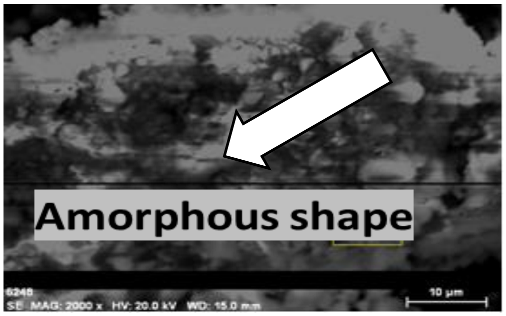

Figure 3.9 SEM Morphology of hydrated Mix M

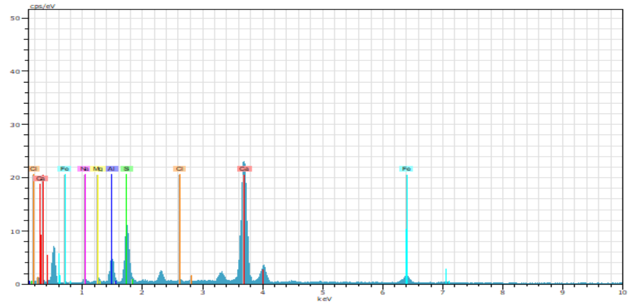

Figure 3.9.1 EDX Chemical constituents of Mix M

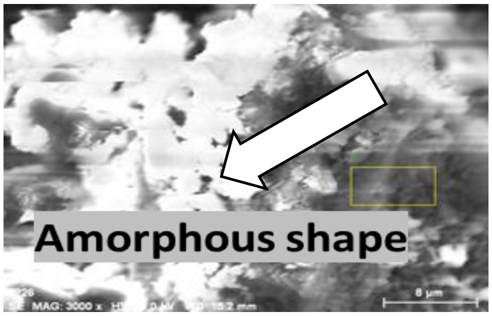

Figure 3.10 SEM Morphology of hydrated Mix P

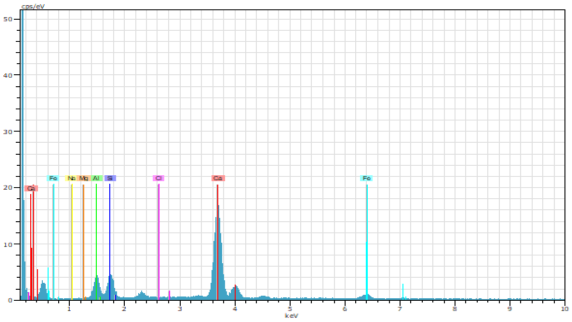

Figure 3.10.1 EDX Chemical constituents of Mix P

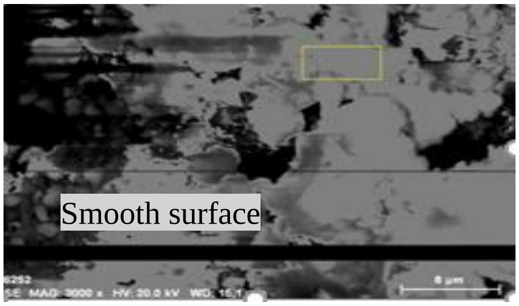

Figure 3.11 SEM Morphology of hydrated Mix F

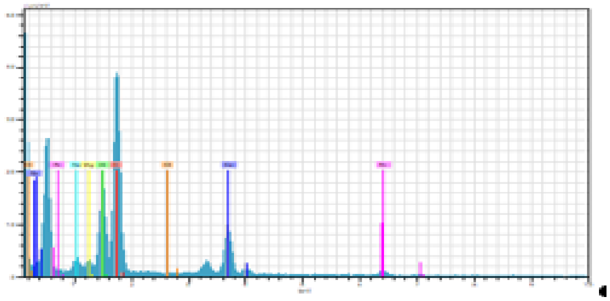

Figure 3.11.1 EDX Chemical constituents of Mix F

Figures 3.9 to 3.11.1 show the morphology and the chemical constituents of 3 different cementitious materials mixes hydrated for (NP) samples.

3.6 Energy Dispersive X- Ray (EDX)

Energy Dispersive X-Ray Analysis is an x-ray technique used to identify the elemental composition of materials. Its applications include materials and product research [98]. The EDX system used at the AMF at the University of Victoria is an attachment to the Electron Microscopy instrument Scanning Electron Microscopy (SEM). A spectrum showing peaks with information corresponding to the different elements that make up the composition of the samples being analysed is the result of the data generated by the EDX imaging capability. This technique can provide quantitative chemical element composition [98].

The procedure for the EDX observation of cementitious repair samples is as follows:

i) EDX set up: during this procedure, the key is to be aware that the resolution limit of EDX is not the same as the resolution of the SEM. This depends on both the specimen and the instrument settings [97].
ii) Determine the necessary accelerated voltage to cause enough excitation in the electron shell of elements contained in the specimens of interest. By setting the accelerating voltage accordingly, characteristic x-rays from the chemical elements likely to be present in the specimen are obtained. It is important to have a good understanding of the electron acceleration voltage value of each chemical element that may be present in the sample that is being analyzed.
iii) Determine the electron energy Eo minimum required. Higher Eo yields higher x-ray counts, which translate into collecting more data quickly.
iv) Adjust the acceleration voltage Energy Eo to get a clear spectrum, so that the elements and peaks present in the sample can be observed.

3.6.1 EDX SPECTRA of Mixes M, P, F and Control (PRO)

In Figures 3.1.1 to 3.4.1 Energy Dispersive X-ray spectra show the effects of exposure to wet / dry sodium chloride cycles of Mixes M, P, F and Control. All PRO Mixes show the presence of several chemical components, mostly Calcium and Silica, however in different %at weight proportion. Table 3.6 below shows a summary of the chemical components present on PRO powder hydrated samples.

3.6.2 EDX SPECTRA Mixes M, P, F and Control (PR&S)

In Figures 3.5.1 to 3.8.1, Energy Dispersive X-ray spectra show the effects of exposure to wet / dry Sodium chloride cycles of Mixes M, P, F and Control. Table 3.6 below shows a summary of the chemical components present on PR&S powder hydrated samples.

3.6.3 EDX SPECTRA Mixes M, P, F (R&S) No ponding

In Figures 3.9.1 to 3.11.1 Energy Dispersive X-ray spectra show the effects of exposure to wet / dry Sodium chloride cycles of Mixes M, P, and F. Table 3.6 below shows a summary of the chemical components present on non-ponded powder hydrated samples.

The purpose of performing the EDX analysis of all three different cementitious materials was to find the chemical composition, especially the Ca / Si ratio present in the three different repair mixes. Table 3.6 shows the chemical composition of three different cementitious repair materials and Control after being analyzed using SEM / EDX technology.

3.7 Chloride Concentration and chemical components

In table 3.6 below, a summary of the chemical components found in the 20 cementitious repair hydrated powder samples is shown. As mentioned previously, a high percentage of Silica and Calcium chemical constituents was mostly present in all the powder samples. Additionally, a small percentage of chloride was observed in all the powder samples, with Mix F showing the lowest amount of chloride by % at weight per sample.

Mix Type	Exposure	Si (*%at)	Ca (*%at)	Al (*%at)	Na (*%at)	Mg (*%at)	Fe (*%at)	Cl (*%at)
M	Ponding Rep	51.84	12.16	26.18	9.22	0.06	0.52	0.023
P		31.98	33.24	22.96	4.25	3.71	3.83	0.020
F		48.87	12.89	3.37	0.28	0.30	1.17	0.003
Control		73.15	12.15	10.67	3.29	0.00	0.96	0.037
Mix Type	Exposure	Si (*%at)	Ca (*%at)	Al (*%at)	Na (*%at)	Mg (*%at)	Fe (*%at)	Cl (*%at)
M	Ponding R&S	31.7	49.56	9.71	3.59	1.73	3.49	0.210
P		18.5	52.66	24.26	0.83	0.57	2.99	0.180
F		47.43	30.62	14.47	1.47	0.91	3.47	0.033
Control		73.15	12.15	10.67	3.29	0.00	0.96	0.037
Mix Type	Exposure	Si (*%at)	Ca (*%at)	Al (*%at)	Na (*%at)	Mg (*%at)	Fe (*%at)	Cl (*%at)
M	No Ponding	50.77	16.11	18.14	5.26	1.27	2.45	0.000
P		88.53	7.56	2.51	0.45	0.24	0.61	0.090
F		56.77	16.11	18.14	5.26	1.27	2.45	0.000

*%at = % atomic weight

Table 3.6 Chemical composition of specimens and characterization of repair materials by EDX analysis

Chapter 4. Results and Discussion

4.1 Visual Observation

After removing the sodium chloride solution from the ponding container at the end of the last wet / dry cycle, specimens were inspected visually. Small cracks were clearly observed on 2 out of 3 of the Mix M repair specimens after completing 16 weeks of exposure to the salt solution. This type of crack could be the result of thermal cracking or drying shrinkage of the material. Signs of rust are clearly noticeable on the substrate concrete of Mix P. Signs of rust are clearly noticeable on 2 out of 2 of the control Mix. No signs of corrosion, cracks or staininig was observed on Mix F. See Figure 4.1.

Corrosion potential, macro cell corrosion, and corrosion current density and rate results on all the specimens confirm that some cementitious materials are more vulnerable than others when exposed to a chloride attack or corrosive environment.

(a) (b) (c) (d)

Figure 4.1 Visual observation of repair mixes and control. a) Mix M, (cracks can be observed); b) Mix P, (corrosion stains on surface; c) Mix F, (no cracks or corrosion stains can be observed); d) Mix Control, (corrosion stains on surface).

4.2 Electrochemical Techniques

As mentioned above, three different types of NDTs, Half Cell Potential (HCP), Linear Polarization Resistance (LPR), and Macrocell Current were performed for all the 21 RC specimens. After curing, the specimens were exposed to wet and dry cycles of sodium chloride for 120 days. The wet and dry cycles were performed to simulate RC structures exposed to a marine environment. This test was done to the ASTM G-109 standard to simulate a marine environment.

4.2.1 Half-Cell Potential (HCP)

Half Cell Potential results or the probability of corrosion for RC specimens prepared with Mixes M, P, F and Control were obtained following ASTM C876. Wet and dry sodium chloride cycles that simulated the exposure of specimens to a marine environment were performed on three different types of specimen set ups, and the monitoring of HCP measurement was done once every 4 weeks for the duration of the test (120 days).

Repair material exposed to chloride only

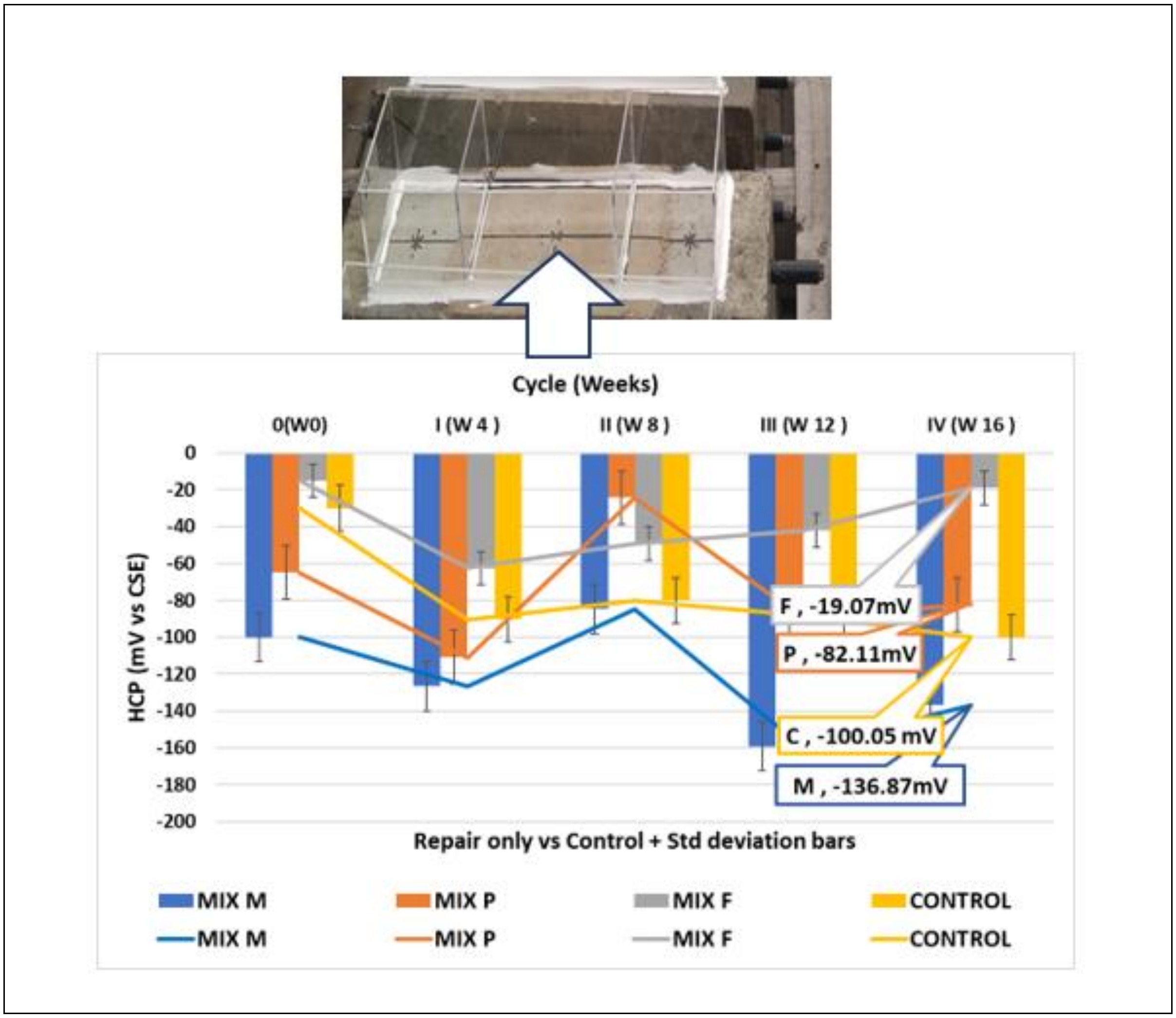

Figure 4.2 HCP Cementitious repair material vs. Control and Std. deviation (PRO)

As shown in Figure 4.2, each plotted point represents one HCP measurement at every cycle for every one of the repair mixes and control exposed to sodium chloride ponding. As can be observed in Figure 4.2, HCP recorded values taken before ponding of the specimens, Mix F data showed the lowest value: (-15 mV) compared to all repair mixes and Control. Then, at the end of the testing period (120 days) Mix F, again, shows the lowest HCP values at -19 mV. Figure 4.2 also indicates the standard deviation bar with information regarding the HCP average data for the samples representing Mixes M, P, F and Control respectively during the sodium chloride wet / dry testing period.

Repair material plus substrate interface exposed to chloride

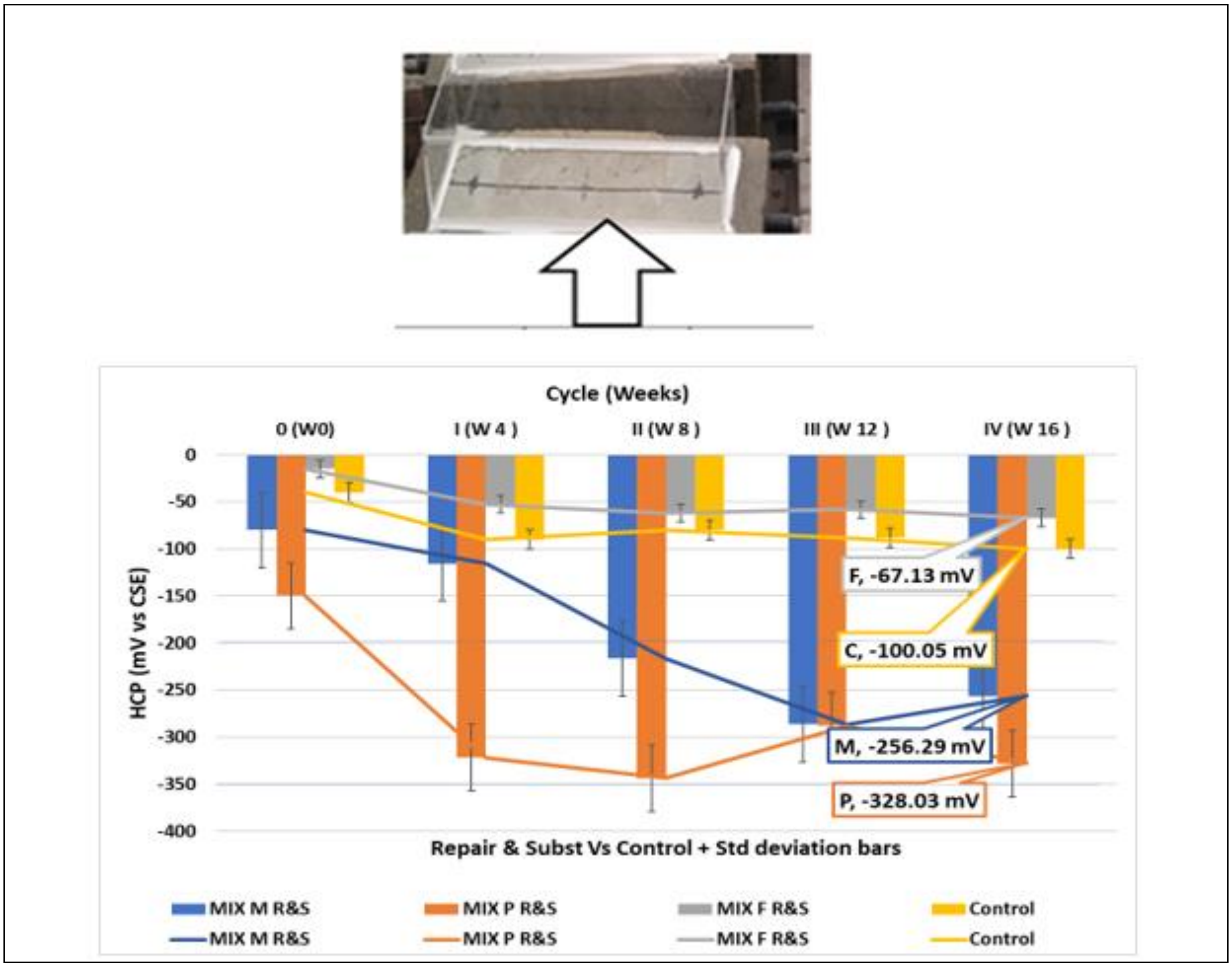

Figure 4.3. HCP Cementitious repair material vs. Control and Std. deviation (PR&S)

As shown in Figure 4.3, each plotted point represents one HCP measurement at every cycle for all of the repair mixes and Control exposed to sodium chloride ponding of repair material & substrate interface. It can be observed that for HCP recorded values taken before ponding of the specimens for Mix F, the data showed the lowest value of all repair mixes and Control. Then, throughout the testing period, Mix F, again, shows the lowest HCP values at the end of the testing period at -67 mV.

The HCP data analysis revealed that corrosion potential in Mixes M and P is between 2 to 3 times higher in the specimens where the sodium chloride ponding setup is expanded to the repair substrate interface as compared to the specimens where only the repair material was exposed to NaCl. This can be explained by the effect of the compatibility of the repair materials to the substrate transition zone between the repair materials as opposed to the substrates that are less electrochemically compatible. This finding agrees with other researchers who have performed related experiments, [32], [21], [99] , including Cusson et al. [100]. Figure 4.3 also indicates the standard deviation bar with information regarding the HCP data for the samples representing Mixes M, P, F and Control respectively during the sodium chloride wet / dry testing period.

The difference in corrosion potential values among Mix M, P, F and Control can be explained by the denser microstructure of Mix F compared to Mixes M, P, and Control. This finding agrees with researchers K. U. Avani et al. [41], who found the use of cementitious materials containing silica fume beneficial for corrosion repair. Their studies show how SF material properties affect chloride transfer into concrete and highlight the importance of a material’s porous structure. The corrosion resistance of concrete repair mortars were also evaluated by Velu Saraswathy et al [21]. Their results showed that modified mortar systems treated with fly ash and micro silica have lesser permeable voids because of the smaller size of the micro silica particles compared to normal cement particles. Less permeable gaps and less water absorption occurred in the cement matrix's denser packing.

D.D. L. Chung et al [36] also investigated the corrosion resistance of cement-based materials containing silica fume content and found that SF improves a broad range of essential features, including steel corrosion resistance, the freeze-thaw durability, abrasion resistance, bond strength with embedded steel rebars, and the resistance to chemical attack, as compared to polymer-modified mortars. Safwan et al. [37] also investigated the resistance of SF concrete to corrosion related damage and found that it outperformed that of regular control concrete.

Repair material plus substrate interface not exposed to chloride

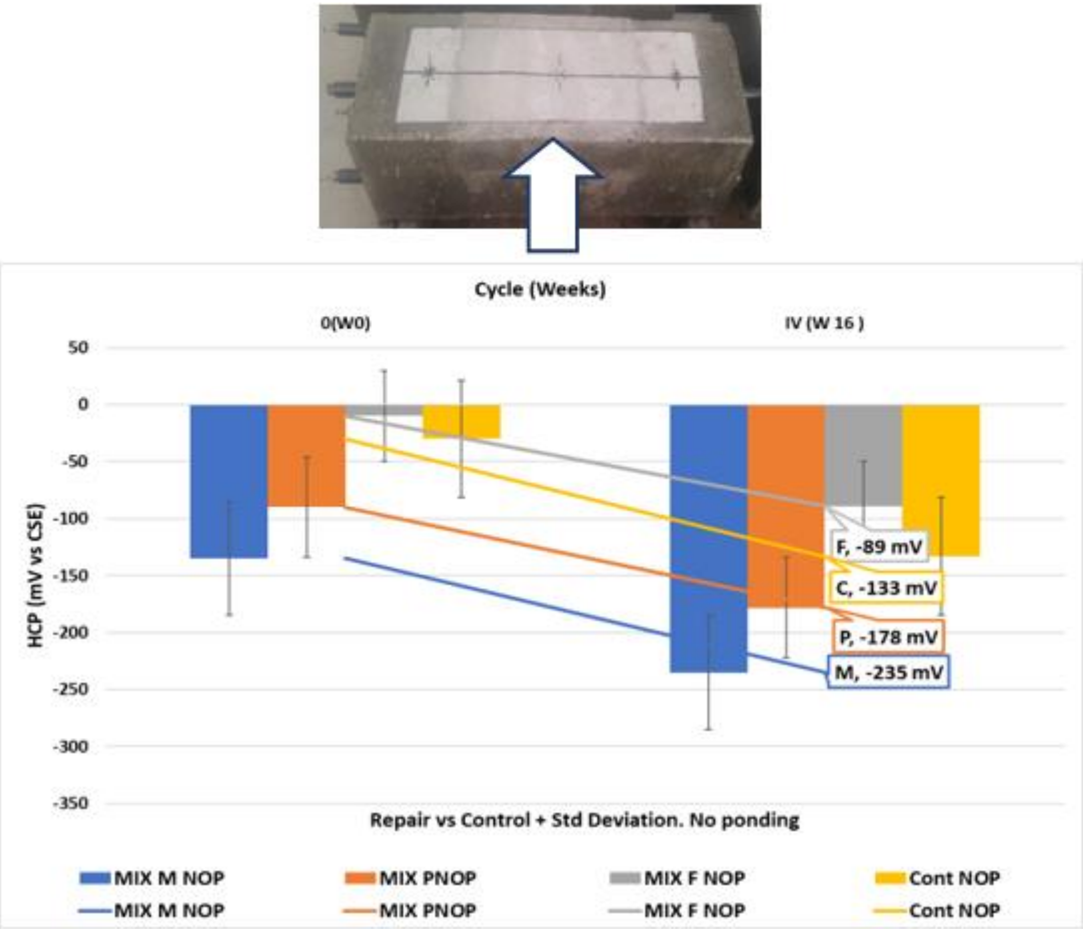

Figure 4.4 HCP Cementitious repair material vs. Control and Std deviation (NP)

As shown in Figure 4.4, each plotted point represents HCP measurement during the testing period (120 days) for each of the repair mixes and control exposed in the lab at 50% RH and 20°C Temperature. As can be observed in Figure 4.4, HCP recorded values taken of the RC material repair specimens, Mix F data showed the lowest value raising from -15 mV to -89 mV of all HCP recorded values for repair mixes and control at the end of testing period. This range of values are in agreement with the values reported by B. Elsener et al. [101]. Figure 4.4 also indicates the standard deviation bar with information regarding the HCP data for the samples representing Mixes M, P, F and Control. Additionally, the difference in corrosion potential values among the three different mixes can be explained by the potentially denser microstructure of Mix F compared to Mix M and P as mentioned above.

4.2.2 Macrocell Corrosion Results

The Macrocell current of RC specimens repaired with three different types of Mixes M, P, F and Control exposed to wet / dry ponding cycles of sodium chloride was assessed by measuring the total charge passing through a 100-ohm resistor every month for the duration of the test following ASTM G-109.

Repair material exposed to chloride only

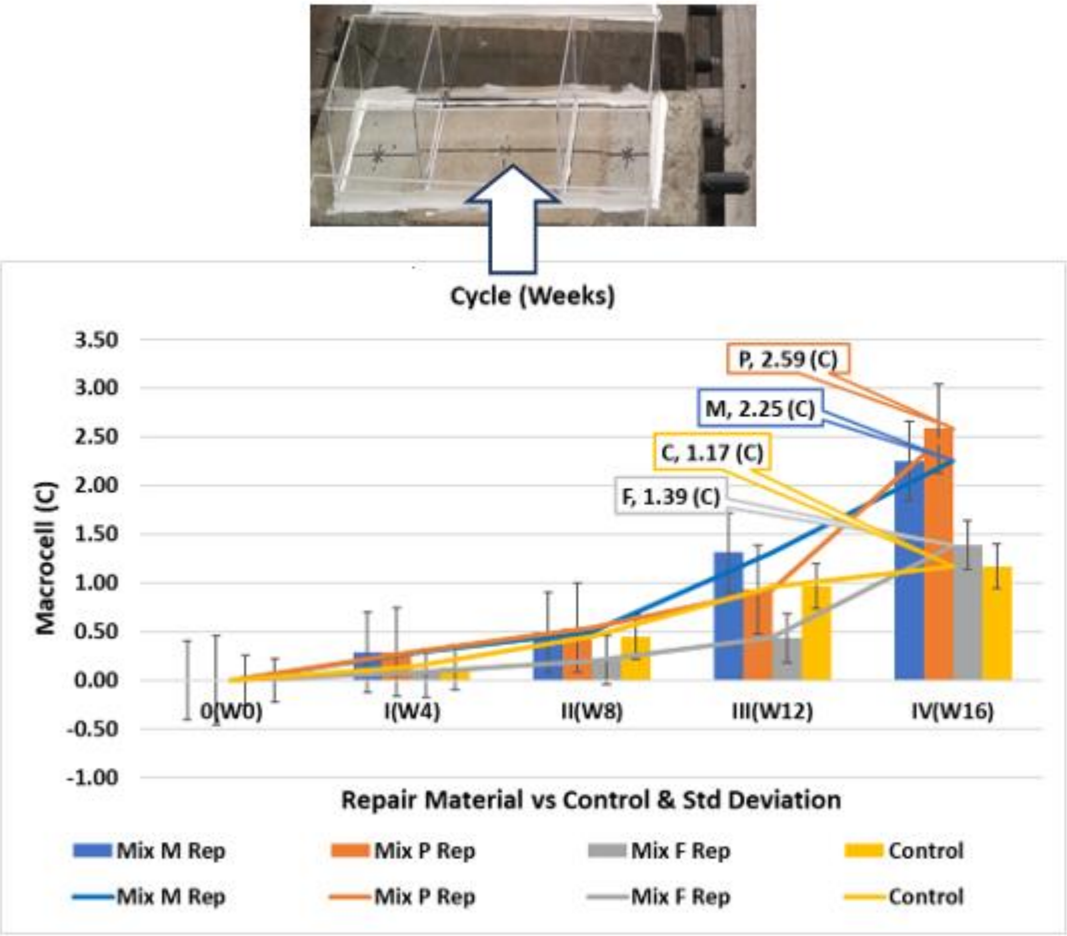

Figure 4.5 MC Cementitious repair material vs. Control. and Std. deviation (PRO)

In Figure 4.5, each plotted point represents the total integrated current of the RC repair specimens and Control exposed to sodium chloride ponding. The current was recorded at every cycle for each of the RC repair mixes and control specimens. As it can be observed in Figure 4.5, the Macrocell current values taken before ponding of the specimens all show zero (0) current passing through for all the mixes and Control. Fluctuation of current values can also be observed throughout the repair mixes and Control during the testing period. At the end of the testing period however, the cumulative current for Mix F shows the lowest value at 0.47 Coulombs, compared to the Macrocell current values for repair mixes M, P and Control. Figure 4.5 also indicates the standard deviation bar with information regarding the Macrocell current data for the samples representing Mixes M, P, F and Control respectively.

Repair material plus substrate exposed to chloride

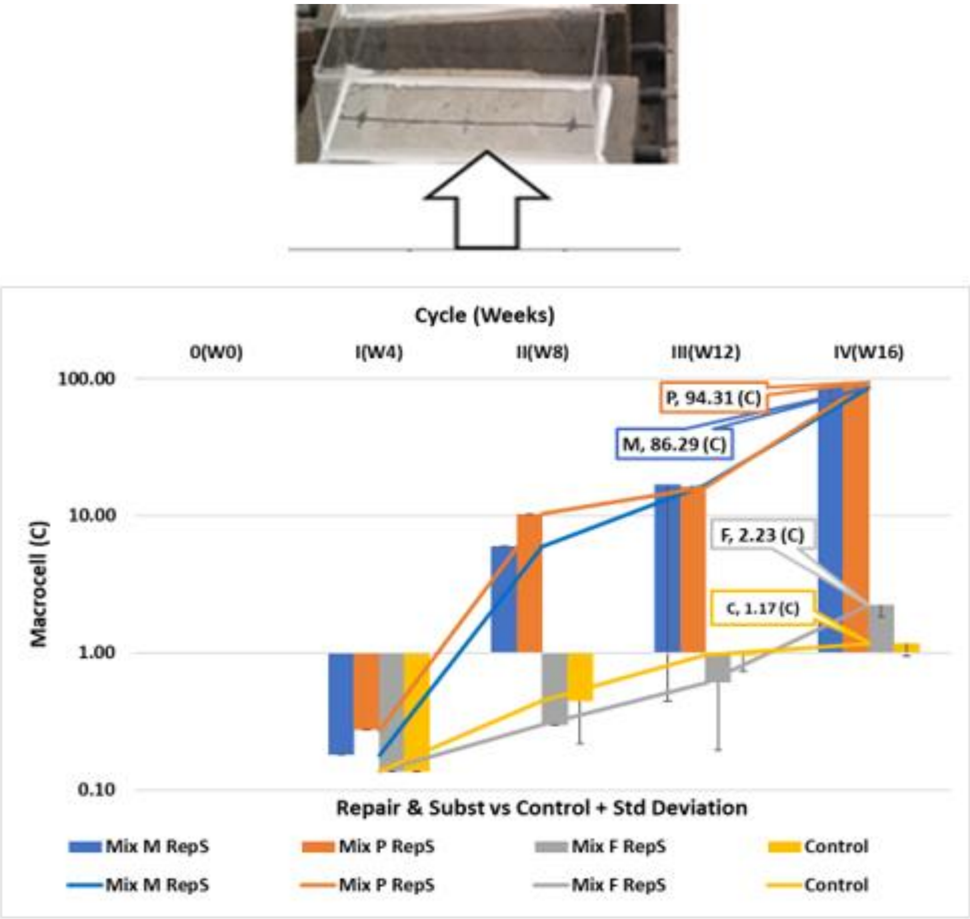

Figure 4.6 MC Cementitious repair material vs. Control. Std deviation (PR&S)

In Figure 4.6, each plotted point represents the total integrated current of the RC repair specimens and control exposed to sodium chloride ponding of the repair cementitious material and substrate interface. As it can be observed in Figure 4.6, the Macrocell current values taken before ponding of the specimens all show zero (0) current passing through for all the mixes and Control. At the end of the testing period, the cumulative currents for Mixes Control and F show the lowest values at (2.27) and (1.17 C) respectively, compared to the corrosion current recorded values for repair mixes M and P: (86.29 C) and (94.31 C) respectively. Figure 4.6 also indicates the standard deviation bar with information regarding the Macrocell current data for the samples representing Mixes M, P, F and Control during the wet / dry testing period.

The macrocell current data analysis for RC repair specimens & substrate interface revealed that the total accumulated current passing through the macrocell is around 35 times higher for Mixes M, and P, and only 1.6 times higher for Mix F in the specimens where the sodium chloride ponding setup expanded to the transition zone area. The wide difference found in the macrocell current results between different ponding set up for mixes M, P and F can be attributed to the compatibility between repair material and substrate of the repair.

Mailvaganam, N. P. and Taylor, D. A. [39] reported on the compatibility of repair systems for concrete structures. Their experimental investigation revealed that it is necessary to think of the repair and substrate as components of a composite system, which consists of different materials, in order to understand how different factors affect the performance of repair systems. Even though materials vary, the objective must be to improve physical and chemical property compatibility. The Daniel Cusson et al. [40] research studies reported the importance of comprehensive data on the performance of repair products. A significant portion of early repair failures in North American concrete buildings have been linked to incompatibility between repair materials and substrate concrete. Also, the use of concrete cementitious materials with low permeability is a crucial factor in the long-term durability of RC structures repair. Chloride ion penetration or diffusion is better resisted by low permeability concrete. This prevents oxygen, water, and chlorides from getting to the steel reinforcing bars.

K. U. Aavani et al. [41] found the use of silica fume beneficial for corrosion repair. Their studies show how SF’s material properties affect chloride transfer into concrete and highlight the importance of a material’s porous structure. Cusson et al. [100] observed that after 3 years of assessing patch repairs that contained corrosion inhibitors, the potential difference between the patch and the substrate increased over time. Also, Pruckner, F., and Gjørv, O.E [102] reported that the electrochemical potential imbalance can be as high as 500 mV because of differences in physical properties such as porosity and chemical composition.

Repair material plus substrate interface not ponded

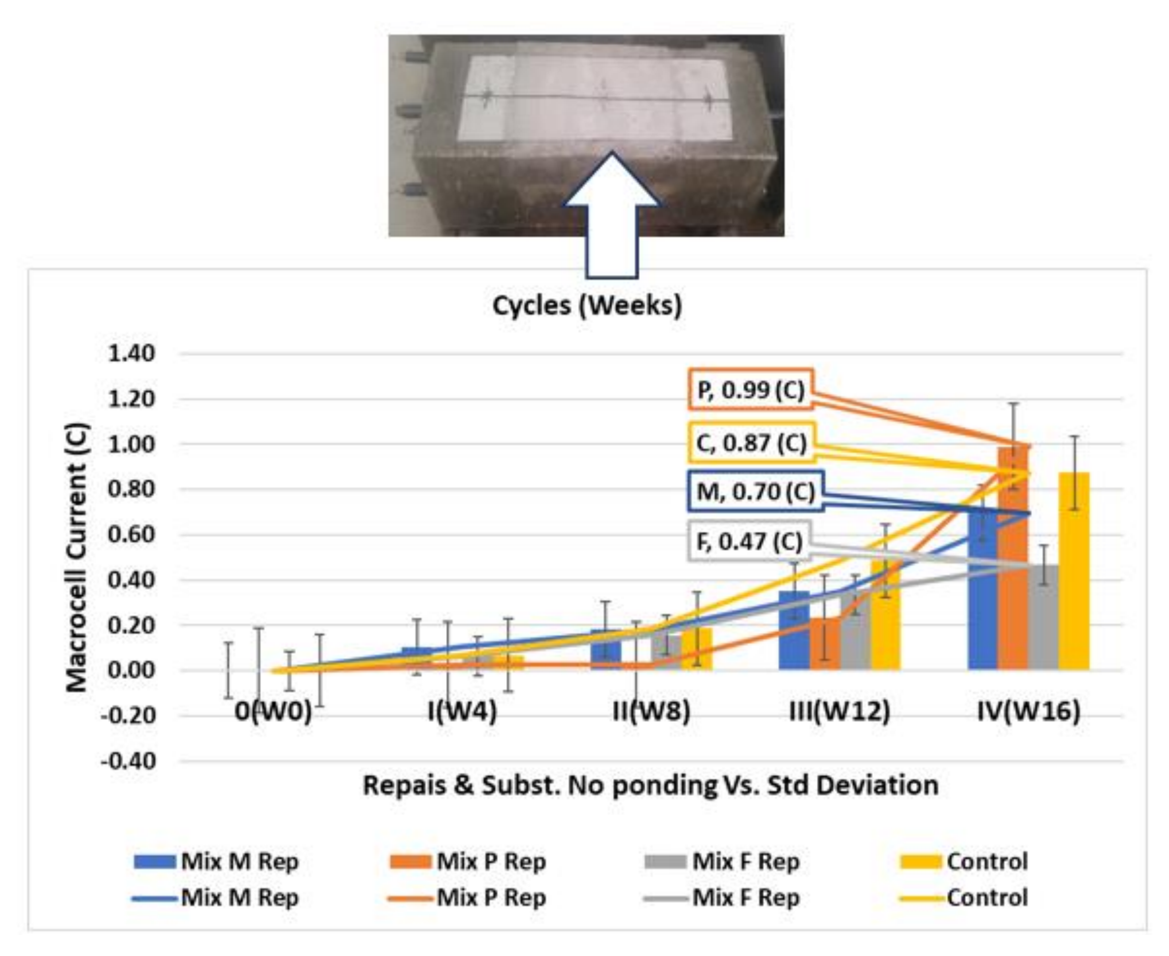

Figure 4.7 MC Cementitious repair material vs. Control. Std. deviation (NP)

In Figure 4.7, each plotted point represents the total integrated current of the RC repair specimens and Control exposed to 50% RH and 20°C Temperature at the lab environment. The macrocell current values taken before ponding of the specimens all show zero (0) current passing through for all the mixes and Control. Fluctuation of current values can also be observed throughout the repair mixes and Control during the testing period. At the end of the testing period however, the cumulative current for Mixes F and M show the lowest corrosion current value: (0.47 C) and (0.70 C) respectively, compared to the corrosion current values for mixes P and Control: (0.99 C) (0.87 C) respectively. Figure 4.7 also indicates the standard deviation bar with information regarding the Macrocell current data for the samples representing Mixes M, P, F and Control during the known RH and Temperature exposure period.

The Macrocell current data analysis for RC repair exposed in the lab environment revealed that mix P and Control present the highest value of current charge passing with time. This finding indicates that RC repair Mix F is the more resistant to current passing compared to repairs M, P and Control. This can be explained by the effect of the larger surface area, dense packing cement matrix and less permeability that the Silica Fume provides to repair material Mix F. This observation agrees with the findings from V. G. Papadakis [103].

4.2.3 Linear Polarization Resistance

Corrosion Current Density and Rate Results

Repair material only exposed to chloride and Corrosion Density

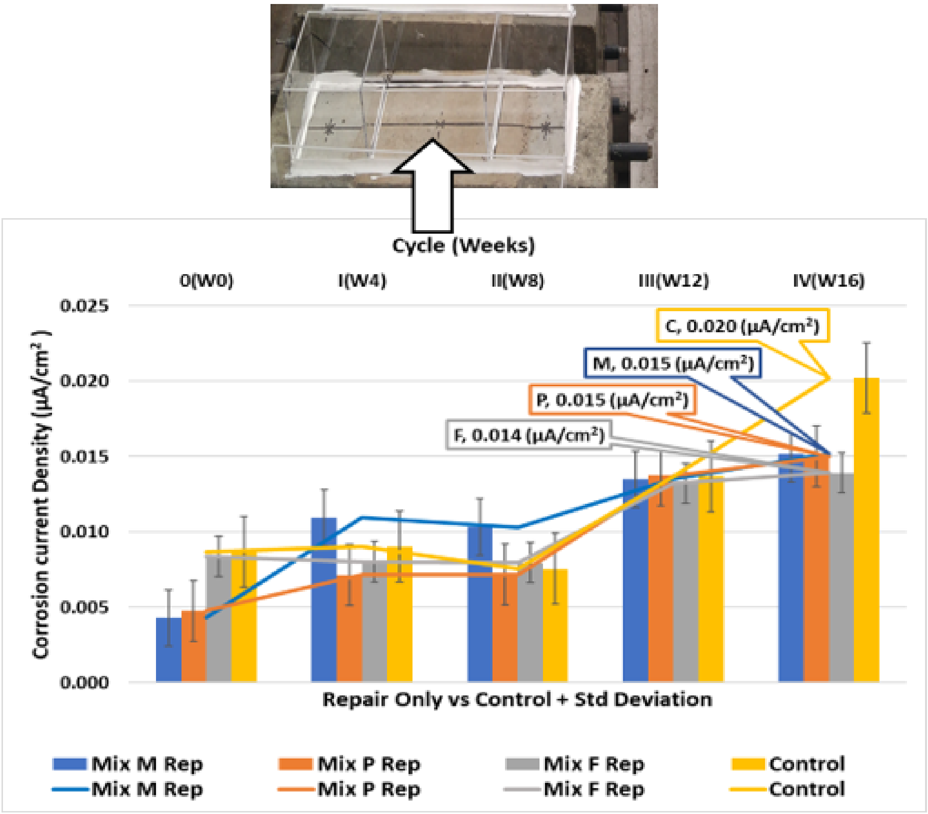

Figure 4.8 CCD Cementitious repair material vs. Control. Std. deviation (PRO)

In Figure 4.8, each plotted point represents the corrosion current density data from the LPR method for the RC repair mixes and Control. The corrosion current density values at the end of the testing period (120 days) show very similar values for Mixes P and F. Control sample is showing the highest corrosion current density value recorded (0.020 µA/ cm^2). Fluctuation of current values can also be observed throughout the repair mixes and Control during the testing period. At the end of the testing period however, the corrosion current for Mix F shows the lowest corrosion current values: (0.014 µA/ cm^2) compared to the corrosion current recorded values for repair mixes M, and Control. Figure 4.8 also indicates the standard deviation bar with information regarding the corrosion current density data for the samples representing Mixes M, P, F and Control respectively.

While the corrosion current density and rate result of each of the repair material specimens indicates that Mix F presents the lowest corrosion rate during the 16 weeks of exposure, the repair material identified as Mix P showed the highest corrosion rate result during the 16 weeks of exposure. The results show the importance of Silica Fume content in cementitious materials to protect RC structures against exposure to sodium chloride environments.

Repair material only exposed to chloride. Corrosion Rate

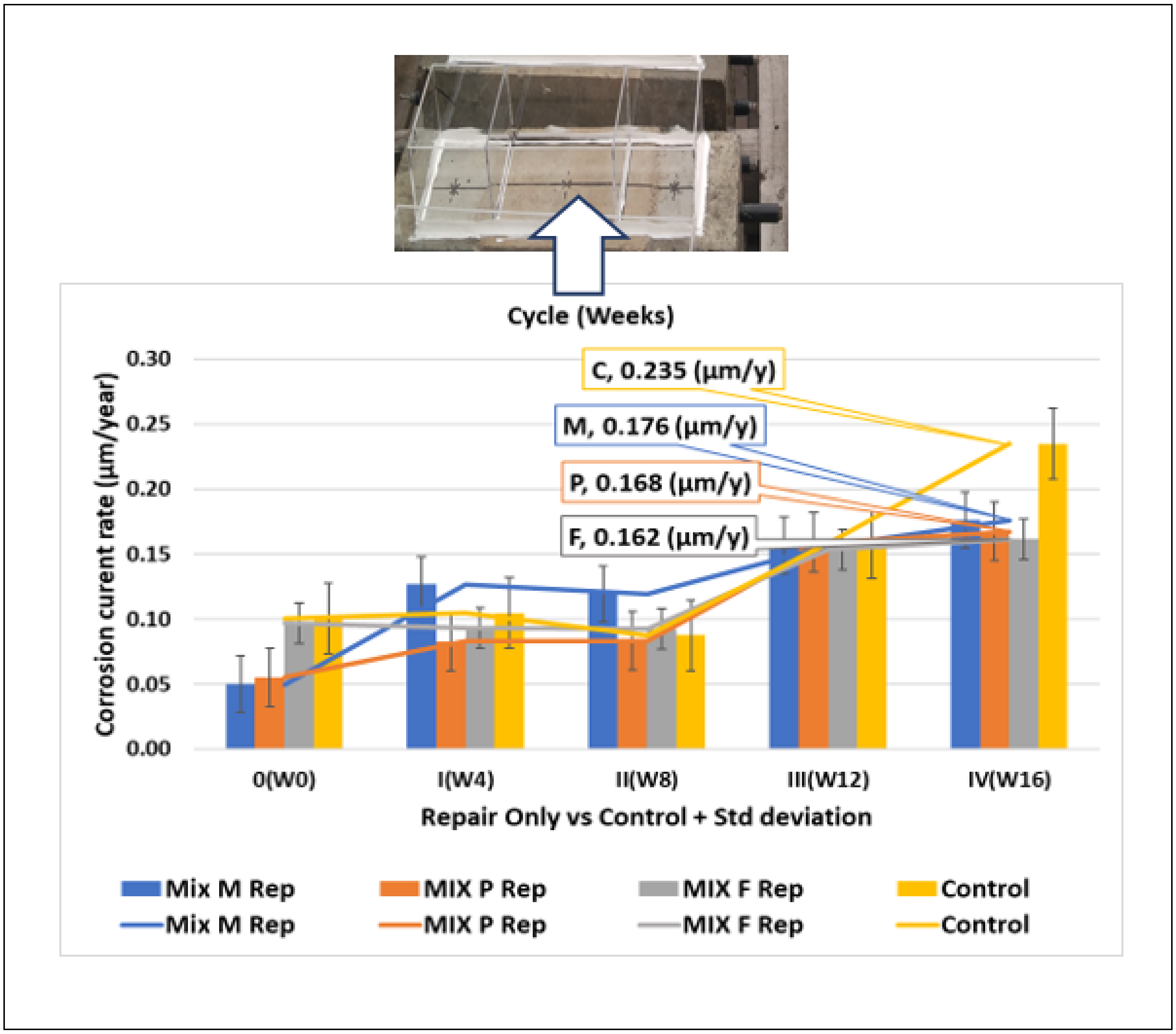

Figure 4.9. CCR Cementitious repair material vs. Control. Std. deviation (PRO)

In Figure 4.9, each plotted point represents the corrosion rate obtained using the LPR method at every cycle for the RC repair mixes and Control exposed to sodium chloride ponding of the repair material only. The corrosion rate at the end of the testing period (120 days) shows Mix F as the lowest value at (0.162 µm/year) compared to the corrosion rate values for repair mixes M, P and Control. Control sample is showing the highest corrosion rate (0.235 µm/year). Fluctuation of corrosion rate values can be observed during the testing period. Figure 4.9 indicates the standard deviation bar with information regarding the corrosion rate data for the samples representing Mixes M, P, F and Control respectively. The corrosion rate result at the end of the testing period for all the mixes is considered low according to the range that can be seen in table 2.1, with the corrosion rate for mix F being the lowest one of all at CR = 0.162 µm/year.

Repair material plus substrate exposed to chloride. Corrosion Rate

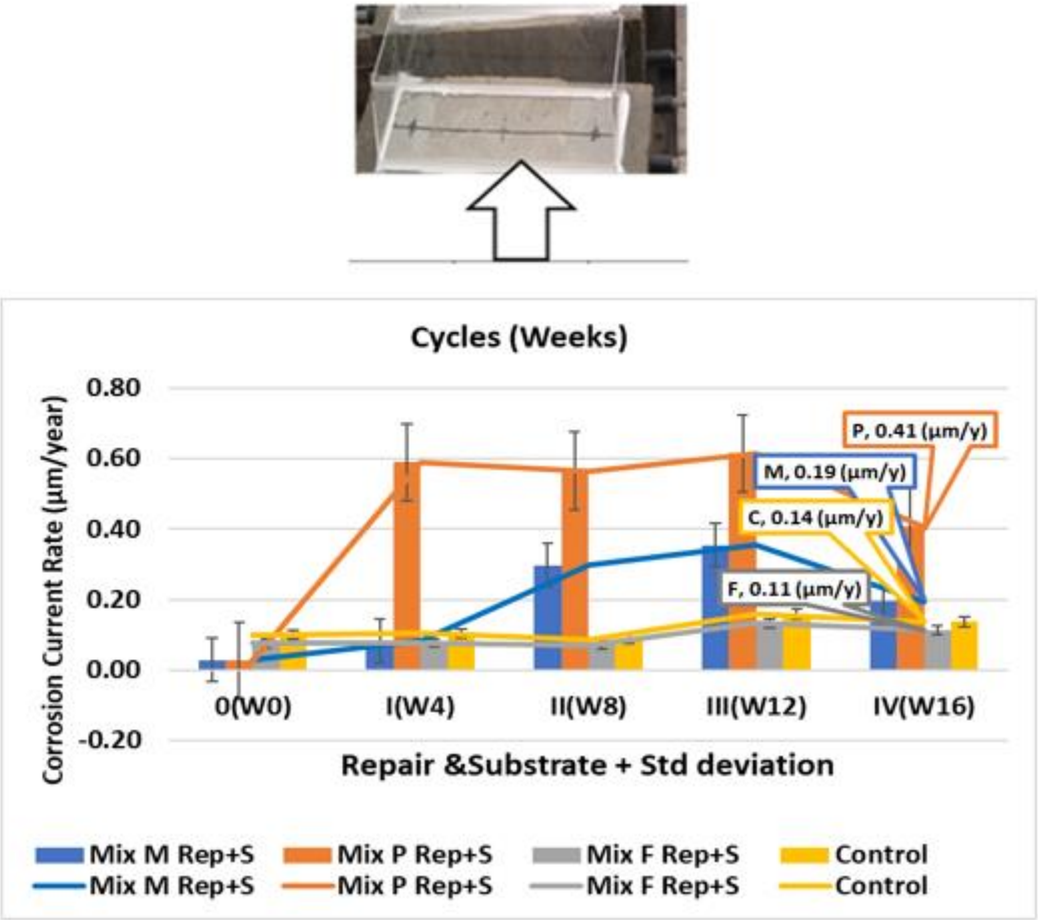

Figure 4.10 CCR Cementitious repair material vs. Control Std. deviation (PR&S)

In Figure 4.10, each plotted point represents the corrosion rate obtained using the LPR method at every cycle for every one of the RC repairs mixes and exposed to sodium chloride & substrate interface. The corrosion rate values at the end of the testing period (120 days) show Mix F as the lowest value at (0.11 µm/year) compared to the corrosion values for repair mixes M, P and Control. The P sample is showing the highest corrosion rate (0.41 µm/year). Figure 4.10 also indicates the standard deviation bar with information regarding the corrosion rate data for the samples representing Mixes M, P, F and Control. The corrosion rate result at the end of the testing period for all the mixes is considered low according to the range described in table 2.1. The corrosion rate for mix F is the lowest one of all at CR = 0.11 µm/year.

In this figure 4.10, we can observe how mixes M and P fluctuate in a less stable way compared to Mixes F and Control when exposed to sodium chloride. This is because repair mixes M and P are not as thermodynamically stable as mixes F and Control.

Repair material plus substrate exposed to chloride. Corrosion Density

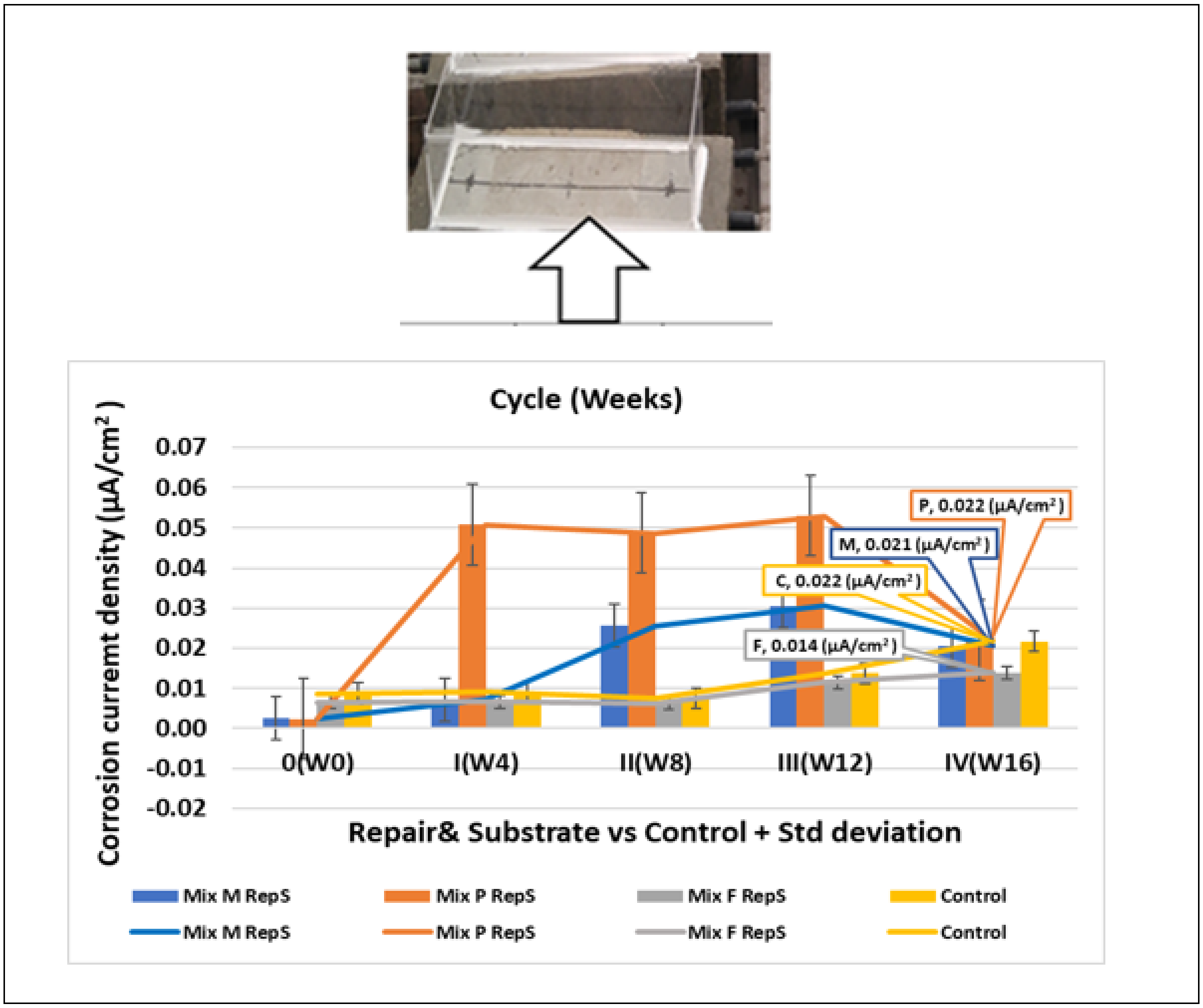

Figure 4.11. CCD Cementitious repair material vs. Control. Std. deviation (PR&S)

In Figure 4.11, each plotted point represents the corrosion current density obtained using the LPR method for every one of the RC repairs mixes and control specimens exposed to sodium chloride and substrate interface. The corrosion current density values at the end of the testing period (120 days) show Mix F as the lowest value at 0.014 µA/cm^2. Compared to the corrosion values for repair mixes M, P and Control, the control sample is showing the highest corrosion current density value recorded (0.022 µA/cm^2). Figure 4.11 also indicates the standard deviation bar with information regarding the corrosion rate data for the samples representing Mixes M, P, F and Control. In this graphic we can observe how mixes M and P fluctuate in a less stable way compared to Mixes F and Control when exposed to sodium chloride. This is because repair mixes M and P are not as thermodynamically stable as Mixes F and Control.

Repair material plus substrate not exposed to chloride. Corrosion Density

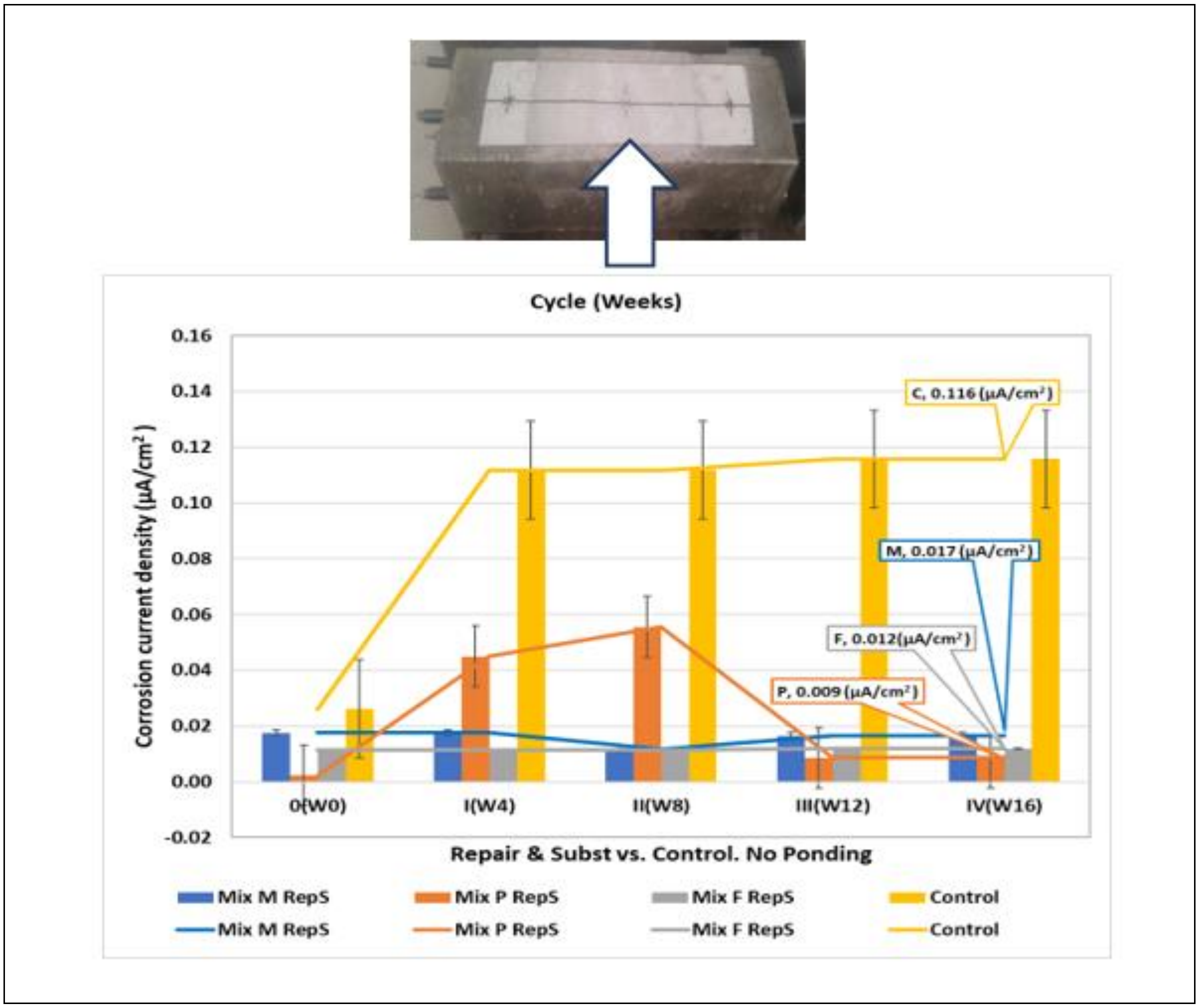

Figure 4.12 CCD Cementitious repair material vs. Control Std. deviation (NP)

In Figure 4.12, each plotted point represents the corrosion current density data from using the LPR method for each of the RC repair mixes and control specimens not exposed to chloride. The corrosion current density values at the end of the testing period (120 days) with Mix P and F as the lowest values at 0.009 µA/cm^2, and 0.012 µA/cm2 respectively compared to the corrosion values for repair mixes M, and Control.

Control sample is showing the highest corrosion current density value at 0.116 µA/cm^2. Fluctuation of corrosion current values can also be observed during the testing period. Figure 4.12 also indicates the standard deviation bar with information regarding the corrosion rate data for the samples representing Mixes M, P, F and Control.

Repair material plus substrate not exposed to chloride. Corrosion Rate

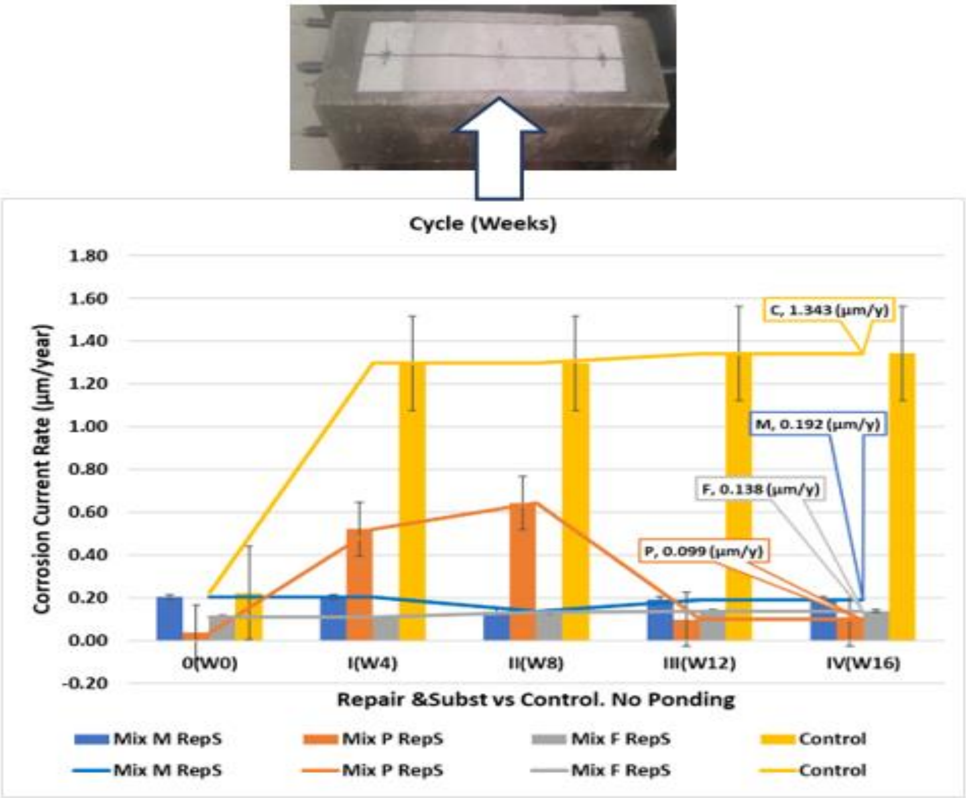

Figure 4.13 CCR Cementitious repair material vs. Control. Std. deviation (NP)

In Figure 4.13, each plotted point represents the corrosion rate obtained using the LPR method for each of the RC repair mixes and Control specimens. The corrosion rate values at the end of the testing period show Mixes P and F were the lowest at 0.099 and 0.138 µm/year respectively. Control sample is showing the highest corrosion rate value at 1.343 µm/year. Fluctuation of corrosion rate values can also be observed during the testing period. Figure 4.13 also indicates the standard deviation bar with information regarding the corrosion rate data for the samples representing Mixes M, P, F and Control. The corrosion rate result at the end of the testing period for all the mixes is considered low according to the range described at table 2.1, with the corrosion rate for mix P being the lowest at CR = 0.099 µm/year.

The author believes that casting more specimens at lab RH and Temperature could help in elucidating the results in terms of corrosion current and corrosion rate values for specimens not exposed to sodium chloride ponding.

4.3 Scanning Electron Microscope (SEM) and Energy Dispersive X-Ray Analysis (EDX)

4.3.1 Influence of microstructure (SEM) analysis of repair materials in corrosion of RC

From figures 3.1 to 3.4, figures 3.5 to 3.8 and figures 3.9 to 3.11, SEM analysis shows the difference in microstructure of the three different repair materials and Control. Mixes M, P and Control show a clear amorphous shape while Mix F shows a denser microstructure. Figure 3.1 shows the morphology of hydrated Mix M sample with the formation of agglomerated amorphous shape material. In figure 3.2., the morphology of Mix P also shows formation of agglomerated amorphous shape material. Figure 3.3 shows the formation of spherical shaped particles, and a smoother material shape formation in mix F. In figure 3.4, the morphology of the Control sample also shows formation of agglomerated amorphous shape material. Hydrated samples observed in Figures 3.1 to 3.4 were ponded in sodium chloride for 120 days.

Figure 3.5 shows the morphology of the hydrated Mix M sample, where formation of agglomerated amorphous shape material can be observed. Figure 3.6, morphology of Mix P, also shows the formation of agglomerated amorphous shape material. Figure 3.7, morphology of Mix F, shows the formation of spherically shaped particles, and a denser material shape formation. Figure 3.8, morphology of control sample, shows formation of agglomerated amorphous shape material. Hydrated samples observed on Figures 3.5 to 3.8 were ponded in sodium chloride for 120 days.

Figure 3.9 shows the morphology of the hydrated Mix M sample, where formation of agglomerated amorphous shape material can be observed. Figure 3.10 shows the morphology of Mix P, where formation of agglomerated amorphous shape material can also be observed. Figure 3.11, morphology of Mix F, shows the formation of spherical particles, and a denser material shape formation.

The hydrated repair materials powder samples described above where exposed to a control temp of 20° C and RH of 50% at the lab for 120 days. It can be seen that there are amorphous shapes in Mixes M and P. In Mix F, the formation of spherical particles due to the Silica Fume presence can also be observed. The small fine glassy particles of SF create a denser microstructure for Mix F due to the large surface area of its glassy spheres. This feature makes it less permeable to chloride attack compared to the other repair mixes and control used during this research.

The finding during the assessment of repair materials performed in this research agrees with K. U. Aavani et al. [41], whose research found the use of silica fume to be beneficial for corrosion repair. Their studies show how SF material properties affect chloride transfer into concrete and highlight the importance of a material’s porous structure.

4.3.2 Influence of chemical constituents EDX Analysis on chloride content among mixes

The chemical constituents of all mixes and Control are summarized in Tables 4.1 to 4.3. It can be appreciated that Mix F shows the lowest percentage of chloride content compared to the other mixes, including control, considered in this study for each one of the different ponding configurations as well as no ponding. It can be observed that for RC repaired materials exposed to wet / dry cycles of sodium chloride, Mix F shows the lowest chloride content at 0.003 % at weight of sample compared to Mix M, P and Control, showing a chloride content of: 0.023, 0.020, 0.037 % at weight per sample, respectively.

The concentration of chloride for mixes M, and P is between 4 to 5 times higher than for mix F and Control. For mixes F and Control the chloride concentration values are the lowest at 0.033 and 0.037 % at weight of sample respectively. The concentration of chloride for mixes M and F (no ponding) show the lowest values 0.0 % at weight per sample and Mix P the highest value at 0.09% at weight per sample for RC repaired materials not exposed to wet / dry sodium chloride.

SEM / EDX-ray spectra analysis showed the presence of seven elements (Si, Ca, Al, Na, Mg, Fe, and Cl). It was found that Si, Ca, and Al were the elements with higher at% per weight of sample. From the information obtained during the EDX analysis of hydrated powder samples examined during this research, it can be inferred that a lower Ca / Si ratio will lead to a lower Chloride concentration in the specimens.

Other research, including that of T. Luping et al. [104], has shown that a reduced Ca / Si ratio in the C-S-H chemical structure is believed to alter the surface characteristics of cement gel and reduce the amount of chloride binding in hydrated cement mixes. The results obtained after performing SEM / EDX analysis at the end of the testing period are in good agreement with the NDT findings performed during this research, pointing at the usage of Mix F as the most suitable material for corrosion repair of RC structures.

Repair material only exposed to chloride

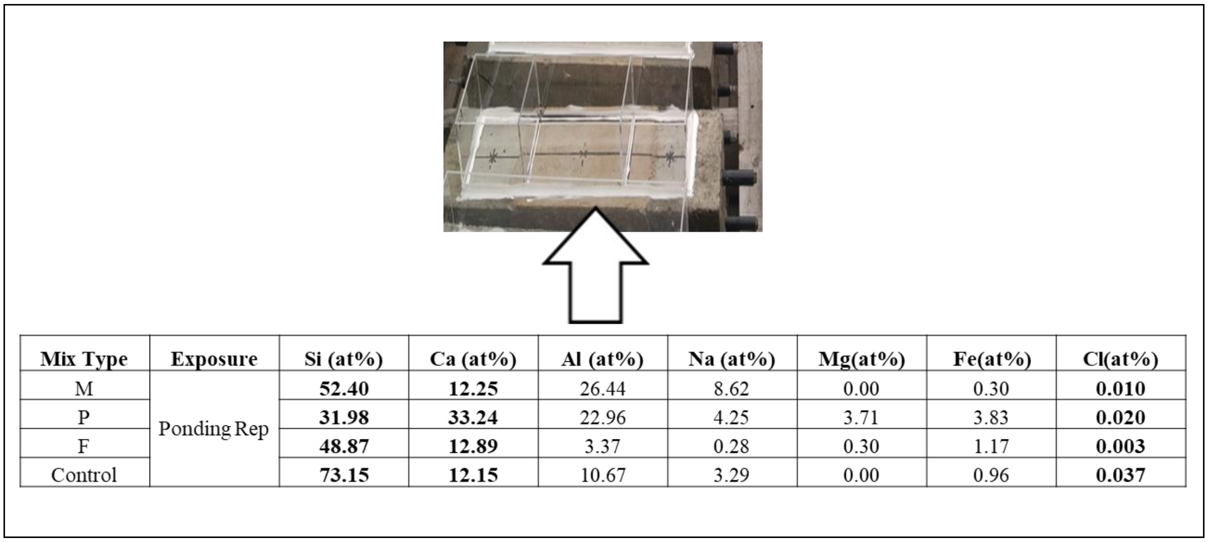

Mix Type	Exposure	Si (at%)	Ca (at%)	Al (at%)	Na (at%)	Mg(at%)	Fe(at%)	Cl(at%)
M	Ponding Rep	**52.40**	**12.25**	26.44	8.62	0.00	0.30	**0.010**
P		**31.98**	**33.24**	22.96	4.25	3.71	3.83	**0.020**
F		**48.87**	**12.89**	3.37	0.28	0.30	1.17	**0.003**
Control		**73.15**	**12.15**	10.67	3.29	0.00	0.96	**0.037**

*%at = % atomic weight

Table 4.1 Characterization of repair material by EDX analysis (%at). Mixes M, P, F and Control (PRO)

Repair material & Substrate exposed to chloride

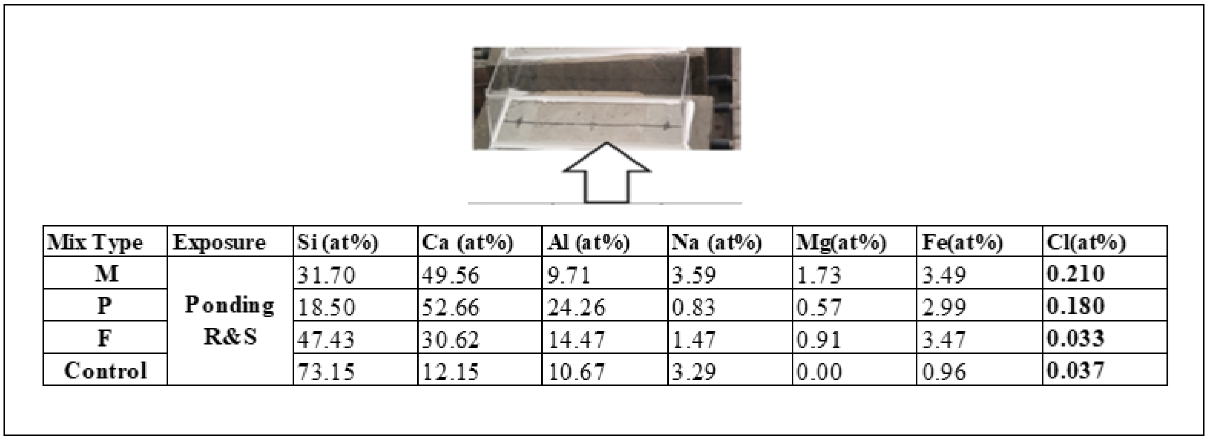

Mix Type	Exposure	Si (at%)	Ca (at%)	Al (at%)	Na (at%)	Mg(at%)	Fe(at%)	Cl(at%)
M	**Ponding R&S**	31.70	49.56	9.71	3.59	1.73	3.49	**0.210**
P		18.50	52.66	24.26	0.83	0.57	2.99	**0.180**
F		47.43	30.62	14.47	1.47	0.91	3.47	**0.033**
Control		73.15	12.15	10.67	3.29	0.00	0.96	**0.037**

*%at = % atomic weight

Table 4.2 Characterization of repair material by EDX analysis (%at). Mixes M, P, F and Control (PR&S)

Repair material & Substrate Not exposed to chloride

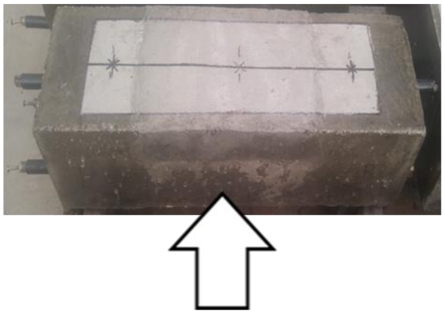

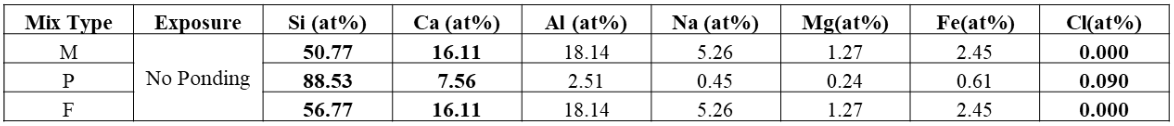

Mix Type	Exposure	Si (at%)	Ca (at%)	Al (at%)	Na (at%)	Mg(at%)	Fe(at%)	Cl(at%)
M	No Ponding	**50.77**	**16.11**	18.14	5.26	1.27	2.45	**0.000**
P		**88.53**	**7.56**	2.51	0.45	0.24	0.61	**0.090**
F		**56.77**	**16.11**	18.14	5.26	1.27	2.45	**0.000**

*%at = % atomic weight

Table 4.3 Characterization of repair material by EDX analysis (at%). Mixes M, P, F (NP)

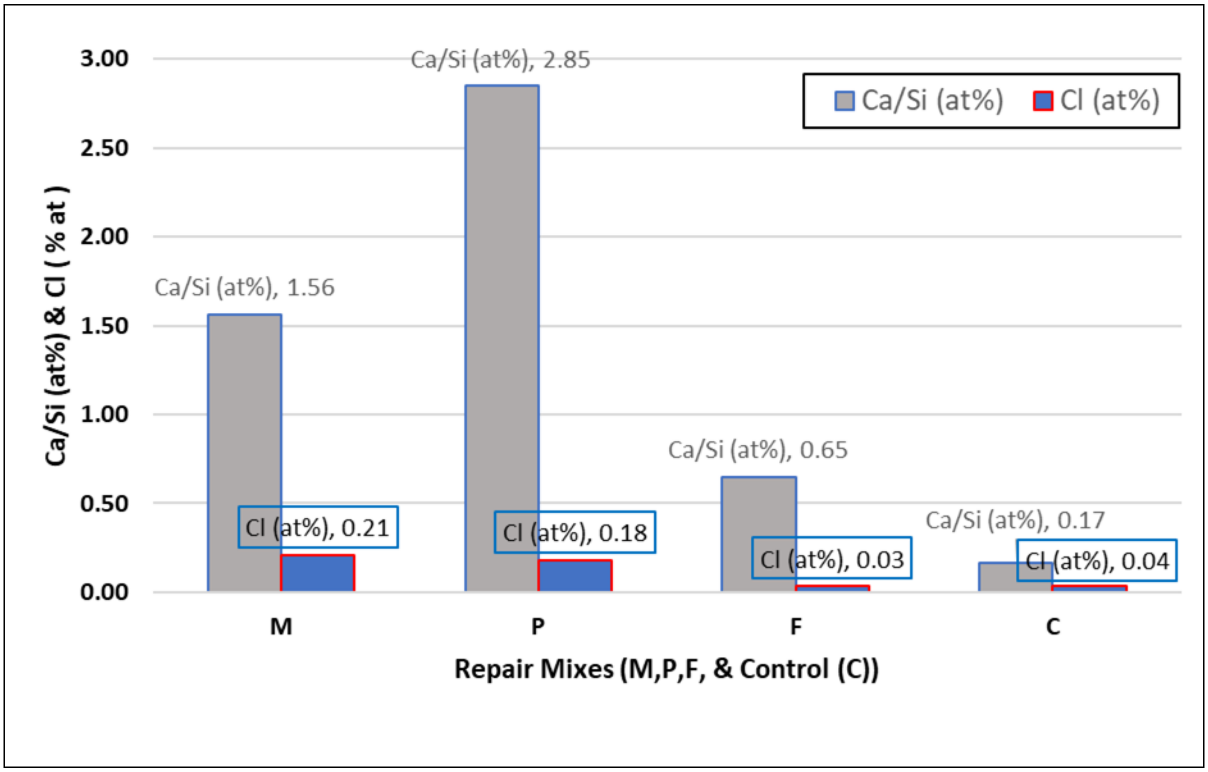

*%at = % atomic weight

Figure 4.14 Ca/Si vs. Cl content. Mixes M, P, F and Control.

In Figure 4.14, it can be observed that there is a relationship between the Ca / Si ratio vs. Cl amount concentration in the repair mixes vs. control. However, for some of the mix samples it was found that the Ca / Si decreasing ratio did not correlate to a decrease of Cl content. The author believes that a binding Isotherm test as the one proposed by T. Luping et al. in [104] could help elucidate the real amount of binding chloride found in the hydrated powder repair mixes.

4.3.3 SEM/EDX effect on corrosion determination (Durability):

The information obtained from SEM / EDX analysis will provide crucial insight into the molecular morphology and structure of the main product of hydrated cementitious based materials such as Calcium silicate hydrates (C-S-H) in corrosion repair cementitious materials. The molecular composition of C-S-H will provide information about the study and improvement of the properties of cementitious materials. The structure of Calcium Silica Hydrate can also affect the chemical and physical properties of cementitious materials like strength, shrinkage, creep of the cement paste, as well as mechanical properties including elastic modulus, fracture risk, and toughness.

Manzano et al. [105] studied the C-H-S mechanical properties by lattice dynamics simulation. Their experimental results showed that an increase in Ca / Si ratio led to a decrease in the volume, shear stress and elastic modulus of C-S-H. Qomi et al. [106] found through molecular dynamics simulation that an increase in the Ca / Si ratio led to a decrease in the indentation modulus, and therefore the calcium-silica layers became defective and the mechanical stiffness and anisotropy decreased. The understanding of SEM / EDS microanalysis provides deep insight into the chemical composition of C-S-H [107]. An improvement in the performance of RC and cementitious repair materials can be achieved through the study in the mechanisms of chloride ions and C-S-H.

4.4 Experimental results and correlation of NDT tests

A correlation model that captures the experimental results obtained from assessing three different types of cementitious repair materials vs. Control using three different types of Electrochemical NDT methods will be presented.

Microsoft excel software was used to present the relationship between NDT results of the repair materials and control performed in this research, along with their potential effects to protect concrete reinforcement steel against corrosion.

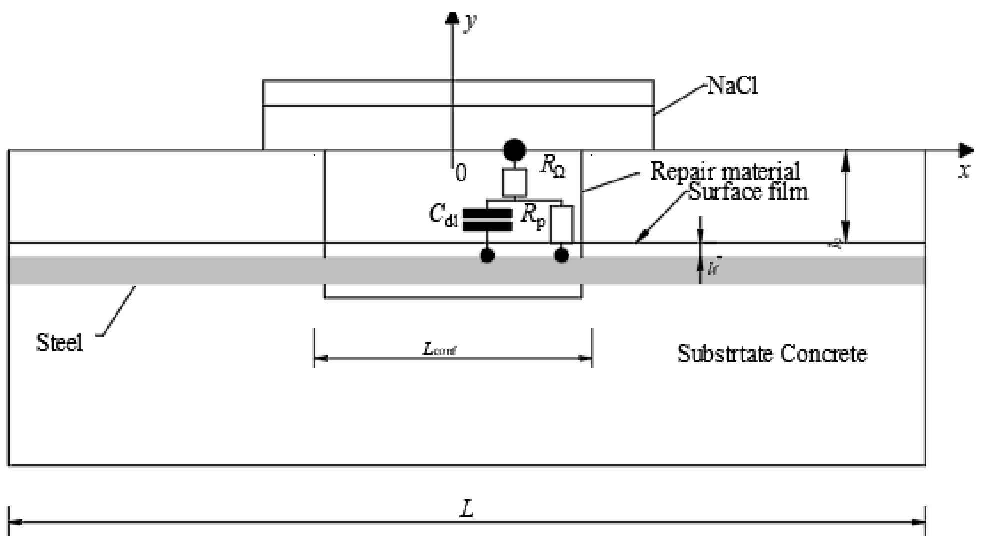

Figure 4.15 Equivalent circuit and schematic set up of experimental RC for corrosion repair

In this research study the Stern-Geary equation, which is derived from the Butler-Volmer kinetic, is used to determine the corrosion current density and corrosion rate using the LPR methodology. The experimental results obtained from performing the Linear polarization Resistance of the RC corrosion repair specimens was used to propose a formulation to calculate the conductivity of three different repair materials vs. the control considered in this study [108].

The theory behind finding the conductivity of the RC repair materials is to have a better understanding of the phenomena involved in the chloride resistance in cement-based materials. The following graphics show a linear fitting since the total electrical conductivity of RC specimens was derived from the Linear Polarization Resistance through the Stern-Geary equation.

Equations and parameters used for formulating the electrical conductivity of RC corrosion repair specimens, are the following:

Stern-Geary Linear Polarization resistance, Rp in Ohm. (As stated in chapter 2)

Equation - Derivation of Buttler- Volmer:

$$Rp = \left(\frac{\partial}{\partial}\frac{\Delta \mathrm{E}}{\iota}\right) i = 0, \frac{dE}{dt} \rightarrow 0 \tag{6}$$

Corrosion Current Icorr:

$$I\mathrm{corr} = \frac{B}{Rp} \tag{7}$$

Stern – Geary constant B:

$$B = \frac{\beta a \, \beta c}{2.303 \, (\beta a \, \beta c)} \tag{8}$$

Corrosion current density, $i$corr

$$i\mathrm{corr} = \frac{I \ \mathrm{corr}}{As} \tag{9}$$

Corrosion rate (Assuming uniform corrosion)

$$CR = \frac{kaw}{nF\delta} \, i\mathrm{corr} = \alpha i\mathrm{corr} \tag{10}$$

Conductivity of steel (σf) :

$$\sigma f = \frac{lf * i\mathrm{corr}}{B} \tag{11}$$

Where lf = thickness of surface film

Conductivity of concrete material (σc)

$$\sigma c = \frac{lc * i\mathrm{corr}}{B} \tag{12}$$

Where lc = thickness of concrete cover

Total Conductivity concrete & steel (σt)

$$\sigma t = \sigma f + \sigma c \tag{13}$$

Experimental values of corrosion current density obtained from performing the LPR test on RC repaired samples exposed to wet / dry NaCl using NDT equipment are considered for obtaining the conductivity of the beam specimens in figure 4.15. The conductivity data was obtained through equations 11 to 13. A linear relationship between conductivity of the RC system and the corrosion current density of the specimen, as expected, was obtained.

Relationship between Corrosion Current Rate vs. Conductivity of RC (PRO)

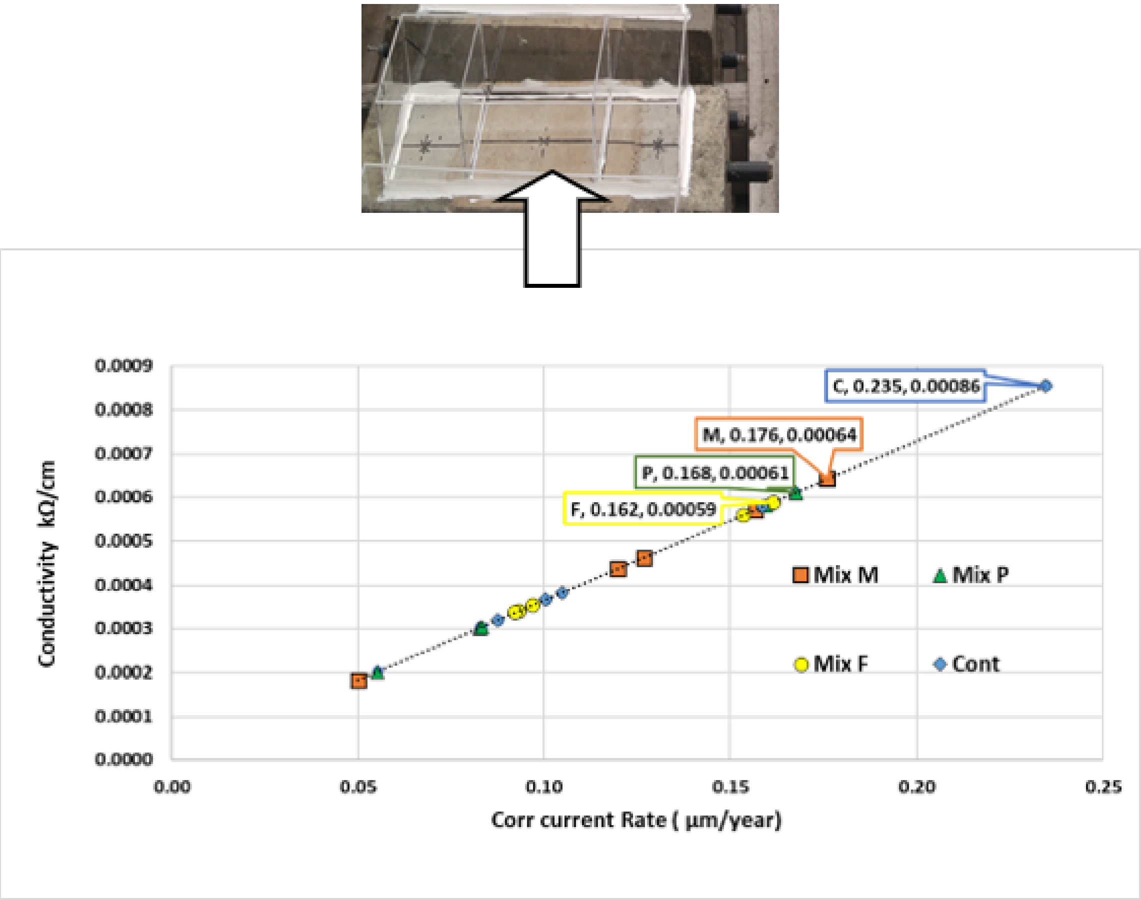

Figure 4.16 CCR vs. Conductivity. Cementitious repair material vs. Control (PRO)

In figure 4.16, we can also observe that the Control sample is the one showing the highest corrosion rate as well as the higher conductivity: 0.235 μm/y and 0.00086 kΩ/cm respectively at the end of the testing period. Followed by Mixes P and M, Mix F shows the lowest corrosion rate and conductivity at 0.162 μm/year and 0.00059 kΩ/cm respectively. Higher conductivity of the RC repair material correlates with higher corrosion current density. The summary of results shown in this graphic is in good agreement with the information obtained from experimental results using other electrochemical techniques performed in this study as well as the SEM and EDX-Ray analysis. All of these tests show Mix F as the best suited for corrosion repair of RC.

Relationship between Corrosion Current Rate vs. Conductivity of RC. Repair & substrate interface (PR&S)

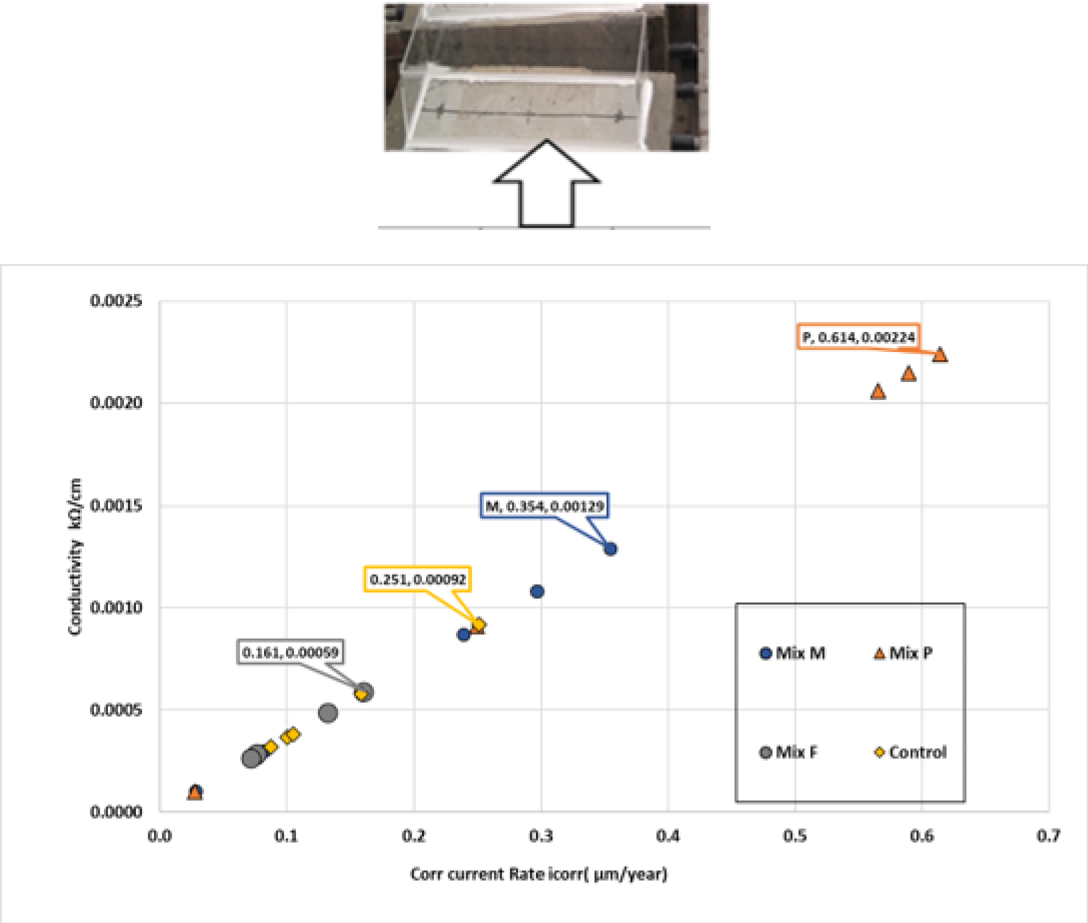

Figure 4.17 CCR vs. Conductivity. Cementitious repair material vs. Control (PR&S)

In Figure 4.17, we can observe that the P sample is the one showing the highest corrosion rate as well as the higher conductivity of electrical signals at 0.614 μm/year and 0.00224 kΩ / cm at the end of the testing period. Mix F showed the lowest corrosion current rate and conductivity at: 0.161 μm/year and 0.00059 kΩ / cm.

Relationship between Corrosion Current Rate vs. Conductivity of RC Repair material & Substrate no ponding

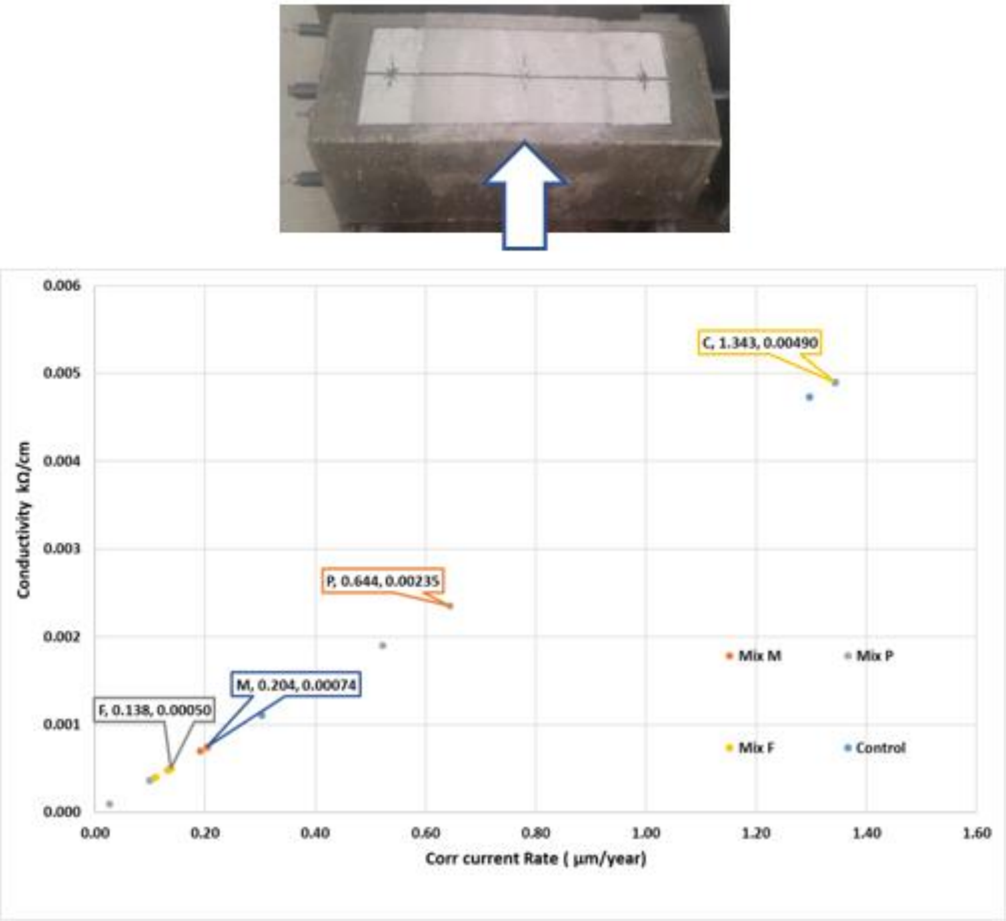

Figure 4.18 CCR vs. Conductivity. Cementitious repair material vs. Control (NP)

Experimental values of corrosion current density obtained from performing the LPR test on RC repaired samples exposed to lab RH and temperature using NDT equipment are considered for obtaining the conductivity of the beam specimens (see Figure 4.15).

In Figure 4.18, we can also observe that the control sample is the one showing the highest corrosion rate as well as the higher conductivity of electrical signals at 1.343 µm/year and 0.0049 kΩ / cm at the end of the testing period. At the end of the testing period, mix F shows the lowest corrosion rate and conductivity value at 0.138 µm/year and 0.00050 kΩ / cm. A linear relationship between conductivity of the RC system and the corrosion current density of the specimen, as expected, was obtained.

Relationship between Corrosion Current Rate vs. Macrocell of RC Repair material (PRO)

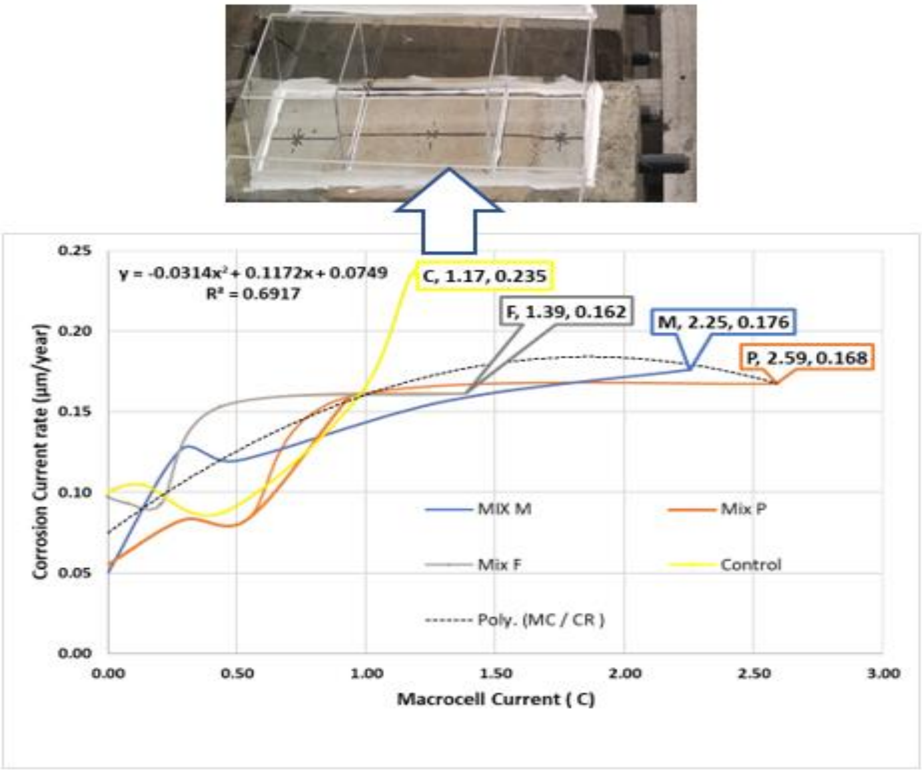

Figure 4.19 CCR vs. Macrocell. Cementitious repair material vs. Control (PRO)

In Figure 4.19, it can be observed that Mixes M, and P show the highest Macrocell current with time, whereas Control and Mix F show the lowest Macrocell current. Additionally, Control specimens show the highest corrosion rate and Mix F the lowest corrosion rate. This difference in Macrocell current and corrosion density rate among mixes could be due to the electrochemical potential difference between control and repair mixes and the chloride ion movement among mixes.

Relationship between Corrosion Current Rate vs. Macrocell current of RC. Repair & substrate interface vs. Control

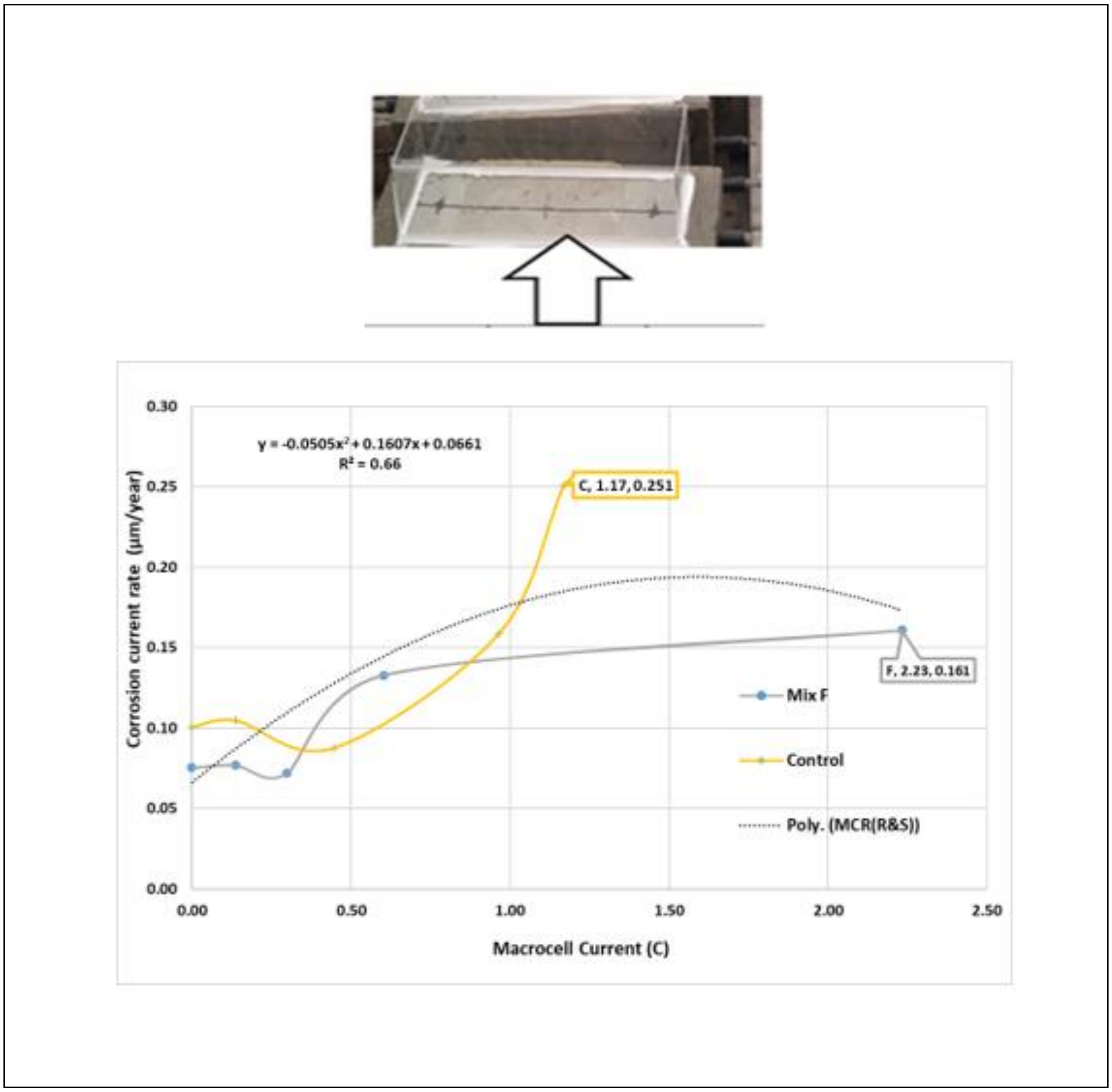

Figure 4.20 CCR vs. Macrocell. Cementitious repair material vs. Control (PR&S).

In Figure 4.20, it can be observed that control mix shows the highest corrosion current with time, whereas Mix F shows the lowest corrosion current with time. Mixes control and F show the lowest Macrocell current. Relationship between NDT methods Macrocell current and corrosion rate can not be established for mixes M, and P due to the great difference in driving potentials between mixes M, P and their substrates. It has been found that the incompatibility between mix repairs and substrate interface exposed to sodium chloride has a great impact in the Macrocell current. This finding has been confirmed by other researchers stated in the literature review.

Relationship between Corrosion Current Rate vs. Macrocell current of RC. Repair vs. Control. No ponding

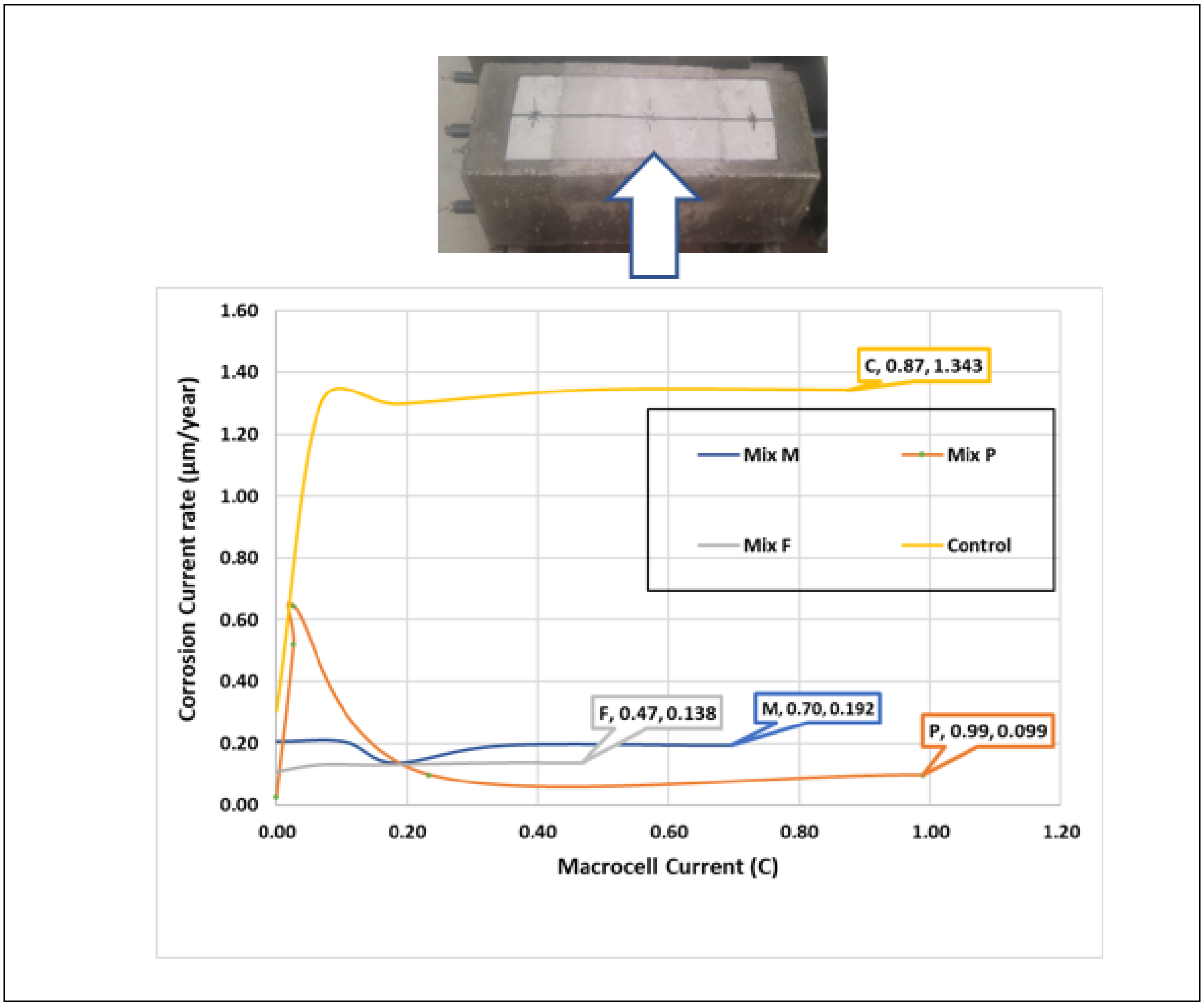

Figure 4.21 CCR vs. Macrocell. Cementitious repair material vs. Control (NP)

In Figure 4.21, it can be observed that Mix F maintains a stable and low corrosion rate and Macrocell current during the testing period. Mixes F and M show the lowest Macrocell current. Mix P shows the highest Macrocell current, and the Control mix shows the highest corrosion rate of all mixes.

Relationship between Corrosion Current Rate vs. HCP of RC Repair Mixes & Control

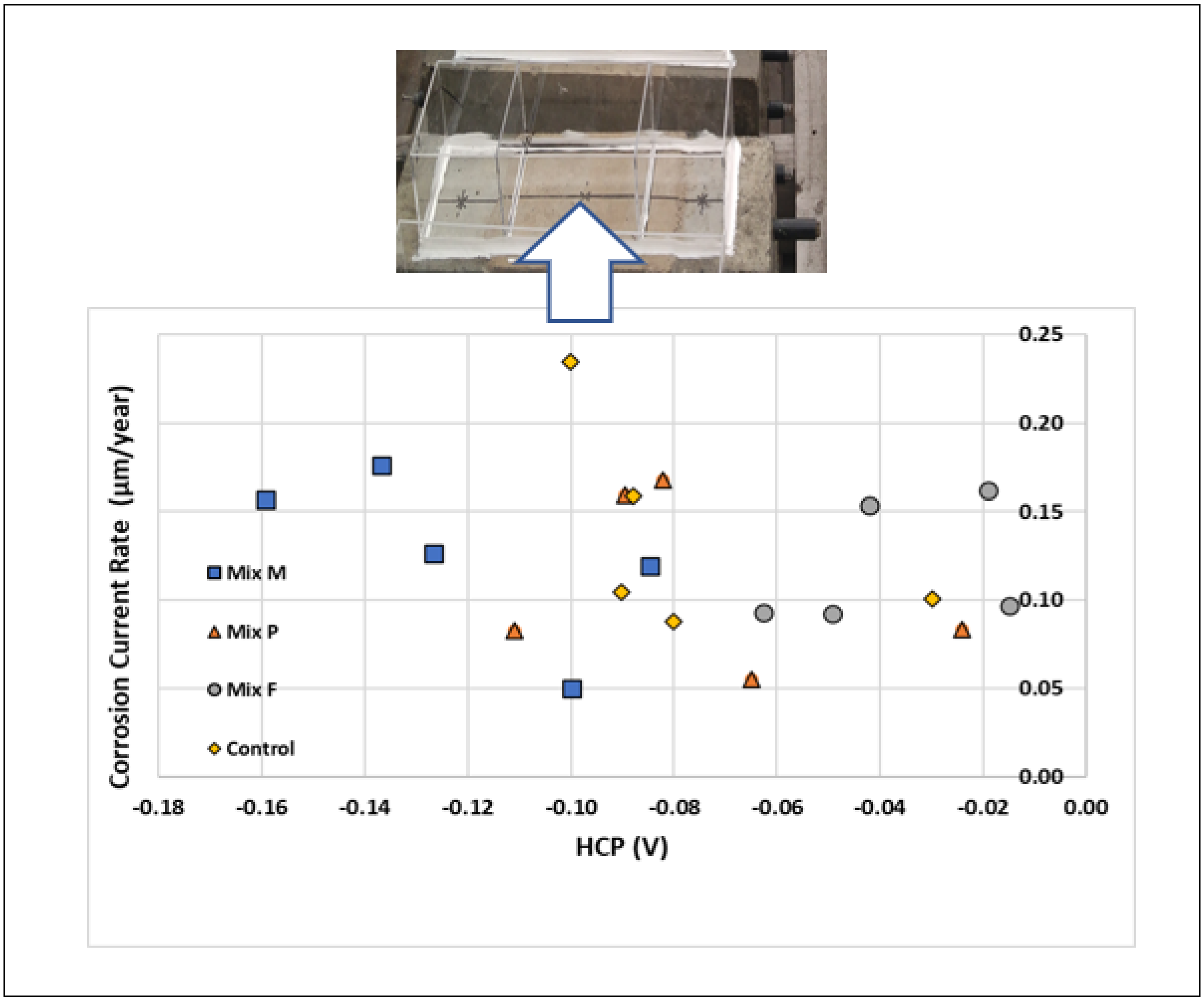

Figure 4.22 CCR vs. HCP. Cementitious repair material vs. Control (PRO)

There are fluctuating corrosion density rate results during the testing period (as shown in Figure 4.22), for all the Mixes, M, P, F, and Control. The Control repair mix shows the highest corrosion potential and corrosion rate of all the mixes, while Mix F shows the lowest HCP and corrosion rate of all the mixes. It can be observed that mix F shows the lowest potential and corrosion rate at the end of testing. No clear relationship can be established between the HCP and Corrosion rate for mixes exposed to sodium chloride during the testing period. The author believes this is due to the difference in driving potentials between the mixes being tested.

Relationship between Corrosion Current Rate vs. HCP of RC Repair & substrate vs. Control

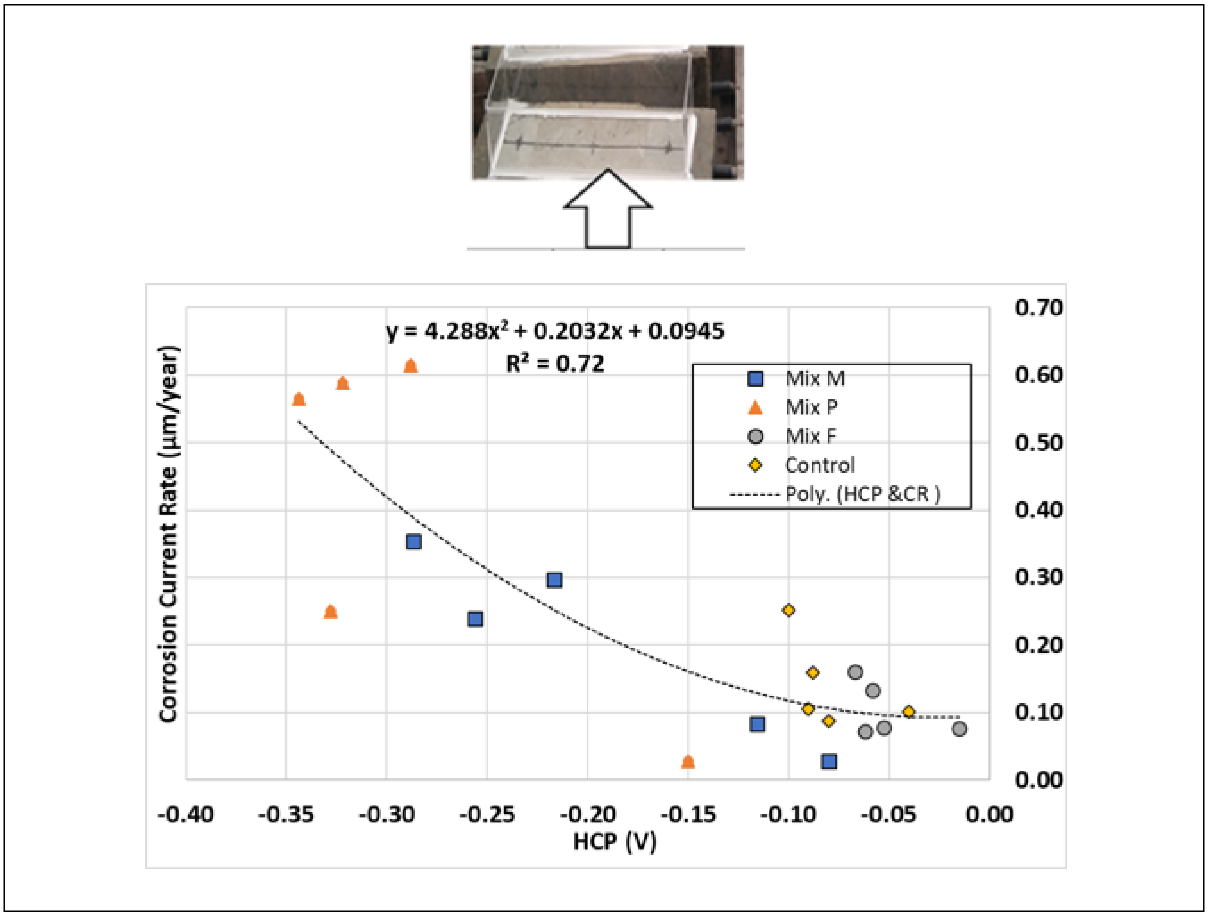

Figure 4.23 CCR vs. HCP Cementitious repair material vs. Control (PR&S)

In Figure 4.23, it can be observed that Mixes F and Control show the lowest corrosion potential and corrosion current of all the mixes. Mixes M and P show the highest HCP and corrosion rate of all the mixes. These results are in agreement with that of other researchers mentioned in the literature review regarding compatibility of materials between repair material and substrate interfaces. The potential differences between mixes M and P make results more scattered compared to those of Mixes F and Control. A second order polynomial equation was chosen to fit this relationship since this is the shape that is drawn from the data obtained after performing both HCP and LPR tests.

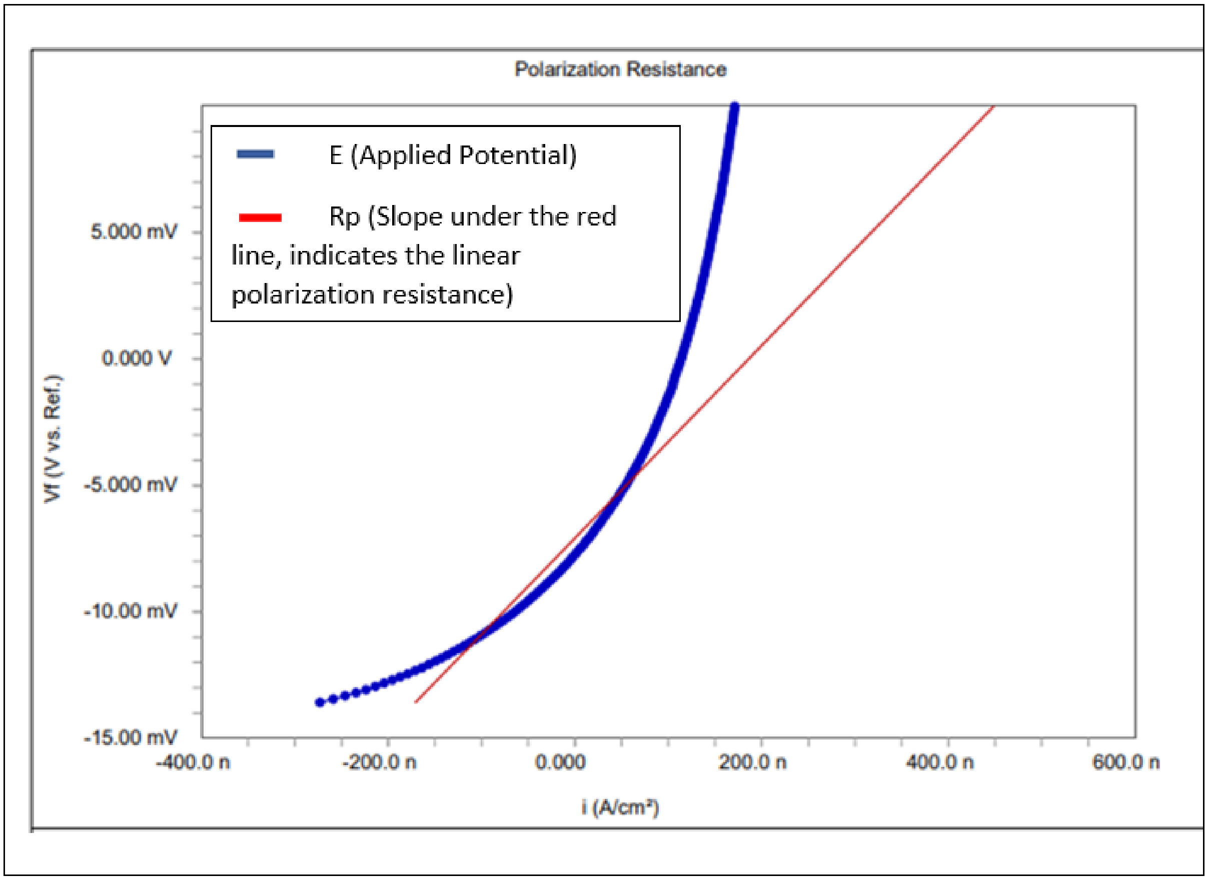

Figure 4.24 Applied potential (E) vs. Corrosion current density (icorr)

In Figure 4.24, a polynomial shape is observed when measuring the Linear Polarization Resistance of repair mixes and Control.

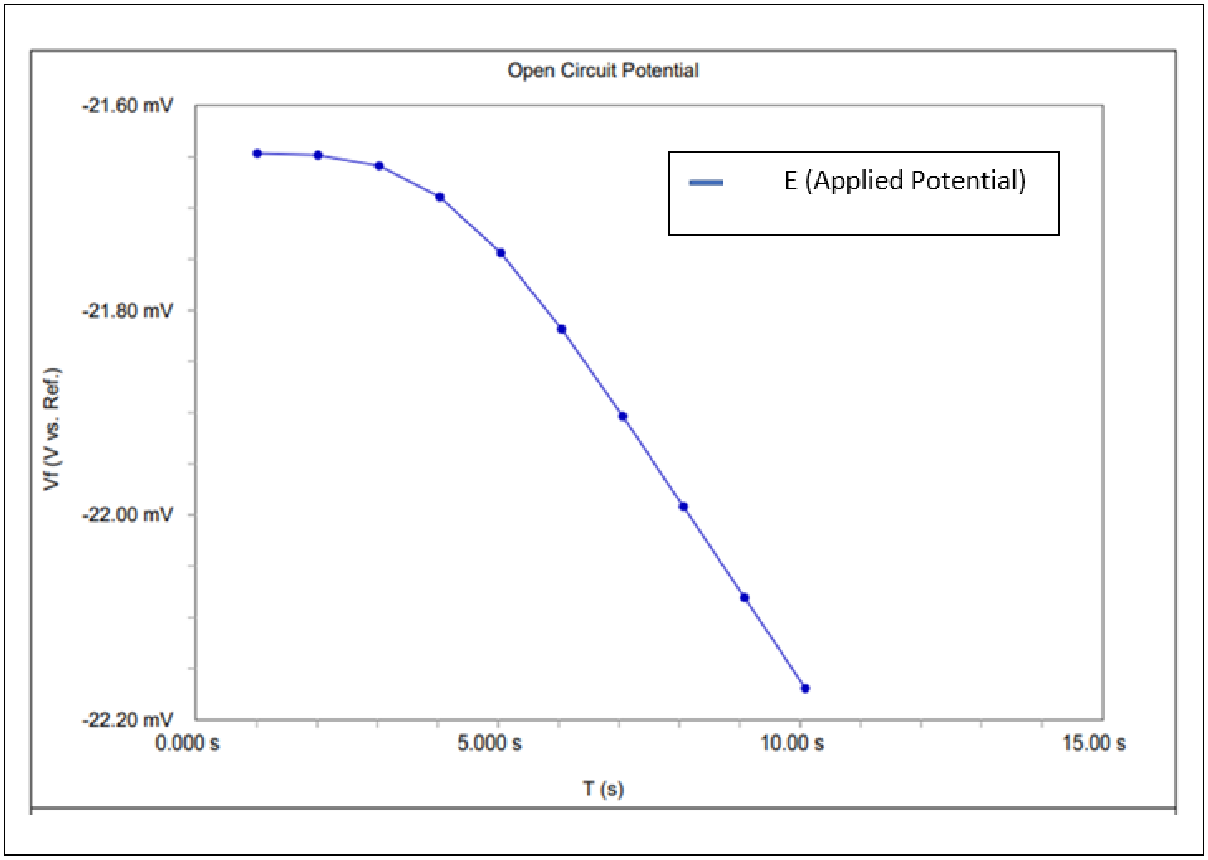

Figure 4.25 Applied potential (E) vs. Time (sec)

In Figure 4.25, a polynomial shape is observed when measuring the Half Cell Potential of repair mixes and Control.

Relationship between Corrosion Current Rate vs. HCP of RC Repair & Control exposed at RH and Temperature. No ponding

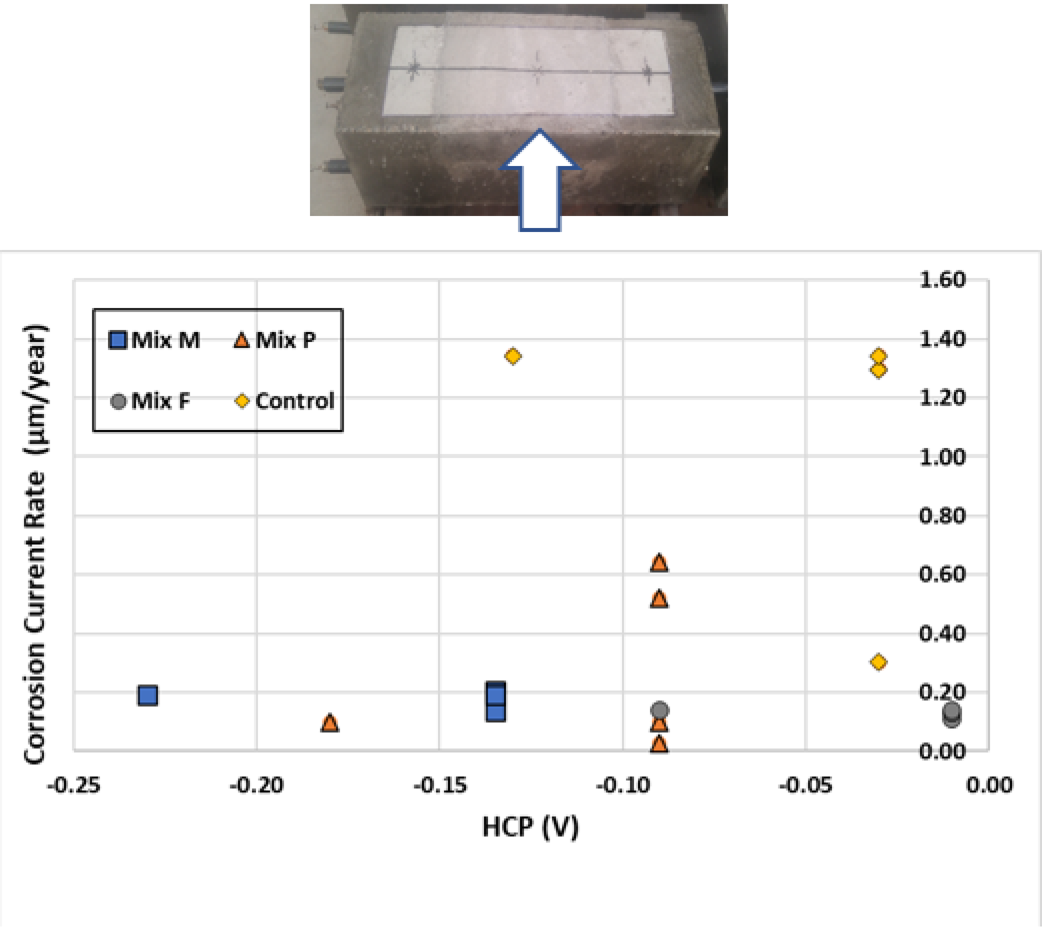

Figure 4.26 CCR vs. HCP Cementitious repair material vs. Control (NP)

In figure 4.26, it can be observed that Mix F shows the lowest corrosion potential and corrosion rate value of all the mixes. Control mix shows the highest corrosion rate. Mixes M and P show the highest HCP of all the mixes.

Chapter 5. Experimental Results / Discussion

5.1 Visual Observations

At the end of the wetting/drying sodium chloride cycles, it was observed that RC specimens treated with cementitious repair Mixes M and P presented some visible cracks. Slight change in color and even signs of corrosion on the surface of Mix P after vacuuming the sodium chloride solution was observed. Mix F, however remained uncracked and free of corrosion stains. For the control mix, there was no sign of cracks at the end of the testing. The author believes that the fact that control specimens were casted continuously, with no repair indentation, had an impact in the visual results of control samples.

5.2 Electrochemical Techniques

After performing HCP, LPR and Macrocell electrochemical tests on three different types of cementitious repair material under chloride exposure, it is observed that all the values from the NDT's methods in terms of degree of corrosion activity led to results were Mix F outperformed Mixes M, P and control when exposed to sodium chloride, even though the Mix F had a built-in indentation when exposed to sodium chloride compared to control.

Additional research like the one performed by Raghav et al [99], reported that some chemical components such as silica fume being present in cement-based materials can react with concrete. SF can provide a physical contribution by filling the spaces found in the interfacial region of cement grains. This physical contribution is known as particle packing. Chemically, due to the high percentage (>90%) of highly amorphous SiO_2, SF cement-based materials lead to the formation of hardened concrete.

5.3 Bond and compatibility of cementitious repair materials:

The effectiveness of repair cementitious materials to delay / retard corrosion in RC exposed to high-chloride environments is highly dependant on how the repair and substrate material react as a system to sodium chloride attack.

Song et al [109], reported an improvement of the bond strength at an interface between the repair and substrate material was caused by the C-S-H secondary reaction between the silica fume in UHPC and the $Ca(OH)_2$ in the old concrete substrate. This improvement was observed through mechanical testing and SEM observation.

5.4 Efficiency of cementitious repair materials

Structural:

Research conducted by S. Tang et al. [107] found that a cement mortar repair material modified with a small amount of polypropylene fibers and silica fume showed improved interfacial bond mechanical properties. They observed improvement between interfacial transition zones of substrates and repairs.

Durability:

External additives and the type of substrate to receive the repair can affect the quality of the repair material. An increase in roughness of the existing concrete has been proposed by Feng et al [110] to enhance the bond strength and mechanical interlock between the substrate and the repair. In addition, Xiong et al [111] reported that the adhesion between the repair layer and the substrate interfacial transition could be improved by incorporating a silane coupling agent. P. Stutzman et al [75], reported that an improvement could be achieved regarding the bond strength and toughness of the interface between repair materials and concrete by applying nano-silica-modified silane as an interfacial coupling agent between the repair and a concrete structure.

Sodium Chloride resistance and repair-substrate compatibility:

As per the NDT results performed through all different repair materials vs. control, it was determined that Mix F and Control substrate materials had the best sodium chloride-induced corrosion resistance compared to Mixes M and P. This finding is attributed to electrochemical compatibility with the substrate.

Best performing corrosion repair:

As per the three different NDTs, and through SEM / EDX analysis performed during this experimental research, it was concluded that that Mix F was the most suited repair material for corrosion repair of RC structures.

Chapter 6. Conclusions

Results of the experimental study of using electrochemical methods to assess the effectiveness of cementitious materials for corrosion repair can be summarized as follows:

The usage of electrochemical techniques to measure corrosion potential (HCP), Macrocell corrosion, and Linear Polarization performed in this study proved to be useful techniques to assess the effect of three different types of cementitious repair materials and control when under chloride exposure and without chloride exposure, as well as for the degree of corrosion where each of the different types of cementitious repair materials developed at the end of the testing period.

The chemical components contained in Mix F (silica fume), make it a more desirable repair due to its higher surface area, less available void space and less permeable environment for ion movement. Additionally, it provides electrochemical compatibility with the substrate when exposed to sodium chloride. Experimental results for Mix F show a lower corrosion potential, corrosion rate and Macrocell corrosion compared to repair Mix M and Mix P when exposed to sodium chloride.

SEM / EDX technology provided more information about the morphology and chemical composition of these three different repair materials, plus the control after being exposed to chlorides. It was found that Mix F had the lowest chloride content by atomic percentage compared to mixes M, P and control after performing SEM / EDX analysis.

A careful evaluation of the physical and chemical exposure of the repair material should be conducted before a final selection is made. As well, the physical and chemical compatibility of the repair and substrate must be of primary concern.

The findings of this study will contribute to the development and choosing of a repair material that is adequate to the corrosion repair of RC structures exposed to high sodium chloride environments. Findings also show the importance of electrochemical compatibility between repair materials and substrates when exposed to wet / dry sodium chloride cycles.

A modelling procedure that resembles the experimental set up conducted in this research was performed. A relationship between the three different NDT methods and the effect of three different cementitious repair materials applied to the substrate of a RC system for corrosion repair was found. This information will give us insight as to which repair material to choose for a RC structure that is exposed to NaCl.

6.1. Future work and Recommendations

After assessing the performance of three different cementitious repair materials against the control using three different types of NDTs, there are still many aspects that need to be investigated further in the area of corrosion repair material and NDT methods. The need for further investigation of the following points will provide a better understanding of corrosion repair materials, as well as improvement for faster NDT methods to assess the corrosion repair of RC structures.

1. The effectiveness of cementitious repair materials can be affected by their chemical composition and ability to withstand chloride attacks. It would be recommended to investigate other cementitious repair materials containing nanosilica and other nanowaste materials in order to reduce the carbon footprint emission and measure their resistance to chloride attack.
2. Conduct assessment of corrosion rate on materials exposed to a natural marine environment on site and in a Laboratory control environment and compare the difference in results.
3. Develop a data base of the chloride binding properties of different cementitious repair materials. Use this data to determine possible parameters for predicting Chloride diffusion and creating service life calculation models of RC exposed to a chloride environment.
4. Standardize the type of corrosion repair materials to be used for corrosion repair treatment, maximizing compatibility with existing concrete substrates.
5. Explore the application and use of UAV devices for assessment of corrosion repair of RC structures.

Bibliography

[1] “Corrosion of Steel in Concrete: Understanding, Investigation and Repair, Second Edition,” *Routledge & CRC Press*. https://www.routledge.com/Corrosion-of-Steel-in-Concrete-Understanding-Investigation-and-Repair/Broomfield/p/book/9780367864705 (accessed Sep. 21, 2021).

[2] American Concrete Institute, Ed., *Guide to materials selection for concrete repair*. Farmington Hills, Mich: American Concrete Institute, 2014.

[3] D. W. Hobbs, “Concrete deterioration: Causes, diagnosis, and minimising risk,” *International Materials Reviews*, vol. 46, no. 3, pp. 117–144, 2001, doi: 10.1179/095066001101528420.

[4] Y. S. Ariningsih, D. Nuralinah, and A. W. W. Saputra, “Diffusion of chloride from seawater into the concrete analysis: a literature review on implemented approaches,” *IOP Conf. Ser.: Earth Environ. Sci.*, vol. 930, no. 1, p. 012015, Dec. 2021, doi: 10.1088/1755-1315/930/1/012015.

[5] “American Concrete Institute - 2014 - Guide to materials selection for concrete repair.pdf.” Accessed: Feb. 19, 2022. [Online]. Available: https://www.concrete.org/Portals/0/Files/PDF/Previews/546.3R-14_preview.pdf

[6] “What is Ponding? - Definition from Corrosionpedia,” *Corrosionpedia*. http://www.corrosionpedia.com/definition/2933/ponding (accessed Nov. 27, 2022).

[7] “Balestra - 2020 - Service Life and Durability of Reinforced Concrete.pdf.” Accessed: Oct. 25, 2022. [Online]. Available: https://link-springer-com.ezproxy.library.uvic.ca/content/pdf/10.1007/978-3-030-47302-0_2

[8] “Marine-Environment Classification,” *Hoists.com*. https://hoists.com/resources/special-applications/marine-environment-classification/ (accessed Nov. 27, 2022).

[9] “Passive Layer - an overview | ScienceDirect Topics.” https://www.sciencedirect.com/topics/engineering/passive-layer (accessed Nov. 27, 2022).

[10] “Corrosion of Embedded Materials.” https://www.cement.org/learn/concrete-technology/durability/corrosion-of-embedded-materials (accessed Oct. 21, 2022).

[11] O. E. Gjorv, O. Vennesland, and A. H. El-Busaidy, “DIFFUSION OF DISSOLVED OXYGEN THROUGH CONCRETE,” *Materials Performance (MP)*, vol. 25, no. No.12, Dec. 1986, Accessed: Feb. 22, 2022. [Online]. Available: https://trid.trb.org/view/395058

[12] A. C. A. Muller, K. L. Scrivener, J. Skibsted, A. M. Gajewicz, and P. J. McDonald, “Influence of silica fume on the microstructure of cement pastes: New insights from 1H NMR relaxometry,” *Cement and Concrete Research*, vol. 74, pp. 116–125, Aug. 2015, doi: 10.1016/j.cemconres.2015.04.005.

[13] “Electrochemical behavior of mild steel in concrete: Influence of pH and carbonate content of concrete pore solution - ScienceDirect.” https://www.sciencedirect.com/science/article/pii/S0013468605003713 (accessed Feb. 22, 2022).

[14] “222R-01 Protection of Metals in Concrete Against C.pdf.” Accessed: Feb. 20, 2022. [Online]. Available: http://civilwares.free.fr/ACI/MCP04/222r_01.pdf

[15] ACI Committee 318 and American Concrete Institute (ACI), *Building code requirements for structural concrete (ACI 318-14): an ACI standard and commentary on building code requerements for structural concrete (ACI 318R-14) : an ACI report*. Farmington Hills, Michigan: American Concrete Institute, ACI, 2014.

[16] “Corrosion Effects on Bond Strength in Reinforced Concrete,” *SJ*, vol. 96, no. 6, 1999, doi: 10.14359/765.

[17] M. Durand-Charre, *Microstructure of Steels and Cast Irons*. Springer Science & Business Media, 2004.

[18] M. F. Montemor, A. M. P. Simões, and M. G. S. Ferreira, “Chloride-induced corrosion on reinforcing steel: from the fundamentals to the monitoring techniques,” *Cement and Concrete Composites*, vol. 25, no. 4, Art. no. 4, May 2003, doi: 10.1016/S0958-9465(02)00089-6.

[19] Gartner, T. Kosec, and Legat, “Monitoring the Corrosion of Steel in Concrete Exposed to a Marine Environment,” *Materials*, vol. 13, p. 407, Jan. 2020, doi: 10.3390/ma13020407.

[20] Y. Du, L. Clark, and A. Chan, “Impact of reinforcement corrosion on ductile behavior of reinforced concrete beams,” *ACI Structural Journal*, vol. 104, pp. 285–293, May 2007.

[21] S. Velu and H.-W. Song, “Evaluation of Cementitious Repair Mortars for Corrosion Resistance,” *Portugaliae Electrochimica Acta*, vol. 26, pp. 417–432, Jan. 2007, doi: 10.4152/pea.200805417.

[22] M. Manera, Ø. Vennesland, and L. Bertolini, “Chloride threshold for rebar corrosion in concrete with addition of silica fume,” *Corrosion Science*, vol. 50, pp. 554–560, Feb. 2008, doi: 10.1016/j.corsci.2007.07.007.

[23] G. Nery de Araújo Neto, G. Hüsken, and H.-C. Kühne, *Design of a cementitious coating system for corrosion protection: materials*. 2014.

[24] P. Azarsa, R. Gupta, and A. Biparva, “Assessment of self-healing and durability parameters of concretes incorporating crystalline admixtures and Portland Limestone Cement,” *Cement and Concrete Composites*, vol. 99, pp. 17–31, May 2019, doi: 10.1016/j.cemconcomp.2019.02.017.

[25] “Corrosion Repair - an overview | ScienceDirect Topics.” https://www.sciencedirect.com/topics/engineering/corrosion-repair (accessed Nov. 27, 2022).

[26] K. Gadri and A. Guettala, “Evaluation of bond strength between sand concrete as new repair material and ordinary concrete substrate (The surface roughness effect),” *Construction and Building Materials*, vol. 157, pp. 1133–1144, Dec. 2017, doi: 10.1016/j.conbuildmat.2017.09.183.

[27] S. Sajedi, F. Ghasemzadeh, I. Harsini, M. Shekarchi, and B. Mohammadi, *Behavior of Bonded Concrete Overlays under Restrained Shrinkage*. 2011.

[28] B. Wang and R. Gupta, “Analyzing bond-deterioration during freeze-thaw exposure in cement-based repairs using non-destructive methods,” *Cement and Concrete Composites*, vol. 115, p. 103830, Jan. 2021, doi: 10.1016/j.cemconcomp.2020.103830.

[29] M. Panjehpour, A. Abdullah, A. Ali, and R. Demirboga, “A Review for Characterization of Silica Fume and Its Effects on Concrete Properties,” *International Journal of Sustainable Construction Engineering and Technology*, vol. 2, Dec. 2011.

[30] V. Logeswaran, “A Study on Compatibility of Concrete Repair Materials,” p. 21, 2020.

[31] F. Dehn, H.-D. Beushausen, M. G. Alexander, and P. Moyo, Eds., *Concrete repair, rehabilitation and retrofitting IV: proceedings of the 4th International Conference on Concrete Repair, Rehabilitation and Retrofitting (ICCRRR 2015), Leipzig, Germany, 5-7 October 2015*. Boca Raton London New York Leiden: CRC Press, a Balkema book, 2015.

[32] G. Venkiteela, M. Klein, H. Najm, and P. N. Balaguru, “Evaluation of the Compatibility of Repair Materials for Concrete Structures,” *International Journal of Concrete Structures and Materials*, vol. 11, no. 3, pp. 435–445, 2017, doi: 10.1007/s40069-017-0208-5.

[33] R. R. Pattnaik and P. Rangaraju, “Relationship between properties and compatibility of repair materials with substrate concrete,” *Indian Concrete Journal*, vol. 88, pp. 20–31, Dec. 2014.

[34] R. Pattnaik, “INVESTIGATION INTO COMPATIBILITY BETWEEN REPAIR MATERIAL AND SUBSTRATE CONCRETE USING EXPERIMENTAL AND FINITE ELEMENT METHOD,” p. 168.

[35] S. Yang, N. Kim, J. Kim, and J. Park, “Experimental measurement of concrete thermal expansion,” *Journal of the Eastern Asia Society for Transportation Studies*, vol. 5, Jan. 2003.

[36] D. D. L. CHUNG, “Improving cement-based materials by using silica fume,” *Journal of materials science*, vol. 37, no. 4, pp. 673–682, 2002, doi: 10.1023/A:1013889725971.

[37] S. Khedr, A. Idriss, and D. McDonald, “Resistance of Silica-Fume Concrete to Corrosion-Related Damage,” *Journal of Materials in Civil Engineering*, vol. 8, pp. 177–178, Jan. 1996, doi: 10.1061/(ASCE)0899-1561(1995)7:2(102).

[38] D. Wang, X. Zhou, Y. Meng, and Z. Chen, “Durability of concrete containing fly ash and silica fume against combined freezing-thawing and sulfate attack,” *Construction and Building Materials*, vol. 147, pp. 398–406, Aug. 2017, doi: 10.1016/j.conbuildmat.2017.04.172.

[39] N. P. Mailvaganam and D. A. Taylor, “Compatibility of repair systems for concrete structures,” p. 23.

[40] D. Cusson and N. P. Mailvaganam, “Durability of repair materials,” p. 8.

[41] K. U. Aavani, A. Aneesha, B. X. Thomas, S. Vandana, and A. Paul, “Review on investigation of corrosion behavior of reinforced concrete with supplementary cementitious materials,” *Sustainability, Agri, Food and Environmental Research*, vol. 10, no. 1, Art. no. 1, 2022, doi: 10.7770/safer-V10N1-art2539.

[42] M. Asi and O. S. B. Al-Amoudl, “IN-SITU TESTING OF CONCRETE,” p. 17.

[43] “compass,” Sep. 15, 2021. https://compass.astm.org/document/?contentCode=ASTM%7CC0876-15%7Cen-US (accessed Sep. 15, 2021).

[44] V. L. Satish, “Half Cell Potential Studies for Durability Studies of Concrete Structures in Coastal Environment,” p. 11.

[45] “compass.” https://compass.astm.org/document/?contentCode=ASTM%7CG0059-97R20%7Cen-US (accessed Dec. 19, 2022).

[46] M. G. Grantham, B. Herts, and J. Broomfield, “The use of linear polarisation corrosion rate measurements in aiding rehabilitation options for the deck slabs of a reinforced

concrete underground car park," *Construction and Building Materials*, vol. 11, no. 4, Art. no. 4, Jun. 1997, doi: 10.1016/S0950-0618(97)00040-8.

[47] "compass." https://compass.astm.org/document/?contentCode=ASTM%7CG0109-21%7Cen-US (accessed Dec. 19, 2022).

[48] D. Trejo and C. Halmen, "Corrosion Performance Tests for Reinforcing Steel in Concrete: Technical Report," p. 252.

[49] M. Pour-Ghaz, O. Isgor, and P. Ghods, "Quantitative Interpretation of Half-Cell Potential Measurements in Concrete Structures," *Journal of Materials in Civil Engineering - J MATER CIVIL ENG*, vol. 21, Sep. 2009, doi: 10.1061/(ASCE)0899-1561(2009)21:9(467).

[50] B. Elsener, C. Andrade, J. Gulikers, R. Polder, and M. Raupach, "Half-cell potential measurements—Potential mapping on reinforced concrete structures," *Mat. Struct.*, vol. 36, no. 7, pp. 461–471, Aug. 2003, doi: 10.1007/BF02481526.

[51] E. Sassine, S. Laurens, R. François, and E. Ringot, "A critical discussion on rebar electrical continuity and usual interpretation thresholds in the field of half-cell potential measurements in steel reinforced concrete," *Materials and structures*, vol. 51, no. 4, pp. 1–12, 2018, doi: 10.1617/s11527-018-1221-0.

[52] C. Andrade and C. Alonso, "Test methods for on-site corrosion rate measurement of steel reinforcement in concrete by means of the polarization resistance method," *Mat. Struct.*, vol. 37, no. 9, pp. 623–643, Nov. 2004, doi: 10.1007/BF02483292.

[53] "compass." https://compass.astm.org/document/?contentCode=ASTM%7CG0109-07R13%7Cen-US (accessed Aug. 29, 2021).

[54] D. Trejo and C. Halmen, "Corrosion Performance Tests for Reinforcing Steel in Concrete: Technical Report," p. 252.

[55] E. Choorackal, O. Nanayakkara, J. Xia, and S. Jones, "Macrocell Corrosion Formation in Concrete Patch Repairs - A Laboratory Study," *Key Engineering Materials*, vol. 711, pp. 68–75, Sep. 2016, doi: 10.4028/www.scientific.net/KEM.711.68.

[56] S. Jäggi, H. Böhni, and B. Elsener, "Macrocell corrosion of steel in concrete – experiments and numerical modelling," *Corrosion of Reinforcement in Concrete: Monitoring, Prevention and Rehabilitation Techniques*, Dec. 2007, doi: 10.1533/9781845692285.75.

[57] B. Elsener, "Macrocell corrosion of steel in concrete – implications for corrosion monitoring," *Cement & concrete composites*, vol. 24, no. 1, pp. 65–72, 2002, doi: 10.1016/S0958-9465(01)00027-0.

[58] S. Qian, J. Zhang, and D. Qu, "Theoretical and experimental study of microcell and macrocell corrosion in patch repairs of concrete structures," *Cement and Concrete Composites*, vol. 28, no. 8, pp. 685–695, Sep. 2006, doi: 10.1016/j.cemconcomp.2006.05.010.

[59] C. Chalhoub, R. Francois, D. Garcia, S. Laurens, and M. Carcasses, "Macrocell corrosion of steel in concrete: Characterization of anodic behavior in relation to the chloride content," *Materials and Corrosion*, vol. 71, Mar. 2020, doi: 10.1002/maco.201911398.

[60] H. H. Song and P. Yalagandula, "Real-time End-to-end Network Monitoring in Large Distributed Systems," in *2007 2nd International Conference on Communication*

Systems Software and Middleware, Jan. 2007, pp. 1–10. doi: 10.1109/COMSWA.2007.382612.

[61] "Linear Polarization - an overview | ScienceDirect Topics." https://www.sciencedirect.com/topics/earth-and-planetary-sciences/linear-polarization (accessed Nov. 27, 2022).

[62] "Polarization Resistance - an overview | ScienceDirect Topics." https://www.sciencedirect.com/topics/chemistry/polarization-resistance (accessed Nov. 27, 2022).

[63] "What is a Polarization? - Definition from Corrosionpedia," *Corrosionpedia*. http://www.corrosionpedia.com/definition/896/polarization-electrochemistry (accessed Nov. 27, 2022).

[64] M. Stern and A. L. Geary, "Electrochemical Polarization: I . A Theoretical Analysis of the Shape of Polarization Curves," *J. Electrochem. Soc.*, vol. 104, no. 1, Art. no. 1, Jan. 1957, doi: 10.1149/1.2428496.

[65] M. Stern, "Electrochemical Polarization: II . Ferrous-Ferric Electrode Kinetics on Stainless Steel," *J. Electrochem. Soc.*, vol. 104, no. 9, Art. no. 9, Sep. 1957, doi: 10.1149/1.2428653.

[66] M. Stern, "Electrochemical Polarization: III . Further Aspects of the Shape of Polarization Curves," *J. Electrochem. Soc.*, vol. 104, no. 11, Art. no. 11, Nov. 1957, doi: 10.1149/1.2428438.

[67] "What is Corrosion Rate? - Definition from Trenchlesspedia." http://www.trenchlesspedia.com/definition/2732/corrosion-rate (accessed Dec. 01, 2022).

[68] B. Borgard, C. Warren, S. Somayaji, and R. Heidersbach, "Mechanisms of Corrosion of Steel in Concrete," in *Corrosion Rates of Steel in Concrete*, pp. 174–188. doi: 10.1520/STP25023S.

[69] S. G. Millard, D. Law, J. H. Bungey, and J. Cairns, "Environmental influences on linear polarisation corrosion rate measurement in reinforced concrete," *NDT & E International*, vol. 34, no. 6, Art. no. 6, Sep. 2001, doi: 10.1016/S0963-8695(01)00008-1.

[70] H.-W. Song and V. Saraswathy, "Corrosion Monitoring of Reinforced Concrete Structures - A Review," *Int. J. Electrochem. Sci.*, vol. 2, p. 28, 2007.

[71] R. Rodrigues, S. Gaboreau, J. Gance, I. Ignatiadis, and S. Betelu, "Reinforced concrete structures: A review of corrosion mechanisms and advances in electrical methods for corrosion monitoring," *Construction and Building Materials*, vol. 269, p. 121240, Feb. 2021, doi: 10.1016/j.conbuildmat.2020.121240.

[72] S. K. Verma, S. S. Bhadauria, and S. Akhtar, "Monitoring Corrosion of Steel Bars in Reinforced Concrete Structures," *The Scientific World Journal*, vol. 2014, p. e957904, Jan. 2014, doi: 10.1155/2014/957904.

[73] "Chapter 14. Sample Preparation for and Examination With The Scanning Electron Microscope - Petrographic Methods of Examining Hardened Concrete: A Petrographic Manual, July 2006 - FHWA-HRT-04-150." https://www.fhwa.dot.gov/publications/research/infrastructure/pavements/pccp/04150/chapt14.cfm (accessed Mar. 28, 2022).

[74] F. Mokobi, “Scanning Electron Microscope (SEM)- Definition, Principle, Parts, Images,” *Microbe Notes*, Mar. 11, 2022. https://microbenotes.com/scanning-electron-microscope-sem/ (accessed Jul. 08, 2022).

[75] P. Stutzman, “Scanning electron microscopy imaging of hydraulic cement microstructure,” *Cement and Concrete Composites*, vol. 26, no. 8, pp. 957–966, Nov. 2004, doi: 10.1016/j.cemconcomp.2004.02.043.

[76] A. Sharif, “Review on Advances in Nanoscale Microscopy in Cement Research,” *Micron*, vol. 80, Sep. 2015, doi: 10.1016/j.micron.2015.09.010.

[77] “QUIKRETE® Portland Cement Type (GU) – Target Products Ltd.” https://www.targetproducts.com/portfolio-item/type-gu-general-use-type-10-cement/ (accessed Feb. 12, 2022).

[78] C01 Committee, “Specification for Portland Cement,” ASTM International. doi: 10.1520/C0150_C0150M-20.

[79] C09 Committee, “Specification for Concrete Aggregates,” ASTM International. doi: 10.1520/C0033_C0033M-18.

[80] “compass.” https://compass.astm.org/document/?contentCode=ASTM%7CC1157_C1157M-20A%7Cen-US (accessed Mar. 06, 2022).

[81] “compass.” https://compass.astm.org/document/?contentCode=ASTM%7CC0260_C0260M-10AR16%7Cen-US (accessed Mar. 06, 2022).

[82] “compass.” https://compass.astm.org/document/?contentCode=ASTM%7CC0494_C0494M-19%7Cen-US (accessed Mar. 06, 2022).

[83] “masteremaco-t-430-tds.pdf.” Accessed: Sep. 22, 2021. [Online]. Available: https://assets.master-builders-solutions.com/en-us/masteremaco-t-430-tds.pdf

[84] “1_3000182-planitop-x-en_81c9db47eac8427b8607a1626bb67641.pdf.” Accessed: Sep. 22, 2021. [Online]. Available: https://cdnmedia.mapei.com/docs/librariesprovider10/products-documents/1_3000182-planitop-x-en_81c9db47eac8427b8607a1626bb67641.pdf?sfvrsn=d94b2cb8_0

[85] “DS-flowcrete.pdf.” Accessed: Sep. 22, 2021. [Online]. Available: https://www.targetproducts.com/PDFs/DS-flowcrete.pdf

[86] “compass.” https://compass.astm.org/document/?contentCode=ASTM%7CC0231_C0231M-17A%7Cen-US (accessed Mar. 06, 2022).

[87] “compass.” https://compass.astm.org/document/?contentCode=ASTM%7CC0143_C0143M-20%7Cen-US (accessed Mar. 06, 2022).

[88] “compass.” https://compass.astm.org/document/?contentCode=ASTM%7CC0192_C0192M-19%7Cen-US (accessed Mar. 06, 2022).

[89] American Concrete Institute, Ed., *Guide to materials selection for concrete repair*. Farmington Hills, Mich: American Concrete Institute, 2014.

[90] "Sodium chloride, 99+%, ACS reagent, Thermo Scientific | Fisher Scientific." https://www.fishersci.com/shop/products/sodium-chloride-99-acs-reagent-thermo-scientific/AC424290250 (accessed Mar. 06, 2022).

[91] "Reference 600+ Potentiostat/Galvanostat 5 MHz EIS." https://www.gamry.com/potentiostats/reference-600-plus/ (accessed Nov. 25, 2021).

[92] Introduction to Stainless Steels. Accessed: Mar. 06, 2022. [Online]. Available: https://www.asminternational.org/documents/10192/1849770/06940G_Chapter_1.pdf/53f29213-5dd6-4499-9959-841477b385b9

[93] "fluke_289_multimeter_manual.pdf." Accessed: Mar. 06, 2022. [Online]. Available: http://www.myflukestore.ca/pdfs/cache/www.myflukestore.ca/fluke/multimeter/289/manual/fluke_289_multimeter_manual.pdf

[94] A. L. Geary, "Electrochemical Polarization," *JOURNAL OF THE ELECTROCHEMICAL SOCIETY*, p. 9, 1957.

[95] C. Andrade *et al.*, "Test methods for on-site corrosion rate measurement of steel reinforcement in concrete by means of the polarization resistance method," *Materials and Structures/Materiaux et Constructions*, vol. 37, pp. 623–643, Nov. 2004, doi: 10.1617/13952.

[96] P. Azarsa, R. Gupta, P. Azarsa, and A. Biparva, "Durability and Self-Sealing Examination of Concretes Modified with Crystalline Waterproofing Admixtures," *Materials*, vol. 14, Oct. 2021, doi: 10.3390/ma14216508.

[97] "SEM-Hitachi-S-4800-Instruction-Manual.pdf." Accessed: Jul. 08, 2022. [Online]. Available: https://www.scu.edu/media/school-of-engineering/photos/cns/SEM-Hitachi-S-4800-Instruction-Manual.pdf

[98] "Energy Dispersive X-Ray Analysis (EDX)." https://www.intertek.com/analysis/microscopy/edx/ (accessed Jul. 08, 2022).

[99] M. Raghav, T. Park, H. Yang, S.-Y. Lee, K. Subbiah, and H.-S. Lee, "Review of the Effects of Supplementary Cementitious Materials and Chemical Additives on the Physical, Mechanical and Durability Properties of Hydraulic Concrete," *Materials*, vol. 14, p. 7270, Nov. 2021, doi: 10.3390/ma14237270.

[100] D. Cusson, S. Qian, and T. Hoogeveen, "Field performance of concrete repair systems on highway bridge," *ACI Materials Journal*, vol. 103, Sep. 2006.

[101] B. Elsener, C. Andrade, J. Gulikers, R. Polder, and M. Raupach, "Half-cell potential measurements—Potential mapping on reinforced concrete structures," *Materials and structures*, vol. 36, no. 7, pp. 461–471, 2003, doi: 10.1007/BF02481526.

[102] F. Pruckner and O. Gjørv, "Patch repair and macrocell activity in concrete structures," *ACI Materials Journal*, vol. 99, pp. 143–148, Mar. 2002.

[103] V. G. Papadakis, "Effect of supplementary cementing materials on concrete resistance against carbonation and chloride ingress," *Cement and Concrete Research*, vol. 30, no. 2, pp. 291–299, Feb. 2000, doi: 10.1016/S0008-8846(99)00249-5.

[104] T. Luping and L.-O. Nilsson, "Chloride binding capacity and binding isotherms of OPC pastes and mortars," *Cement and Concrete Research*, vol. 23, no. 2, pp. 247–253, Mar. 1993, doi: 10.1016/0008-8846(93)90089-R.

[105] H. Manzano, J. Dolado, A. Bustos, and A. Ayuela, "Mechanical Properties of Crystalline Calcium-Silicate-Hydrates: Comparison with Cementitious C–S–H Gels,"

Physica Status Solidi a-Applications and Materials Science, vol. 204, pp. 1775–1780, Jun. 2007, doi: 10.1002/pssa.200675359.

[106] M. J. Abdolhosseini Qomi *et al.*, “Combinatorial molecular optimization of cement hydrates,” *Nat Commun*, vol. 5, no. 1, p. 4960, Dec. 2014, doi: 10.1038/ncomms5960.

[107] S. Tang *et al.*, “Structure, Fractality, Mechanics and Durability of Calcium Silicate Hydrates,” *Fractal Fract*, vol. 5, no. 2, p. 47, May 2021, doi: 10.3390/fractalfract5020047.

[108] Mapping Corrosion of Steel in Reinforced Concrete Structures. Tang Luping. SP Swedish National Testing and Research Institute Building Technology SP REPORT 2002:32. Accessed: Aug. 06, 2022. [Online]. Available: https://www.diva-portal.org/smash/get/diva2:962223/FULLTEXT01.pdf

[109] “Song et al. - 2022 - Cement-Based Repair Materials and the Interface wi.pdf.” Accessed: Jul. 17, 2022. [Online]. Available: https://mdpi-res.com/polymers/polymers-14-01485/article_deploy/polymers-14-01485.pdf?version=1649235632

[110] S. Feng, H. Xiao, and Y. Li, “Influence of interfacial parameters and testing methods on UHPC–NSC bond strength: Slant shear vs. direct tensile testing,” *Cement & concrete composites*, vol. 131, pp. 104568-, 2022, doi: 10.1016/j.cemconcomp.2022.104568.

[111] G. Xiong, B. Luo, X. Wu, G. Li, and L. Chen, “Influence of silane coupling agent on quality of interfacial transition zone between concrete substrate and repair materials,” *Cement and Concrete Composites*, vol. 28, no. 1, pp. 97–101, Jan. 2006, doi: 10.1016/j.cemconcomp.2005.09.004.

[112] “Hitachi S-4800 FESEM - University of Victoria.” https://www.uvic.ca/research/advancedmicroscopy/about/microscopes/sem/index.php (accessed Oct. 21, 2022).

Appendix A Material Specifications

Cementitious Repair Material. Mix F

Target Flowcrete: Is one of the repair materials for corrosion repair termed as Mix F for the purpose of this study.

Data sheet provided by the supplier is shown below.

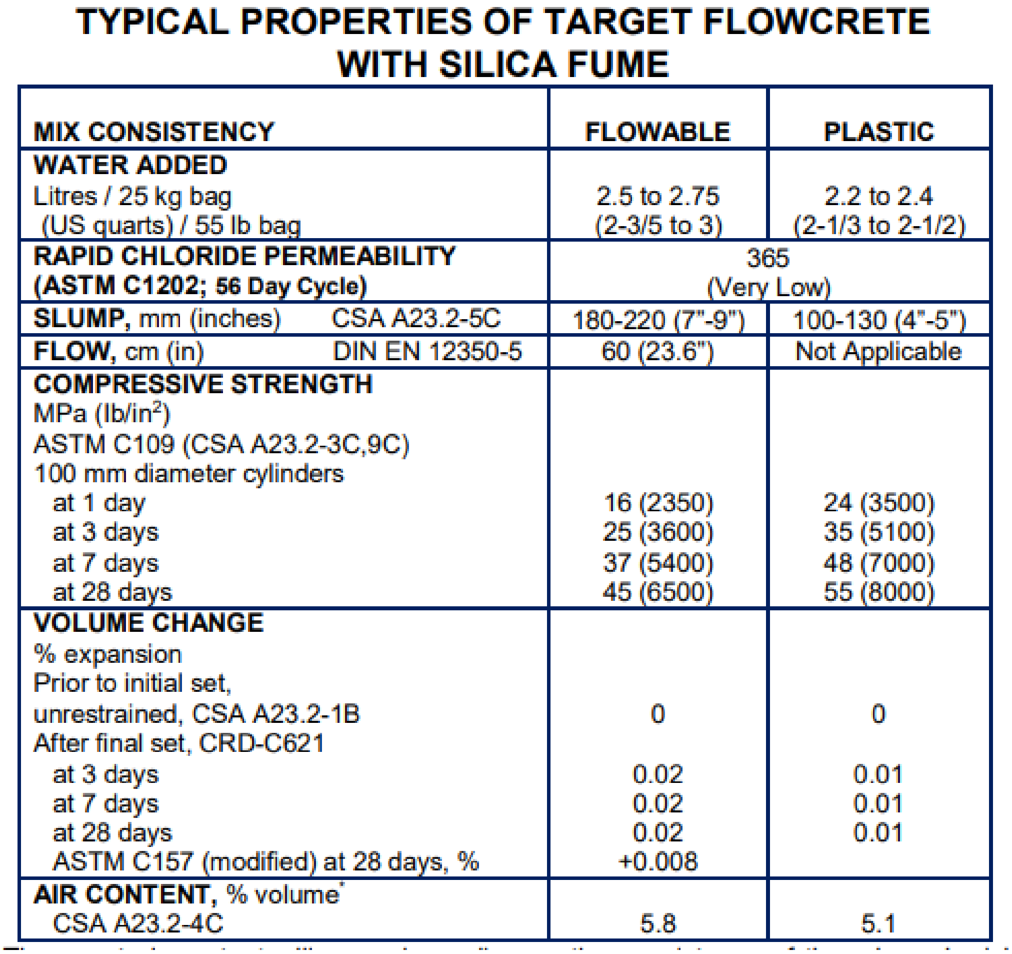

TYPICAL PROPERTIES OF TARGET FLOWCRETE WITH SILICA FUME

MIX CONSISTENCY	**FLOWABLE**	**PLASTIC**
WATER ADDED Litres / 25 kg bag (US quarts) / 55 lb bag	2.5 to 2.75 (2-3/5 to 3)	2.2 to 2.4 (2-1/3 to 2-1/2)
RAPID CHLORIDE PERMEABILITY (ASTM C1202; 56 Day Cycle)	365 (Very Low)	
SLUMP, mm (inches) CSA A23.2-5C	180-220 (7"-9")	100-130 (4"-5")
FLOW, cm (in) DIN EN 12350-5	60 (23.6")	Not Applicable
COMPRESSIVE STRENGTH MPa (lb/in^2) ASTM C109 (CSA A23.2-3C,9C) 100 mm diameter cylinders		
at 1 day	16 (2350)	24 (3500)
at 3 days	25 (3600)	35 (5100)
at 7 days	37 (5400)	48 (7000)
at 28 days	45 (6500)	55 (8000)
VOLUME CHANGE % expansion Prior to initial set, unrestrained, CSA A23.2-1B	0	0
After final set, CRD-C621		
at 3 days	0.02	0.01
at 7 days	0.02	0.01
at 28 days	0.02	0.01
ASTM C157 (modified) at 28 days, %	+0.008	
AIR CONTENT, % volume* CSA A23.2-4C	5.8	5.1

Cementitious Repair Material. Mix P

Planitop X: Is one of the repair materials termed as Mix P for the purpose of this study.

Data sheet provided by the supplier is shown below.

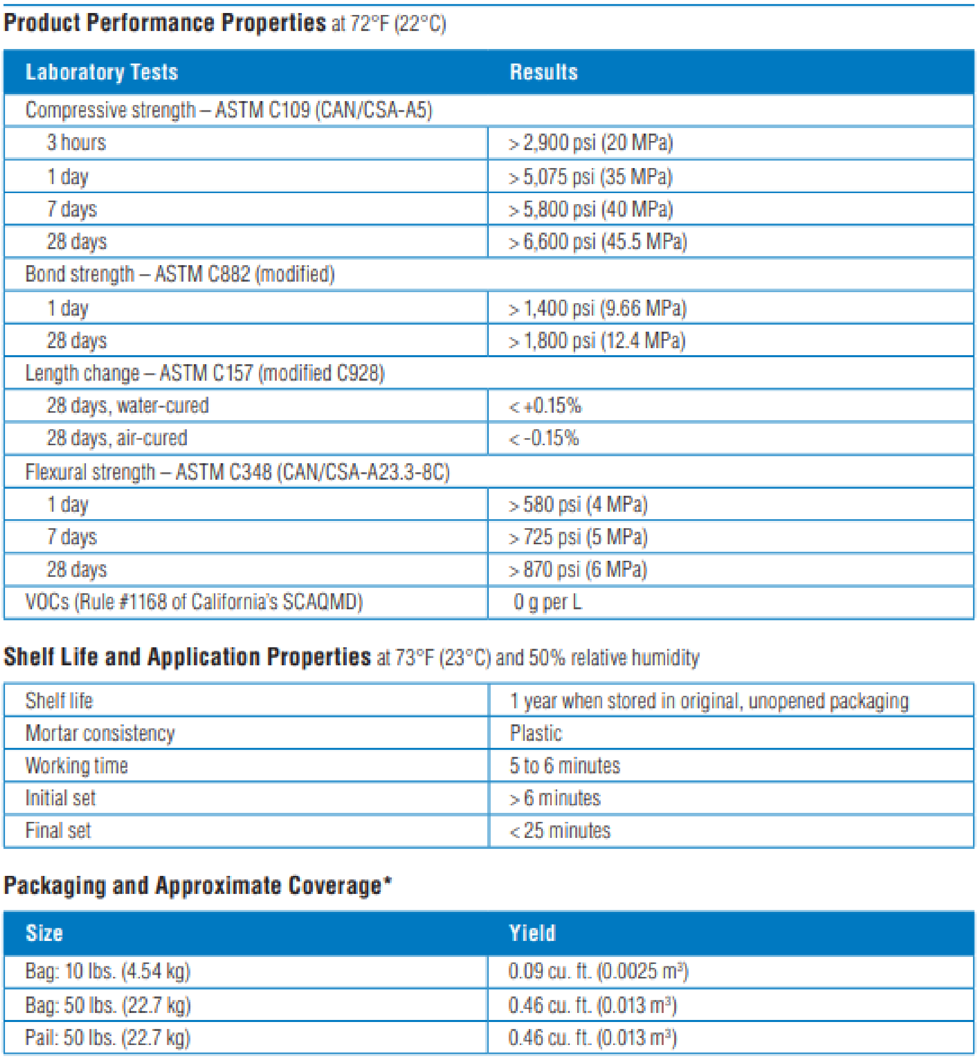

Product Performance Properties at 72°F (22°C)

Laboratory Tests	Results
Compressive strength – ASTM C109 (CAN/CSA-A5)	
3 hours	> 2,900 psi (20 MPa)
1 day	> 5,075 psi (35 MPa)
7 days	> 5,800 psi (40 MPa)
28 days	> 6,600 psi (45.5 MPa)
Bond strength – ASTM C882 (modified)	
1 day	> 1,400 psi (9.66 MPa)
28 days	> 1,800 psi (12.4 MPa)
Length change – ASTM C157 (modified C928)	
28 days, water-cured	< +0.15%
28 days, air-cured	< -0.15%
Flexural strength – ASTM C348 (CAN/CSA-A23.3-8C)	
1 day	> 580 psi (4 MPa)
7 days	> 725 psi (5 MPa)
28 days	> 870 psi (6 MPa)
VOCs (Rule #1168 of California's SCAQMD)	0 g per L

Shelf Life and Application Properties at 73°F (23°C) and 50% relative humidity

Shelf life	1 year when stored in original, unopened packaging
Mortar consistency	Plastic
Working time	5 to 6 minutes
Initial set	> 6 minutes
Final set	< 25 minutes

Packaging and Approximate Coverage*

Size	Yield
Bag: 10 lbs. (4.54 kg)	0.09 cu. ft. (0.0025 m³)
Bag: 50 lbs. (22.7 kg)	0.46 cu. ft. (0.013 m³)
Pail: 50 lbs. (22.7 kg)	0.46 cu. ft. (0.013 m³)

Cementitious Repair Material. Mix M

Master Emaco T 430: Is one of the repair materials termed as Mix M for the purpose of this study. Data sheet provided by the supplier is shown below

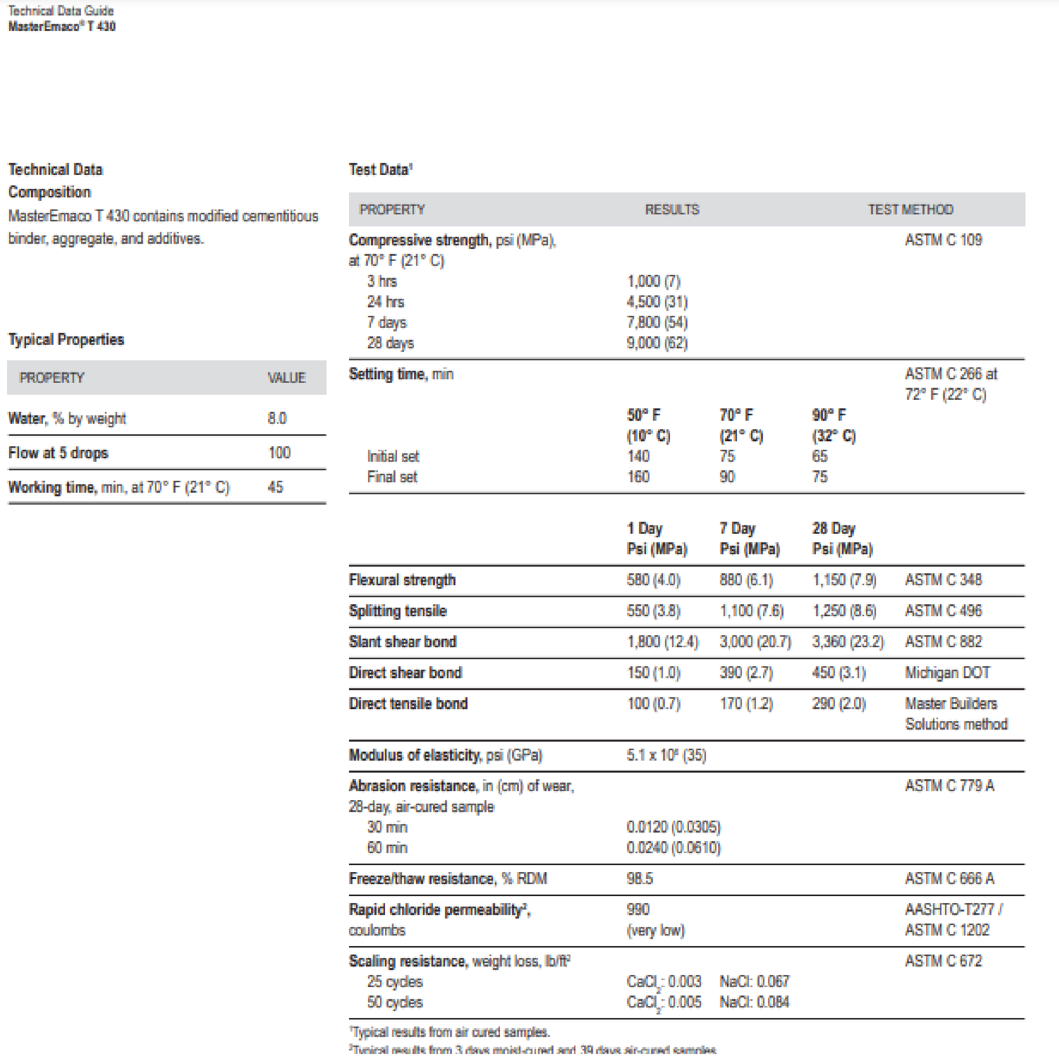

Technical Data Guide
MasterEmaco® T 430

Technical Data
Composition
MasterEmaco T 430 contains modified cementitious binder, aggregate, and additives.

Typical Properties

PROPERTY	VALUE
Water, % by weight	8.0
Flow at 5 drops	100
Working time, min, at 70° F (21° C)	45

Test Data[1]

PROPERTY	RESULTS			TEST METHOD
Compressive strength, psi (MPa), at 70° F (21° C)				ASTM C 109
3 hrs	1,000 (7)			
24 hrs	4,500 (31)			
7 days	7,800 (54)			
28 days	9,000 (62)			
Setting time, min				ASTM C 266 at 72° F (22° C)
	50° F (10° C)	**70° F (21° C)**	**90° F (32° C)**	
Initial set	140	75	65	
Final set	160	90	75	
	1 Day Psi (MPa)	**7 Day Psi (MPa)**	**28 Day Psi (MPa)**	
Flexural strength	580 (4.0)	880 (6.1)	1,150 (7.9)	ASTM C 348
Splitting tensile	550 (3.8)	1,100 (7.6)	1,250 (8.6)	ASTM C 496
Slant shear bond	1,800 (12.4)	3,000 (20.7)	3,360 (23.2)	ASTM C 882
Direct shear bond	150 (1.0)	390 (2.7)	450 (3.1)	Michigan DOT
Direct tensile bond	100 (0.7)	170 (1.2)	290 (2.0)	Master Builders Solutions method
Modulus of elasticity, psi (GPa)	5.1×10^6 (35)			
Abrasion resistance, in (cm) of wear, 28-day, air-cured sample				ASTM C 779 A
30 min	0.0120 (0.0305)			
60 min	0.0240 (0.0610)			
Freeze/thaw resistance, % RDM	98.5			ASTM C 666 A
Rapid chloride permeability[2], coulombs	990 (very low)			AASHTO-T277 / ASTM C 1202
Scaling resistance, weight loss, lb/ft²				ASTM C 672
25 cycles	$CaCl_2$: 0.003	NaCl: 0.067		
50 cycles	$CaCl_2$: 0.005	NaCl: 0.084		

[1] Typical results from air cured samples.
[2] Typical results from 3 days moist-cured and 39 days air-cured samples.

Appendix B. Equipment specifications

Gamry Potentiostat / Galvanostat. Reference 600+

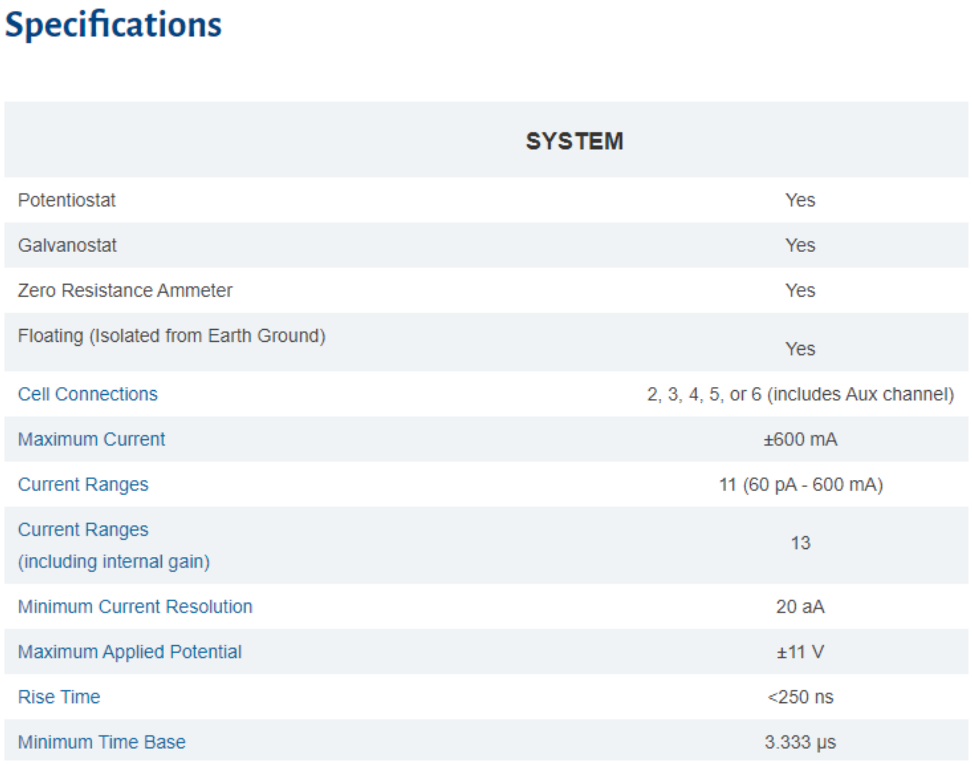

Specifications

SYSTEM	
Potentiostat	Yes
Galvanostat	Yes
Zero Resistance Ammeter	Yes
Floating (Isolated from Earth Ground)	Yes
Cell Connections	2, 3, 4, 5, or 6 (includes Aux channel)
Maximum Current	±600 mA
Current Ranges	11 (60 pA - 600 mA)
Current Ranges (including internal gain)	13
Minimum Current Resolution	20 aA
Maximum Applied Potential	±11 V
Rise Time	<250 ns
Minimum Time Base	3.333 µs

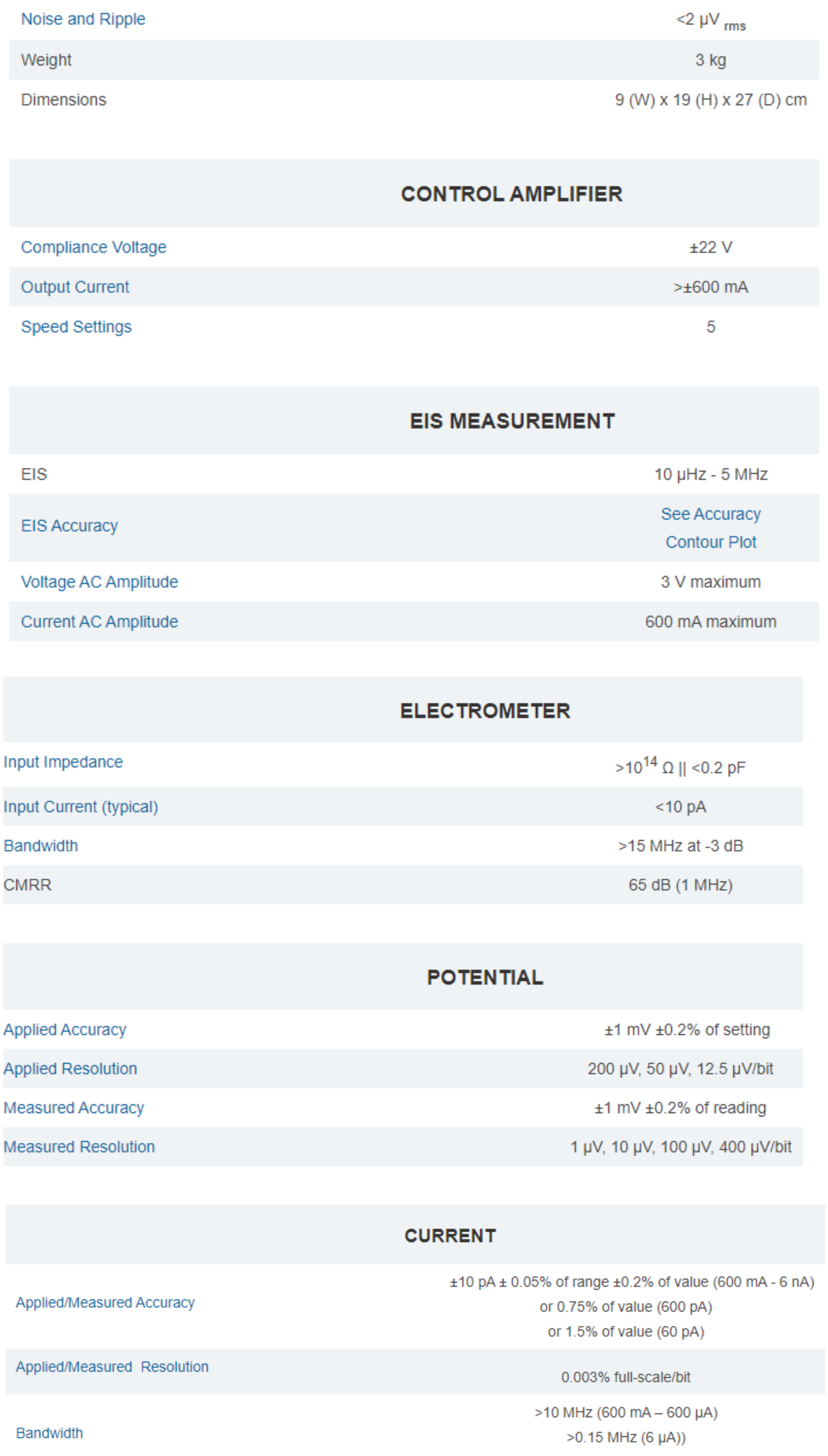

Noise and Ripple	<2 μV_{rms}
Weight	3 kg
Dimensions	9 (W) x 19 (H) x 27 (D) cm

CONTROL AMPLIFIER	
Compliance Voltage	±22 V
Output Current	>±600 mA
Speed Settings	5

EIS MEASUREMENT	
EIS	10 µHz - 5 MHz
EIS Accuracy	See Accuracy Contour Plot
Voltage AC Amplitude	3 V maximum
Current AC Amplitude	600 mA maximum

ELECTROMETER	
Input Impedance	>10^{14} Ω || <0.2 pF
Input Current (typical)	<10 pA
Bandwidth	>15 MHz at -3 dB
CMRR	65 dB (1 MHz)

POTENTIAL	
Applied Accuracy	±1 mV ±0.2% of setting
Applied Resolution	200 µV, 50 µV, 12.5 µV/bit
Measured Accuracy	±1 mV ±0.2% of reading
Measured Resolution	1 µV, 10 µV, 100 µV, 400 µV/bit

CURRENT	
Applied/Measured Accuracy	±10 pA ± 0.05% of range ±0.2% of value (600 mA - 6 nA) or 0.75% of value (600 pA) or 1.5% of value (60 pA)
Applied/Measured Resolution	0.003% full-scale/bit
Bandwidth	>10 MHz (600 mA – 600 µA) >0.15 MHz (6 µA))

Appendix C SEM/EDX Equipment Specifications

Advance Microscopy Facility

Hitachi S-4800 FESEM Extension EDX [112]

- 0.5 kVv to 30kV acceleration voltage
- 1nm resolution at 15kV, 1.4nm at 1Kv
- Magnification from 30x to 800,000x
- Maximum specimen size = 100nm
- Super ExB filter technology
- Dry vacuum system
- X+Y motorized eucentric stage with trackball interface (tilt and Z by manual control)
- Ring-type YAG backscatter detector
- Bruker Quantax EDS System for X-ray spectroscopy

Appendix D.

Measurement of fresh properties of concrete, preparation, and testing of RC repaired specimens

Figure D1.1 Air Content Test

Figure D2.1 Slump Test

Figure D3.1 Molding preparation of specimens

Figure D4.1 Demolding of specimens (substrate and C)

Figure D5.1 Curing of specimens

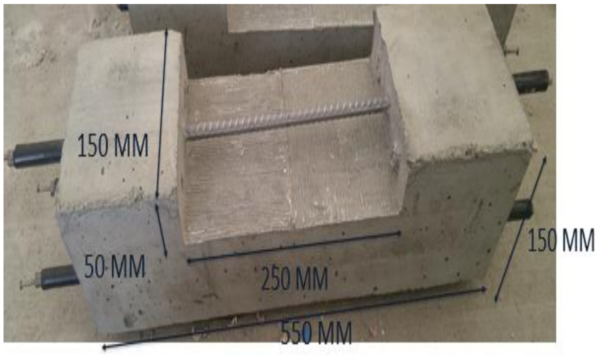

Figure D6.1 Preparation of repair material indentation

Figure D7.1 Casting of repair material Mix M

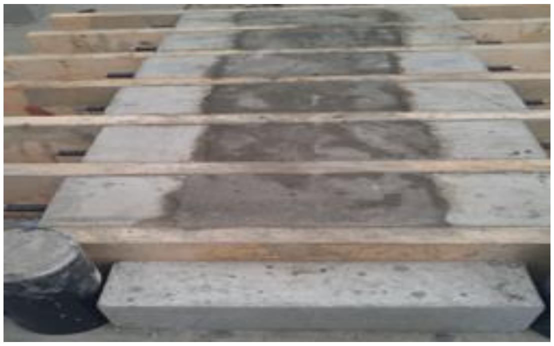

Figure D8.1 Casting of repair material Mix F

Figure D9.1 Casting of repair material Mix P

Figure D10.1 Ponding of repair & substrate interface

Figure D11.1 Ponding of repair materials. M, P, F and C   Figure D12.1 No ponding of repair materials M, P, F and C

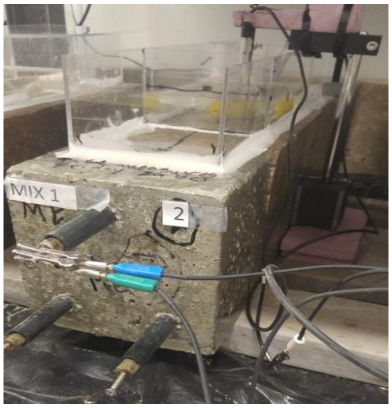

Figure D13.1Macrocell testing, Figure. D14.1 LPR and HCP testing, no ponding. Figure. D15.1. LPR and HCP testing, ponding